ABSTRACT

Title of Document:	OF MICE AND MATH: A SYSTEMS BIOLOGY MODEL FOR ALZHEIMER'S DISEASE
	Christina Rose Kyrtsos Doctor of Philosophy 2011
Directed By:	Dr. John S. Baras Professor Institute for Systems Research

Alzheimer's disease (AD) is the most prevalent neurodegenerative disorder in the US, affecting over 1 in 8 people over the age of 65. There are several well-known pathological changes in the brains of AD patients, namely: the presence of diffuse beta amyloid plaques derived from the amyloid precursor protein (APP), hyper-phosphorylated tau protein, neuroinflammation and mitochondrial dysfunction. Recent studies have shown that cholesterol levels in both the plasma and the brain may play a role in disease pathogenesis, however, this exact role is not well understood. Additional proteins of interest have also been identified (ApoE, LRP-1, IL-1) as possible contributors to AD pathogenesis. To help understand these roles better, a systems biology mathematical model was developed. Basic principles from graph theory and control analysis were used to study the effect of altered cholesterol, ApoE, LRP and APP on the system as a whole. Negative feedback regulation and the

rate of cholesterol transfer between astrocytes and neurons were identified as key modulators in the level of beta amyloid. Experiments were run concurrently to test whether decreasing plasma and brain cholesterol levels with simvastatin altered the expression levels of beta amyloid, ApoE, and LRP-1, to ascertain the edge directions in the network model and to better understand whether statin treatment served as a viable treatment option for AD patients. The work completed herein represents the first attempt to create a systems-level mathematical model to study AD that looks at intercellular interactions, as well as interactions between metabolic and inflammatory pathways.

OF MICE AND MATH: A SYSTEMS BIOLOGY MODEL FOR ALZHEIMER'S
DISEASE

By

Christina Rose Kyrtsos

Dissertation submitted to the Faculty of the Graduate School of the
University of Maryland, College Park, in partial fulfillment
of the requirements for the degree of
Doctor of Philosophy
2011

Advisory Committee:
Professor John S Baras, Chair
Professor Hey-Kyoung Lee
Professor Mary-Ann Ottinger
Professor William Bentley
Assistant Professor Silvina Matysiak

Dedication

I would like to dedicate this work to all of the people who have been a part of this 5 year journey known as a PhD. This has been a process of not only studying what factors may contribute to Alzheimer's disease, but also a process of finding myself and my niche in the world- I can't say that I've experienced such intellectual and personal growth for many years. From the study groups and dinners first year, to the time spent working in lab with fellow lab mates, to all of the activities that I've done with friends, co-workers, faculty and staff, it's been a well-rounded experience.

I would also like to dedicate this work to my family: to my dad who introduced me to math and science by proving Fermat's last theorem on the bathroom wall, taking us to science museums, doing circuits with us and letting us read his college textbooks when we were little and had no clue what they were talking about; to my mom who taught me persistence, patience and kindness, and for instilling in me a love of chemistry and biology; to my sisters, Catherina, Dianna, Angela, Susana and Gabriella, for always being there through all of our misadventures of childhood; and to my little brothers Alex and Nicki for just being awesome. This work is especially dedicated to Nicki who is one of my main motivations for studying neuroscience.

Acknowledgements

Several people have played very important roles in finishing this work. First off, I would like to thank my co-advisor Dr. Hey-Kyoung Lee for all of her time spent helping with the biology side of this project, from the design of the experiments, to troubleshooting and analysis, she has been a great resource and an excellent mentor. I would also like to thank the other members of my committee, Dr. Mary Ann Ottinger, Dr. Silvina Matysiak and Dr. William Bentley, for their insightful support throughout the dissertation process. My main advisor, Dr. John S Baras, has been a continued source of support and guidance, serving as an excellent mentor and teacher. It still amazes me how many different projects he can be working on at the same time and still get things done well; he is definitely a great role model for being a professor.

I would also like to thank the undergraduate students who have helped with the biology experiments: Ryan Fitch, for his help with the HPLC, Western blotting and immunohistochemistry work; Sara Husson, for her help with Western blotting and immunohistochemistry; Danielle Buccine, for her help with the cholesterol assays and immunohistochemistry; and Allen Paisner, for his help analyzing confocal images. Their efforts have helped to make this thesis possible and hopefully they have gained some valuable lab experience that they can take with them (I know I've gained some valuable mentoring experience).

My co-workers from both of the labs that I work in have also played an integral part in preparing for my thesis. I would particularly like to thank my office mates- Pedram Hovarshti and Tao Jiang- for their help and patience while I went through the dissertation process. My other co-workers- Ion Matei, Elena Stai,

Vasiliki Pouli, Hua Chen, ShanShan Zhang, Christoforos Somarkis and Anup Menon- were also great lab mates. I would also like to thank Lihua Song for teaching me how to do Western blotting, Angela Lee and Cara Jacobs for teaching me how to do immunohistochemistry, and Emily Petrus for her help with mice.

Finally, I would like to thank those faculty and staff members who gave me compassionate support throughout the process: Dr. Marta Hopkinson for her support and help with the student group that I helped run; Dr. Isabel Lloyd, for her help, support and guidance throughout the entire process and as the main mentor in the Sloan Program; Ann Anonsen, Michelle French and Katie Helene for always being a listening ear; and last but not least, to Allison Bennett for being there when I needed it most.

Table of Contents

List of Tables

List of Figures

Chapter 1: Introduction

Alzheimer's disease (AD) is the most common form of dementia, affecting more than 4.5 million individuals in the US alone [65]. This number is expected to triple in the next four decades as the most affected age group (those over 65) surpasses 12 million. The cost of care for individuals with AD is staggering- over $140 billion annually, which is also expected to rise in correlation with the affected number of individuals. The exact cause of AD is uncertain, though at least two distinct forms of the disease are known to exist: early-onset and late-onset.

Early-onset AD is related to mutations in the amyloid precursor protein (APP) and presenilin, which increase the cleavage rate of APP into the amyloidogenic beta amyloid (Aβ). Individuals with Down Syndrome (DS; also known as trisomy 21) also commonly have early-onset AD because the gene for APP is located on chromosome 21. Late-onset AD has been linked to age, the presence of the apolipoprotein ε4 allele, cerebrovascular disease, cardiovascular disease (including atherosclerosis) and high plasma cholesterol, though the exact interactions between these co-occurring diseases are not well understood.

Regardless of the disease trigger(s), the resultant pathological characteristics are similar and involve the buildup of Aβ in the brain parenchyma, deposition of Aβ in the cerebral blood vessels (as cerebral amyloid angiopathy, CAA), as well as the presence of neurofibrillary tangles (NFTs). Loss of hippocampal and cortical neurons has been observed [113]. Neuroinflammation with corresponding activation of

microglia has also been observed, as well as alterations in blood-brain barrier (BBB) permeability [121, 156-159, 6-67]. A combination of these cellular and sub-cellular changes is believed to lead to the symptoms most commonly associated with AD, including: gradual loss of memory, personality changes, depression, inability to communicate, and loss of voluntary muscle movements [94].

Even with the significant advances that have been made in the field of AD research, there is still no clear understanding between causality and observation of secondary symptoms. Specifically, no systems-level, biomolecular reaction network exists to describe how different biomolecules that are known or thought to be involved in the pathogenesis are interrelated. The goals of this dissertation were:

1) To develop an interaction network model of the biomolecular processes involved in AD pathogenesis using systems biology and graph theory as the basis for analysis.

2) To study the role of brain cholesterol and inflammation in the disease process via:

   a. Experimental methods that simultaneously decrease the level of brain cholesterol and neuroinflammation, and provide semi-quantitative data points for the effect of a network perturbed by such a decrease.

   b. Computational methods that utilize experimental data to describe connections and connection strengths between components in the network to determine key nodes.

This dissertation represents the first (known) attempt to create a systems biology model to better understand the processes that are co-occurring in AD and how these processes may trigger AD pathogenesis.

Chapter 2: Background

History of neuroscience

The human mind has been the center of much study and discussion since ancient times. The earliest surviving manuscript referencing the brain and brain surgery is a collection of papyrus documents from Egypt dating back to 3000 BC. It is not until nearly 2500 years later that Hippocrates describes the importance of the brain in intelligence and in feeling sensations. This view is debated among several other prominent philosophers of the era, including Aristotle who believed that the heart was the source of sensations and mental processes. Herophilus and his student, Erasistratus, conducted anatomical studies of the brain and believed that the ventricles were the source of human intellect and the soul. Galen (129-199 AD) was the first to describe the brain, spinal cord and nerves as one system, the nervous system, and to conclude that the soul does not reside in the ventricles of the brain through experimental observation.

Further understanding of the brain and nervous system paused during the Middle Ages, and resumed during the Renaissance and thereafter, with contributions by several major physicians and philosophers. In 1543, Andreas Vesalius argued that brain function derives from the tissue surrounding the ventricles (the cortex and other regions of the brain), and not the ventricles. The term "hippocampus" was introduced by Aranzi in 1564. Description of the anatomy of cerebral blood vessels began to

appear in 1609 when Guilio Casserio published drawings of the circle of Willis (a circle of arteries located at the base of the brain). This work was expanded on by Thomas Willis in 1664 who published a work discussing the function of the arteries at the base of the brain that now carry his name.

The 18th century brought significant advances in the anatomical knowledge of the central nervous system, including description of the composition of cerebrospinal fluid, and identification of foramen of Monroe, the stripe of Gennari, the fovea and the insula.   It was also the first time that electrical impulses in nerves were studied in an animal model. The first hospitals dedicated to helping those affected by mental illness also opened during the 18th century.

Neuroscience flourished in the 19th century. Basic anatomy and physiological functions of identified regions were described. In 1837, Jan Purkyne (Purkinje) successfully identified neuronal nuclei and associated processes in cerebellar cells. Robert Remak described the difference between myelineated and unmyelineated cells in 1836; Schwann cells were soon after discovered by Theodor Schwann in 1838. In 1850, Augustus Waller first described degenerating neurons. Richard Caton was the first person to record electrical activity from the brain in 1875, beginning the era of using electrical recordings to study brain functionality. Many of the stains and methods that we still use today in histology were developed in the last 30 years of the 19th century (silver nitrate, 1873; hematoxylin to stain myelin, 1885; Nissl stain for neurons, 1894; formaldehyde to fix brains, 1897). This was also the time period wherein Golgi and Ramon y Cajal did their groundbreaking histological work and developed the reticular and cellular theories of neuroscience, respectively.

The 20th century continued this trend of rapid expansion of knowledge. A single paragraph cannot do justice to the vast amount of information gained in the last 111 years, but only touch on some of the key points. Early in the century, glial cells (astrocytes, microglia and oligodendrocytes) were identified and their roles were characterized. Cellular ultrastructure of all neural cell types was obtained in the 1950s with the advent of the electron microscope, providing definitive proof of the validity of Ramon y Cajal's cellular theory for the brain. This led to the development of neural circuit models to study physiological functioning and development in the brain. Neurotransmitters were identified as the key electrochemical signaling molecule within the brain, leading to the concept of excitatory and inhibitory neurotransmitters, a key factor playing a role in a variety of neurological and psychiatric diseases. It was also in this century that Alois Alzheimer first described the symptomology and amyloid beta plaques present in a patient with *presenile degeneration,* a disease that would later take on his name.

Although our understanding of the brain, its anatomy, physiology and development has grown almost exponentially in the last 200 years, there are still many unknowns. Of all of the subfields in biology and medicine, neuroscience is perhaps the last, towering frontier to understand and conquer. With the advent of modern computing capabilities; technological advances in imaging, metabolomics, genomics and proteomics; and development of a mathematical language to help describe the interaction of a large number of biological networks, neuroscientists stand at the crest of a wave with regards to our understanding of the brain and how it works.

Anatomy of the brain

In humans, that brain starts to form during the first 3 weeks of gestation, with the ectoderm forming the neural plate, followed by the neural plate folding and closing to form the neural tube. As development continues, the neural tube starts to take shape into the cerebral hemispheres, cerebellum and pons. Continuing development of the brain proceeds throughout the early years following birth all the way into young adulthood, wherewith neurons are shed, neurons grow slowly, and near-constant pruning of dendrites and wiring/re-wiring occurs. Development of the brain continues until the early- to mid-twenties, when rates begin to converge. Generation of neurons in the dentate gyrus has been shown to continue well into adulthood, however, the rates are quite slow comparatively.

Together, the brain with the spinal cord, are known as the central nervous system (CNS). The CNS can be divided into six majors divisions: spinal cord, medulla, pons and cerebellum, midbrain, diencephalon and cerebral hemispheres. Each of these regions performs a set of tasks; however, these tasks are not necessarily independent or unique from tasks performed by other CNS regions. Each region can also be clearly subdivided into regions containing neuronal cell bodies (gray matter) and regions containing predominantly axons (white matter). White matter is white due to the high concentration of myelin which surrounds the axons. The CNS is surrounded by three layers of meninges which serve a protective, as well as circulatory role. These three meninges are known as the *dura mater,* the *arachnoid mater* and the *pia mater.* The dura mater contains large, low-pressure blood vessels which are part of the cerebral venous system. The arachnoid mater separates the dura

from the pia, creating the subdural space and the subarachnoid space, respectively. The subarachnoid space contains the veins and arteries that provide circulation to the surface of the CNS, as well as cerebrospinal fluid (CSF). The following sections will describe in further detail the brief functions of each brain region aside from the spinal cord.

The brain stem is composed of the medulla, pons, midbrain and cerebellum and has three main functions: (1) to receive sensory information from cranial nerves and control muscles of the head; (2) to regulate the level of arousal via blood pressure regulation and respiratory regulation by the combined effort of the medulla, pons and midbrain; and (3) to act as a multiplexor of information between the spinal cord and higher brain regions. The cerebellum also plays a key role in the control of muscle movement, while the midbrain plays an important role in the control of eye movement.

The most developed regions of the human brain are the diencephalon and the cerebral hemispheres. The diencephalon is subdivided into the *thalamus* and the *hypothalamus*. The thalamus is responsible for transmitting information between the two cerebral hemispheres. The hypothalamus is responsible for regulating release of hormones from the pituitary gland, as well as integrating the functions of the autonomic nervous system. The sagittal fissure separates the two hemispheres of the cerebrum. The cerebrum can be further divided into the cerebral cortex, basal ganglia, amygdala and hippocampus. The basal ganglia, also known as the striatum, contribute to several higher brain functions, including control of movement, cognition and expression of emotions. The cerebral cortex, the highly convoluted region of

neurons found on the surface of the cerebrum, is responsible for the many of the functions attributed to the brain. The cerebral cortex can be divided into four distinct lobes: the frontal lobe, the parietal lobe, the temporal lobe and the occipital lobe.
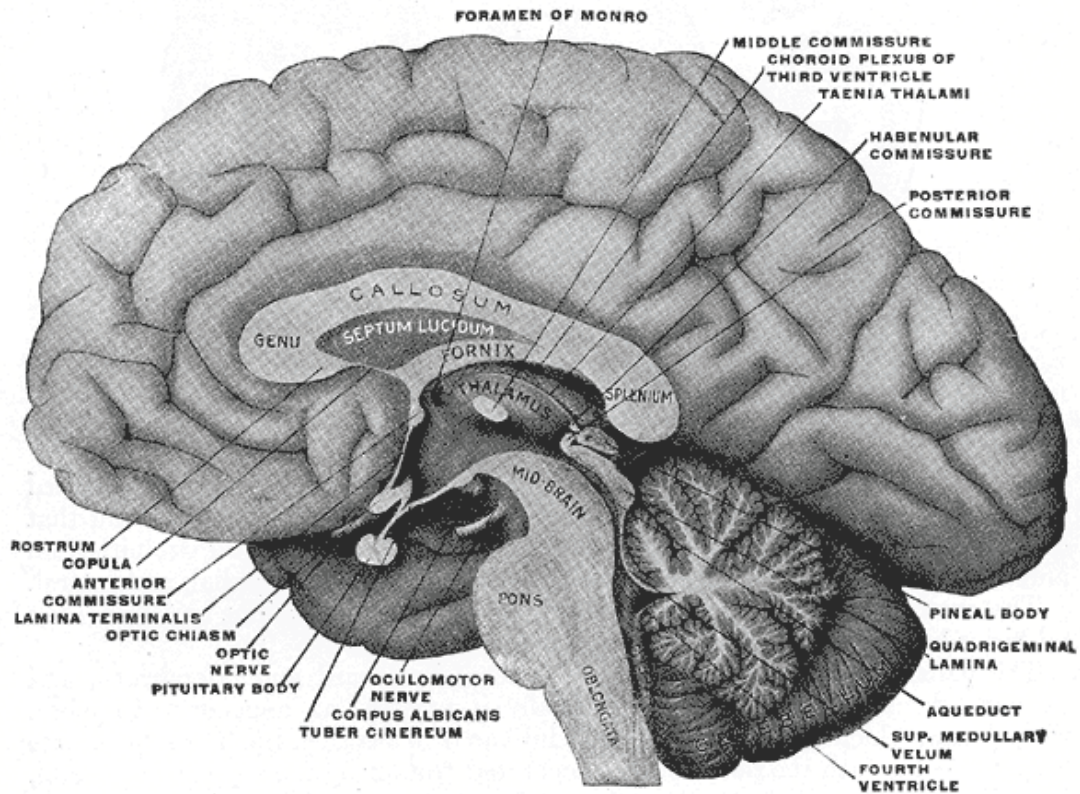
Figure 1: *Sagittal view of right brain hemisphere*. Details of the brain stem (pons, medulla, midbrain and cerebellum) and the diencephalon. Adapted from *Gray's Anatomy*.

The frontal lobe is responsible for many of the higher mental functions of the brain, including suppressing unacceptable social responses, choosing between wrong and right, recognizing consequences and differentiating between objects, events or people. The frontal lobe contains the majority of the neurons that are sensitive to dopamine; dopamine-sensitive neurons are responsible for actions associated with planning, drive, long-term memory, reward and attention. The long-term memories stored in the frontal lobe are often associated with emotion-based memories inputted

from the limbic system. Lesions in the frontal lobe can be associated with loss of creativity and decreased ability to have higher mental processes.

The parietal lobe is responsible for visual-spatial processing, understanding mathematics and abstract, symbolic representations, as well as integrating sensory input from different regions of the body. The temporal lobe plays important roles in processing visual and auditory signals. It contains the auditory cortex. The occipital lobe participates heavily in visual processing and is the origin of dreams.
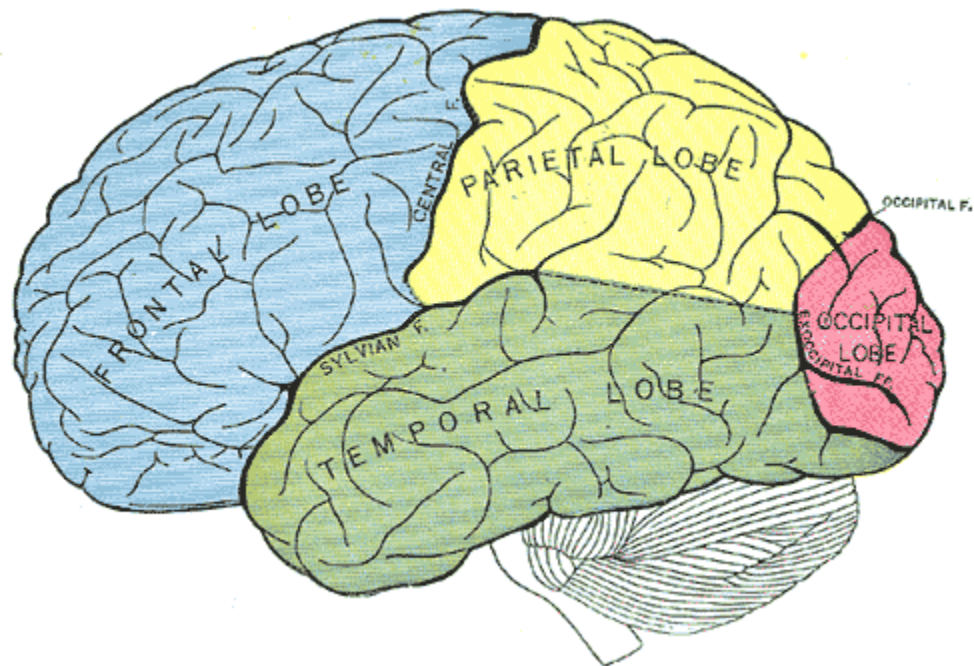
Figure 2: *The four lobes of the cerebral cortex*. Frontal: "moral differentiator", emotion-based memories; Parietal: Visuo-spatial processing, symbolic representation, integrating sensory input; Temporal: Auditory and visual processing, auditory cortex; Occipital: Visual processing, origin of dreams. Adapted from *Gray's Anatomy*.

The final two regions of the cerebral cortex are the amygdala and the hippocampus. The amygdala is believed to be responsible for hormone release, coordination of the autonomic nervous system, and emotional responses. The

hippocampus, the brain region that is initially and most severely affected in AD, is believed to play a role in episodic memory and spatial orientation. The hippocampus can be further subdivided into 4 distinct regions: CA1, CA2, CA3 and DG (**C**ornu **A**mmonis and **d**entate **g**yrus, respectively). Modulatory inputs are received from the dopamine, serotonin, and norepinephrine systems; from the *nucleus reuniens* of the thalamus via CA1; and cholinergic and GABAergic input from the medial septal area. Together, the hippocampus, amygdala, and portions of the midbrain and diencephalon form the *limbic system*, which is believed to be responsible for thought and mood in humans. Disorders of the limbic system often lead to psychiatric disorders.
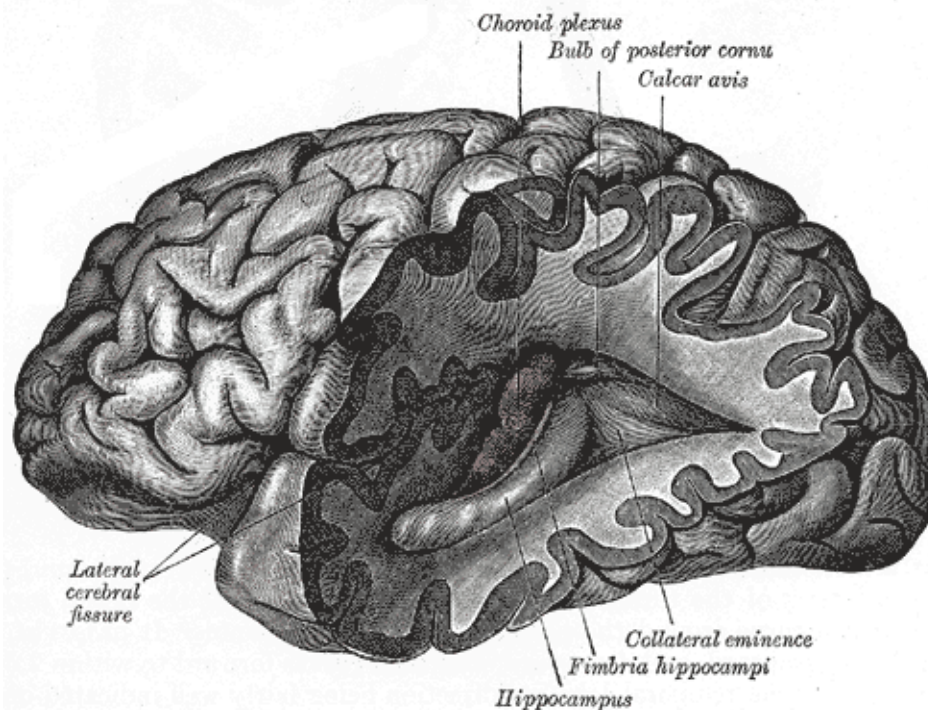
Figure 3: *The hippocampus and surrounding regions*. The hippocampus is believed to be responsible for episodic memory and spatial orientation. Adapted from *Gray's Anatomy*.

Supplying each of these regions of the brain with nutrients and removing waste products is a complicated network of arteries, capillaries and veins. On

average, neurons are less than 50 μm away from an artery, ensuring that they receive an adequate supply of glucose and oxygen for metabolism, and removal of neurotoxic waste products. These vessels are not immune from the buildup of plaques, leading to strokes, poor microcirculation or localized hypoxia, and eventual neuronal cell death. In AD, beta amyloid plaques are found in cerebral blood vessels, which may play a causal role in disease pathogenesis.

Cellular Neurobiology:

At the cellular level, the brain can be divided up into two main types of cells: neurons and glial cells. The average brain contains over 100 billion neurons and more than four times that many glial cells. Neurons are specialized cells that have been terminally differentiated. Their predominant role is to receive incoming electrical signals from neighboring neurons, process the signal, and transmit the corresponding output signal to downstream neurons via the axon and synapse. Glial cells participate in a range of supporting activities, from removing wastes and excess neurotransmitters from the synaptic cleft, to providing dendrites some guidance on where to grow and acting as the brain's immune system.

There is a rich diversity in the types of neurons in the brain. Neurons vary in shape, size and length of axon (morphology), expression of receptors and proteins (proteomic variation), and in physiological function. The basic components of any neuron are: a cell body, the axon, and the dendrites. The dendrites are the location where axons from other neurons synapse onto a neuron, and signals are transmitted to the cell body for further processing. The cell body is the predominant site of protein synthesis and the location where signals are integrated. Action potentials are initiated

12

by the cell body and are transmitted down the axon in generally a unidirectional manner (there are a few exceptions to this). The axon is encased in a layer of myelin, which insulates the axon and allows electrical signals to travel faster. In mammals, the myelin covers distinct areas of the axon while leaving occasional areas un-insulated. These un-insulated areas are known as the *nodes of Ranvier* and give the action potential an appearance of "jumping" from node to node, an observance that has been named *saltatory conduction*. Together, this basic structural unit is capable of receiving, processing, and sending electrochemical signals that serve as the basis of brain function.
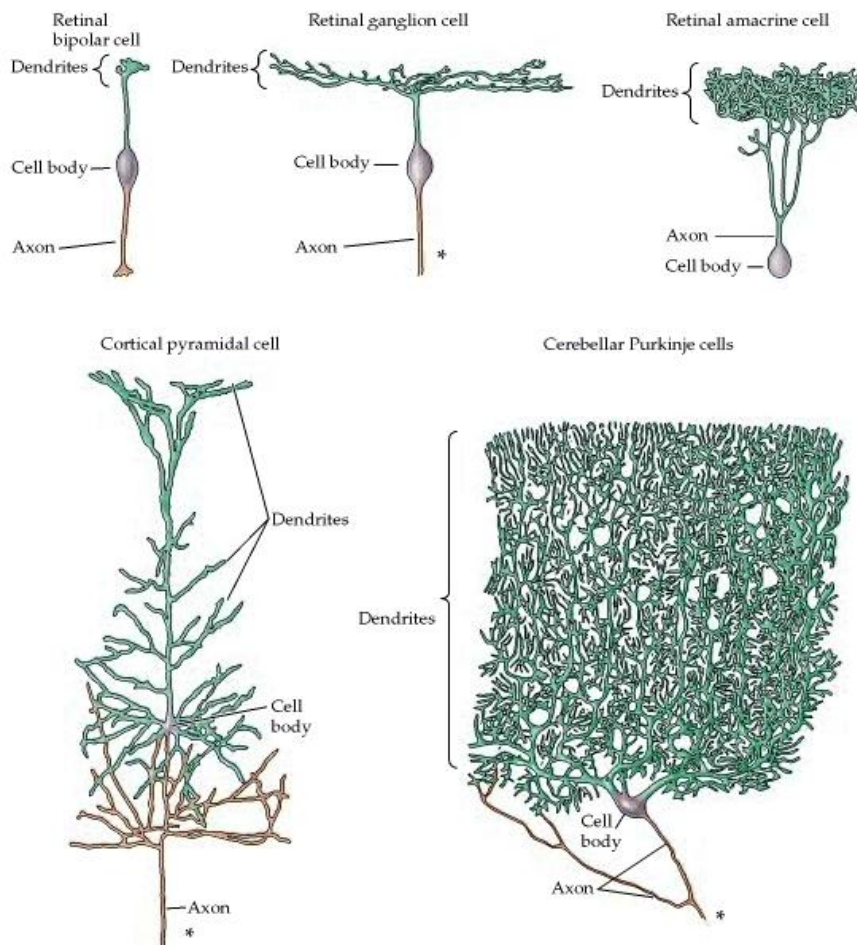
Figure 4: *A sampling of some of the types of neurons that are found in the brain.* Notice how many different variations on the standard textbook neuron (cell body, axon, dendrites) there are, and how the dendritic structure can vary greatly. Adapted from *Neuroscience* by Purves 2nd edition 2001 [115].

At the axon terminal and dendrites, specialized proteins aggregate and help form what is known as the synapse. The synapse is composed of two terminals (pre- and post-) and extracellular space in between the two known as the synaptic cleft. As an action potential reaches the axon terminal, membrane depolarization causes membrane-gated Ca^{2+} to open, triggering the influx of calcium into the pre-synaptic terminal. The increased calcium levels cause synaptic vesicles to move to the pre-synaptic membrane and release neurotransmitter into the synaptic cleft. Neurotransmitter is then bound by receptors at the post-synaptic site, triggering an action potential in the post-synaptic cell. Neurotransmitters can be excitatory, inhibitory or some combination thereof; that is, they can either increase the probability of an action potential (excitatory) or decrease the probability (inhibitory). Used neurotransmitter is released back into the synaptic cleft and either recycled by the pre-synaptic cell or degraded via enzymatic action. The following table lists some of the most common neurotransmitters in the brain, their function and which type of neurotransmitter they are.

Neurotransmitter	Type	Function
Acetylcholine	----	Excitatory
Dopamine	Amine	Excitatory & Inhibitory
Epinephrine	Amine	Excitatory
Nor-epinephrine	Amine	Excitatory
Serotonin	Amine	Excitatory
Glutamate	Amino Acid	Excitatory
Glycine	Amino Acid	Mainly inhibitory
GABA	Amino Acid	Inhibitory

Table 1: *Common neurotransmitters in the brain*. Neurotransmitters belong to one of three main groups: amine, amino acid or acetylcholine. Within this distribution, neurotransmitters can be excitatory, inhibitory, or both to some extent.

Glial cells, derived from the Greek word *glia* meaning glue, are also a very diverse cell type, ranging from Müller cells found in the retina, to astrocytes located in regions throughout the brain. Some cell types are isolated to specific regions of the brain and perform specialized functions, while others are more broadly distributed and perform a wide variety of tasks. Of all glial cells, there are only three main types: astrocytes, oligodendrocytes and microglia. Astrocytes are star-shaped cells that are found in nearly all brain regions. Oligodendrocytes are the oblong, heavily myelin-producing cells that are found surrounding axons in the CNS. Microglia are macrophage cells that function as the brain's immune cells. Astrocytes and oligodendrocytes originate from neural stem cells, whereas microglia originate from the immune system.
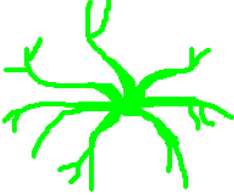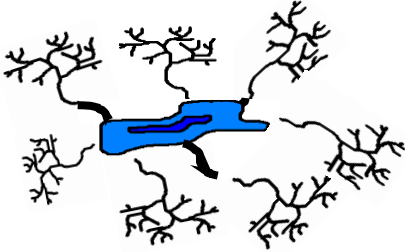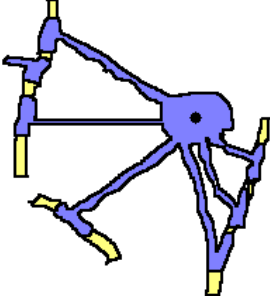
Glial Cell Type	Main Function	Sketch
Astrocytes	Biochemical support	
Microglia	Immune system in brain	
Oligodendrocytes	Provide myelin sheath for axons in CNS	

Table 2: *The major types of glia*. Astrocytes, oligodendrocytes and microglia are the three main types of glial cells found in the CNS. Each serves unique and important roles, helping to maintain normal functioning of neurons and the CNS in general.

Glial cells were initially believed to play only supportive roles in the CNS, particularly for structural support. Research over the last 25 years has shown that glial cells play an increasingly recognized and significant role in the functioning of a normal, healthy CNS. Astrocytes serve a wide variety of roles in the brain. Roles which directly help to maintain neurons include:

- *Provision of needed nutrients* like lactate (metabolic support)

- *Maintenance of physical structure* in the brain (structural support)

Astrocytes also have roles that do not directly support neurons, but are necessary for normal brain function. These roles include:

- *Maintenance of tight junctions at the blood-brain barrier* via release of soluble molecules [74]

- *Control of cerebral blood flow* in combination with neurons [74, 80, 134, 146]

- *Regulation of ion concentration in the extracellular space*. Neurons that are actively firing release potassium into the surrounding environment. Astrocytes have high expression of potassium channels which are responsible for clearing this possible excess in potassium from the extracellular space, particularly at the synaptic cleft. This process is necessary to prevent excess potassium in the extracellular space and subsequent abnormal depolarization (which has been shown to seizures).

- *Promotion of oligodendrocytes myelination*. Extracellular levels of ATP increase due to neuronal electrical activity. In response to this, astrocytes secrete cytokine leukemia inhibitory factor, which in turn promotes myelineation by oligodendrocytes.

- *Regeneration*: Astrocytes fill the void left by injured cells (a glial scar), either helping to repair the damage or replacing cells that cannot regenerate (neurons) [134].

- *Uptake and release of neurotransmitters:* Astrocytes express ATP, glutamate and GABA transporters for neurotransmitters at their plasma membrane. Recent studies have also shown that they release ATP and glutamate in response to calcium waves, which can alter the amount of neurotransmitter present in the synaptic cleft and subsequently the functioning of the synapse [55].

- *Modulation of synaptic connectivity and transmission:* In the CNS, synapses are surrounded by astrocytes, which provide both structural and functional support into the functioning of the synapse. Many of these roles have already been discussed above. This close interaction between the pre- and post-synaptic neurons, as well as the astrocytes, is known as the *tripartite synapse*. Astrocytes have also been shown to have an influence on synaptic connectivity, including synapse formation, functionality, plasticity and eventual elimination [49, 153].
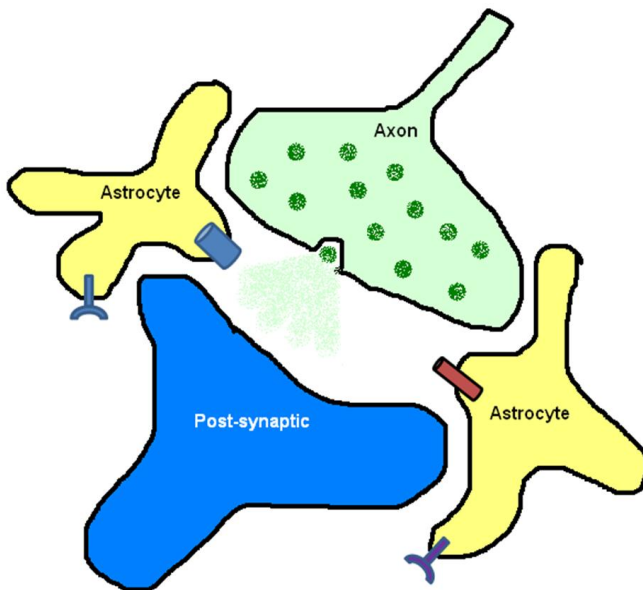
Figure 5: *The Tripartite Synapse Model.* Synapses are ensheathed by astrocytes, which serve pertinent roles in modulating neurotransmitter activity and maintaining normal ionic and pH levels

The brain is an isolated system, relatively speaking, since a healthy,

functioning blood-brain barrier (BBB) prevents the passage of many molecules and substances that would otherwise be toxic or harmful to neurons and other neural cell types. This separation implies that the brain is an "immune privileged" organ; that is, the brain must maintain its own immune system independent of the rest of the body's immune system. Pathogens, infectious agents or toxic compounds that do traverse the BBB must be quickly and efficiently removed from the brain to decrease the inflammation and prevent damage to neurons. Neurons and other cells can also be injured by physical injury or die of natural causes, and need to be removed from the brain to maintain structural homeostasis. Microglia fill this necessary role of resident macrophages, protecting against invading pathogens that are capable of crossing the BBB, as well as clearing unwanted debris.

Although this is such an important role for normal brain functioning, microglia only compose about 20% of all glial cells in the brain. Of mesenchymal origin, microglia are spread relatively uniformly under healthy conditions, and express a phenotype known as 'resting or ramified microglia' [79]. Microglia move constantly within non-overlapping spaces, scavenging for debris and dead or injured cells. Microglia engulf debris via site-directed phagocytosis.

They are also apt sensors of neuronal stress [8], expressing receptors and molecules capable of participating in a large variety of signaling pathways, communicating with neurons via neurotransmitter receptors, with other macroglial cells like astrocytes, and with macrophages and effector molecules of the immune system such as cytokines. When a contagion, lesion or other CNS dysfunction is detected, microglia undergo a transformation from resting to active microglia.

Activated microglia are capable of releasing a variety of molecules at high concentration into the surrounding environment. These molecules can be either beneficial to the nearby cells, aiding in their survival, or detrimental, especially if the microglia remain activated for extended periods of time. It is important to note that activated microglia can migrate towards a site of infection and proliferate, possibly increasing the local level of inflammation. Microglia and their related role in neuroinflammation, have been suggested to be key players in the pathogenesis of AD.

Neurochemistry: The importance of lipids and proteins

Important Biomolecules:

Metabolism in the brain is a highly complex process, encompassing basic glucose metabolism for energy usage, to neurotransmitter synthesis by neurons and myelin synthesis by oligodendrocytes. The main source of energy in the brain is glucose; however, under conditions of starvation, ketone bodies produced from fatty acid metabolism can also provide energy for basic cellular processes. Regulation of many biochemical pathways is often tightly controlled, though can easily be affected by changes in plasma glucose concentrations, oxygen levels, and other hormones. Locally-acting molecules, such as cytokines, paracrine and autocrine hormones, and nitrous oxide can also have significant effects on the metabolic functions of neurons and glial cells.

Although many of the metabolic pathways are highly conserved and expressed across various cell types, expression patterns of lipids and proteins often vary depending on cell type. For example, in the adult brain, cholesterol is only synthesized by astrocytes and oligodendrocytes since it is such an energy intensive

process [12]. The basic metabolic expression profile for the brain can be broken down into five parts corresponding to five main types of cells within the CNS: neuron, astrocyte, microglia, oligodendrocyte and endothelial cell. All cell types express the molecules necessary for:

- energy-producing metabolic processes (glycolysis, the citric acid cycle)

- transcription and translation (RNAases, ribosomes, RNA enzymes, ribozymes)

- anabolic and catabolic biochemical processes (lipid and carbohydrate generation and degradation)

The expression of the remaining types of biomolecules and metabolites are dependent on the functional roles of the individual cell types. For example, neurons have relatively higher expression patterns for neurotransmitters, neurotransmitter receptors, axonal and axonal transport proteins, and synaptic proteins when compared to other CNS cell types, and although they do have functional mitochondrial pathways, do obtain a large percentage of their nutrient intake from nearby astrocytes. Astrocytes express neurotransmitters and their corresponding receptors at a significantly lower levels than neurons, but high levels of potassium and calcium channels, ATP and GABA receptors, and produce C-LIF to modulate myelineation by oligodendrocytes. They are also responsible for producing and transporting cholesterol to neurons in the adult brain. Oligodendrocytes have very high expression profiles for lipids, particularly cholesterol and fatty acids found in cell membranes. Microglia express a large variety of cytokines when activated, as well as many receptors to detect possible pathogens or toxins. Endothelial cells express proteins

necessary transport of molecules across the blood-brain barrier and for formation of tight junctions, as well as many others. The following figure pictorially describes how these pathways vary among different cell types, and demonstrates the importance of differences in the expression of lipidomic, proteomic and inflammatory pathways on the interaction between cell types.

Neuron:
- Neurotransmitters
- Synaptic proteins
- Axonal proteins
- Ion channels
- Other proteins
- Lipids (for membrane)

Astrocytes:
- Low level of neurotransmitters
- Ion channels
- Transport/carrier proteins
- Other proteins
- Cholesterol
- Lipids (for membrane)

Metabolic Pathways

Microglia:
- Cytokines
- Other proteins
- Lipids (for membrane)

Oligodendrocytes:
- Myelin (from cholesterol)
- Other proteins
- Lipids (for membrane)

Figure 6: *Expression Patterns of Different Cell Types in the Brain*. Every cell type in the brain is capable of maintaining its own energy-producing pathway (metabolic pathway), though the expression levels of various proteins, channels and lipids varies across cell type, specialized to the main functions of that cell.

Cholesterol:

Cholesterol is an important steroid molecule, having diverse roles throughout the human body. Its molecular formula is $C_{27}H_{46}O$, atomic molecular weight is 386.65 g/mol and is a white crystalline solid at room and body temperature. It is the main sterol produced by mammals. Only a small amount of cholesterol is produced by plants and fungi, while bacteria produce only trivial amounts. The word cholesterol is derived from the Greek words *chole-* (bile) and *steros* (solid); the suffix

–*ol* is added to recognize that cholesterol is effectively an alcohol (hydroxyl group at the 3' carbon). Cholesterol was first identified in gallstones in 1769 by Francois Poulletier de la Salle, and was later named *cholesterine* by Eugene Chevrul in 1815. The following figure shows the chemical structure

Cholesterol is the main precursor for many very common hormones, including the sex hormones (progesterone, estrogen and testosterone), cortisol and other corticosteroids, and aldosterone produced by the adrenal gland. Cholesterol is also the precursor for molecules such as beta-carotene, needed for vision; geranylgeranylpyrophosphate and farnesyl-PP, needed for memory and learning; and bile, which is produced by the liver and needed to solubilize fats in the intestine and aid in absorption of fat-soluble vitamins (A, D, E and K). Cholesterol is a required precursor for the synthesis of vitamin D and a necessary component of cellular membranes.

Within membranes, cholesterol modulates membrane fluidity in a temperature-dependent manner. Increased cholesterol is believed to decrease membrane fluidity, while decreased cholesterol increases fluidity. This is due partially to the fact that cholesterol is a lipophilic compound; polar head groups in the cellular membrane interact with the hydrophilic hydroxyl group of cholesterol, while the remainder of the cholesterol molecule interacts with the hydrophobic fatty acid tails of membranes. Increased cholesterol levels in cellular membranes have also been shown to decrease membrane permeability to sodium ions and protons, helping to provide an effective ionic barrier for the cell.

Cholesterol has other functions within the cell. At the cell membrane, cholesterol plays several roles: in intracellular transport as a required molecule for the formation of clathrin-coated pits and caveolae in endocytosis; in the formation of lipid rafts important in cellular signaling; and in the myelin sheath as an efficient insulator.

The predominant sites of synthesis are the liver, the intestines and the brain. Cholesterol synthesized by the liver or intestines is only available to cells and organs outside of the CNS; the brain is responsible for synthesizing all of its cholesterol in-house. In the adult brain, only astrocytes are responsible for synthesizing cholesterol [12] since the process is highly energy-intensive. Synthesis proceeds through a 28 step process from HmgCoA to cholesterol. The rate-limiting step in cholesterol synthesis is the conversion of HmgCoA to mevalonate; this has been capitalized on via the development of statins, which inhibit the action of HmgCoA reductase, the enzyme responsible for this conversion. Cholesterol is also an inhibitor of its own synthesis (end-product inhibition); high levels of cholesterol lead to an increased degradation rate of HmgCoA reductase, and subsequently fewer molecules traverse the mevalonate pathway. In essence, this creates a negative feedback loop between cholesterol and HmgCoA reductase.

Cholesterol levels are tightly regulated in the body by the SREBP (sterol-regulatory element binding protein) protein and the end-product inhibition previously discussed. The SREBP pathway is important for up-regulating genes in response to decreased intracellular cholesterol levels, working together with the SCAP (SREBP-cleavage activating protein) protein and Insig-1 to achieve this. In addition to cholesterol end-product inhibition, cholesterol synthesis levels can be reduced when HmgCoA reductase is phosphorylated by AMP-activated kinases, inhibiting the activity of HmgCoA. AMP levels are high when ATP levels are low, thus, if there is mitochondrial dysfunction or a decrease in ATP levels, cholesterol synthesis stops, overriding the SREBP pathway.

Acetyl
CoA

↓

Hmg
CoA

↓

Mevalonate

↓

Isopentenyl PP ⟶ Isoprenoids

↓

Farnesyl PP ⟶ Dolichol
Heme
Ubiquinone
Vitamins A, E, K
Lipid-anchored proteins

↓

Squalene

↓

Cholesterol ⟶ Vitamin D
Bile Acids
Steroid hormones
Cholesterol esters
Modified proteins
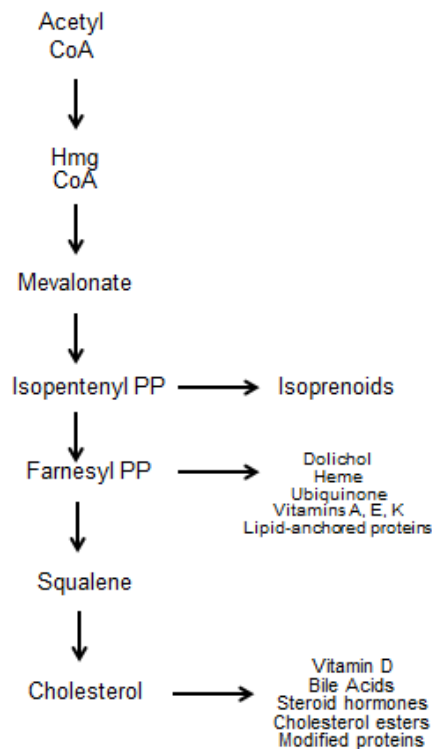
Figure 7: *Cholesterol Synthesis Pathway*. Simplified version of the cholesterol synthesis pathway with important by-products included.

Choline & Acetylcholine:

Both choline and acetylcholine are important biomolecules in the brain. Choline is an essential nutrient (intake required/body does not synthesize) that plays several key roles within the body. It is one of the required precursors for acetylcholine production; it is important in maintaining the structural integrity of cell membranes and in cellular signaling pathways; and it serves as an important molecule in methyl group transfers via its metabolite, betaine, in the SAM-e pathway. Diets low in choline are known to cause fatty liver, kidney necrosis, renal impairment, infertility, growth impairment, bone abnormalities and hypertension. Choline deficiency can be identified by measuring liver enzyme ALT activity (increased levels indicate deficiency). Other methyl group transfer molecules (B6, B12 and folic acid), as well as choline, are known to reduce homocysteine levels, and thus decrease the risk of heart disease. Sources of choline include eggs, liver and peanuts. Some vegetables also contain choline, but in significantly smaller amounts.

Choline may also play an important role in DNA methylation, thus partially controlling the expression pattern of genes (epigenetics). Phosphatidylcholine, a choline metabolite, is also an important precursor molecule for the arachidonate pathway (responsible for producing prostaglandins, pro-inflammatory molecules that act locally), as well as interacting with fatty acids to produce phospholipids at the membrane. Changes in choline levels affect brain function, muscle function, liver and kidney function, and cardiovascular health in a direct manner. Thus, there is a relationship between inflammation, brain health and cardiovascular health that should be elucidated further.

One of the most important role that choline plays within the nervous system is in the production of acetylcholine. Acetylcholine (ACh) has several functions both in the CNS and the PNS. In the PNS, acetylcholine activates muscles and participates in the autonomic nervous system as a neurotransmitter. In the CNS, acetylcholine is the major neurotransmitter in the cholinergic system and is produced in neurons by choline acetyltransferase, an enzyme that combines Acetyl CoA and choline. It is degraded by acetylcholinesterase, an enzyme that has been a key target in AD and is currently one of the few pharmacological treatments available (acetylcholinesterase inhibitor).

ACh has important roles in plasticity, arousal, reward, sensory perception upon waking, attention, and in learning and short-term memory. Experimental evidence has demonstrated that ACh enhances the amplitude of synaptic potentials following long-term potentiation (LTP). Acetylcholine is also responsible for either increasing neuronal excitability or causing inhibition. It is believed that layer-specific differences in the effects of ACh on neurons may help improve the signal-to-noise ratio of cortical processing. This specificity of behavior is also related to the fact that there are two types of acetylcholine receptor: nicotinic and muscarinic. Nicotinic ACh receptors are ionotropic receptors stimulated by nicotine and acetylcholine. These receptors are permeable to sodium, potassium and chloride, and are found in the CNS, the end plates of muscles and in ganglia participating in the autonomic system. Conversely, muscarinic ACh receptors are metabotropic, act on neurons over longer periods of time, and are stimulated by muscarine and acetylcholine. These

receptors are found in the CNS, PNS, upper gastrointestinal tract, lungs, heart and sweat glands.

LRP-1:

The low-density lipoprotein receptor-related protein 1 (LRP-1) is a key receptor within the brain responsible for transporting a variety of molecules. LRP-1 receptors are found both on endothelial cells at the blood-brain barrier, as well as on neurons. At the BBB, LRP-1 transports both free and ApoE-bound beta amyloid basolaterally (from the brain to the blood). LRP-1 receptors are also found on neurons to allow cholesterol to be transported from astrocytes to neurons in the adult brain. Inflammatory cytokines, such as IL-1, are known to up-regulate the expression of LRP-1.

ApoE:

Lipoproteins serve the important role of transporting lipid-soluble molecules, such as cholesterol, through an aqueous environment to their target destination. Brain apolipoproteins, in particular apoE, coordinate the mobilization and re-distribution of cholesterol and phospholipids for the repair, growth and maintenance of myelin and neuronal membranes [28, 110-111]. ApoE is particularly important for synaptic remodeling, and is expressed in astrocytes, cells in the blood vessels and choroid plexus, neural stem cells and injured neurons [71]. Astrocytes have been shown to release cholesterol bound to one of the three different apoE isoforms: ε2, ε3 or ε4. The affinity of the apoE isoforms as a lipid acceptor was: apoE2 > apoE3 = apoE4 in astrocytes, and apoE2 > apoE3 > apoE4 in neurons [99]. The pro-inflammatory cytokine IL-1 is known to upregulate the expression of ApoE.

Neuroinflammation:

The brain's immune system:

For many years, the brain was believed to have its own separate immune system provided by resident macrophages (microglia) that are capable of responding to invading agents and toxins by phagocytosis and secretion of pro-inflammatory cytokines, in combination with protection from pathogens and toxins in the blood by the blood-brain barrier. Under cases of extreme infection, such as meningitis, macrophages could be recruited from the blood to help combat the invading agent, but must be quickly subdued to prevent damage to neurons that are exquisitely sensitive to the effects of cytokines and other pro-inflammatory molecules.

Recent research has shown that this model is not the full picture, and the systemic immune system in fact does interact with the brain and is capable of controlling behavior, neuroendocrine function, synaptic plasticity and neurotransmitter metabolism [24]. Pro-inflammatory cytokines, such as IL-1, that are produced in the periphery are capable of entering the CNS and interacting with the network of cytokines and microglia in the brain to effect these changes. This can lead to significant changes in behavior, including insomnia, anxiety, depression, anorexia, psychomotor retardation and cognitive dysfunction [24]. Individuals with HPA-axis hyper-reactivity (over-reactive stress response) in combination with subclinical depression are at increased risk for developing such cytokine-induced depressive symptoms [23, 117].

Although they are capable of interacting with the brain, cytokines are not able to directly pass through a functional blood-brain barrier. Several routes of passage

28

have been identified, including: active transport by brain endothelial cells; transmission via the vagus nerve; passage through 'leaky' areas of the blood-brain barrier, such as the choroid plexus, or through dysfunctional blood-brain barrier; via activated monocytes; and by activation of brain endothelial cells stimulating release of prostaglandin G2 and nitric oxide [24, 116].   Passage of cytokines through one or more of these routes leads to disruption of the innate cytokine network in the brain, a network of neurons, microglia and astrocytes capable of expressing cytokines and cytokine receptors, and amplifying signals within the cytokine network [62]. Pro-inflammatory cytokines that are normally expressed in the brain include IL-1, IL-1 and TNFα. The signaling cascade modulated by these cytokines can be disrupted by peripheral cytokines, leading to activation of the HPA axis, release of corticotrophin-releasing hormone, and alteration of serotonin, norepinephrine and dopamine usage [100].

Under normal conditions (ie. no peripheral inflammation), the levels of acetylcholine play important roles in maintaining the balance of pro-inflammatory cytokines. Acetylcholine achieves this by binding to nicotinic acetylcholine receptors on microglia, activating a signaling cascade that inhibits the release of pro-inflammatory cytokines. This pathway has no effect on anti-inflammatory cytokines, such as IL-10.

The inflammatory pathway within the brain walks a very thin line between being helpful and being harmful. Over short time periods, pro-inflammatory cytokines can help to remove an invading pathogen or toxin, while producing minimal damage to neurons or glial cells. Over longer periods of time, however, pro-

inflammatory cytokines lead to decreased protein synthesis, decreased cellular energy levels due to decreased uptake and availability of glucose for non-immunological cells, changes in protein and lipid expression levels, and changes in neurotransmitter levels. It is this imbalance in inflammation which may play a key role in AD.

Mechanisms of action:

Interleukin-1 (IL-1) is one of the predominant cytokines produced by brain microglia. The roles of IL-1 in the brain are diverse and cause different effects in different brain regions. The highest density of IL-1 receptors is found on hippocampal cells in the dentate gyrus [11]. IL-1 levels have been shown to increase in response to stress, sleep deprivation, and long-term potentiation via NMDA receptors. Prostaglandin E2, Aβ and glutamate are also known to increase the expression levels of IL-1. IL-4 and interferon-γ are known to decrease levels of IL-1. It is interesting to note that IL-1 enhances neuronal acetylcholinesterase activity, thus increasing the rate at which acetylcholine is degraded (decreasing the level of ACh), though it's production is inhibited by acetylcholine. This in effect is a common network topology with a dual negative feedback loop; the overall result is a switching behavior reminiscent of a clock used in digital logic.

IL-1 is known to have a relatively strong effect on neurotransmitter turnover rates: in the hypothalamus and hippocampus, noradrenaline turnover rates are increased; in the prefrontal cortex, dopamine utilization is increased; and in the hippocampus and prefrontal cortex, serotonin turnover is increased. These changes in neurotransmitter turnover rates may have significant effects on the functions of each of these brain regions. IL-1 is also known to modulate glucocorticoid levels by

decreasing the activation threshold for the hypothalamic-pituitary-adrenal axis (HPA); inhibit the hypothalamic-gonadal axis; increase the production of aldosterone; and cause hypoglycemia by lowering the glucose set point throughout the body.

Within the hippocampus, IL-1 has many of the same effects described above (increased acetylcholinesterase activity in neurons, same activating and inhibiting compounds). IL-1 also causes increased serotonin turnover with an accumulation of tryptophan (the precursor amino acid for serotonin). The amount of glucose available to neurons and other cell types is decreased, limiting energy production as well as production of proteins and lipids. Increased levels of IL-1 that have been sustained for a short duration are known to stimulate the release of prostaglandins and reactive oxygen species into the local environment, enhancing seizure activity and increasing the rate of entry of calcium into cells via NMDA receptors.

Alzheimer's disease Pathology:

Alzheimer's disease (AD) is the most common form of dementia, affecting more than 4.5 million individuals in the US alone [65]. This number is expected to increase almost 3-fold by 2050 as the number of people over 65 (the most affected group of individuals) surpasses 12 million. The cost of care for individuals with AD is staggering- over $140 billion annually, which is expected to rise in correlation with the number of affected individuals. The exact cause of AD is uncertain, though mutations in APP (**a**myloid **p**recursor **p**rotein) and presenilin protein have been linked to early-onset of the disease. Age, the presence of the apolipoprotein ε4 allele, cerebrovascular disease, cardiovascular disease (including atherosclerosis) and high

plasma cholesterol have all been linked to an increased risk of AD later in life. The

following table summarizes the known risk factors for AD.

Risk Factor	Cause	Possible Effects
ApoE4 allele	*Genetic*	Less able to transport cholesterol to neurons, possibly less able to transport Aβ out of brain
APP/PresenilinI mutation	*Genetic*	Increased cleavage of Aβ
APP overexpression	*Genetic; Down syndrome*	Increased APP, suggested increase in Aβ cleavage
Brain infection	*Inflammation*	?
Cerebrovascular disease	*Genetic, inflammation and/or lifestyle*	Increased inflammation, decreased glucose and oxygen transport
Diabetes/insulin resistance	*Genetic, lifestyle and/or inflammation*	Increased inflammation of body system; inadequate transfer of glucose
Dysregulation in steroid periodicity	*Stress/lifestyle*	Alterations in inflammation, neuronal cell death
Decreased levels of neurosteroids, estrogen	*Genetic, stress/lifestyle*	Increased inflammation
Chronically increased cortisol levels	*Stress/lifestyle*	Increased inflammation, alterations in metabolism
Decreased LRP expression	*Genetic, aging*	Decreased Aβ clearance, cholesterol uptake
Transferrin mutation	*Genetic*	Decreased ability to synthesize cholesterol, myelin
Decreased hippocampal volume	*Stress, psychosocial events, injury*	Reduced neuron number increases effects of other alterations
Traumatic brain injury	*Inflammation*	Increased inflammation
Alterations in cholesterol	*Genetic, inflammation and/or lifestyle*	Alterations in Aβ cleavage rate, cellular metabolism; interaction with inflammation

Table 3: *Risk Factors for AD*. AD has several well-known risk factors, including the
ApoE4 allele, cerebrovascular disease, and mutations in APP or presenilin I. A combination
of several of these factors is most likely needed to precipitate onset of AD.

Regardless of the disease trigger, the resultant pathological characteristics are

similar and involve the buildup of amyloid protein in the brain parenchyma and

deposition in cerebral blood vessels (as cerebral amyloid angiopathy, CAA), as well

as the presence of neurofibrillary tangles within affected neurons. Loss of neurons

and synapses in the hippocampus, neocortex and other subcortical regions has been

observed [113]. Activation of microglia (resident CNS macrophages) and

neuroinflammation are also observed, as well as alterations in BBB permeability [66, 121, 156-159]. The combination of these cellular and subcellular changes leads to the symptoms most commonly associated with AD, including: gradual memory loss, personality changes, depression, inability to communicate and loss of voluntary muscle movements [94]. Even with the significant advances that have been made in AD research, there is still no clear understanding of what the causal relationship is between these different symptoms, that is, what is the network connection created between different agents.

AD: A gimesh of pathogenesis theories:

The discovery of parenchymal amyloid plaques and NFTs by Alois Alzheimer in 1906 revolutionized the way that researchers looked at AD, providing the basis where many researchers begin their study. As the wealth of knowledge on AD has grown significantly in the last 20 years, several different theories on the origins and pathogenesis of AD have emerged. Biochemical studies in the 1980s lead to the discovery that the core protein in plaque deposits was beta amyloid (Aβ), leading many researchers to believe that the buildup of Aβ as plaques was the main causative factor in AD. Further studies revealed that cleavage of the amyloid precursor protein (APP) by β-secretase and subsequently by γ-secretase leads to the 39-42 amino acid, amyloidogenic form of Aβ. This monomeric form of beta amyloid often aggregates and forms oligomers, fibrils and eventually plaques. Oligomers range from 2-100 Aβ peptides (1-3 nm in height by 5-10 nm in length), while fibrils are significantly longer and can achieve lengths ~ 200 nm [17]. Oligomeric forms of beta amyloid (<5 nm) have been found to be most neurotoxic [31].

Amyloid Cascade Hypothesis:

Early experimental data points in AD research led to the development of the first major hypothesis for AD pathogenesis: the *amyloid cascade hypothesis*. This hypothesis, developed by Dennis Selkoe [130], states that the high extracellular levels of soluble Aβ oligomers are toxic to neurons, leading to synapse loss, activation of microglia and an inflammatory state. This hypothesis is unable to account for the fact that there are individuals with high brain Aβ levels that do not have symptoms of AD or even cognitive decline. However, since most assays for beta amyloid do not measure oligomeric beta amyloid, there is the chance that plaque load may be increased without having a concurrent increase in the level of Aβ oligomers. This hypothesis does a good job describing the pathological characteristics of AD, but does not describe why there is an initial increase in Aβ, thus, still eluding our understanding of what actually triggers AD. In the familiar forms of AD, the increase in Aβ is due to a mutation in APP or PS1, however, this mutation is not seen in late-onset AD.

Figure 8: *Amyloid Cascade Hypothesis.* Simplified version of the amyloid cascade hypothesis.

Neurotransmitter Hypothesis:

Another early hypothesis for the cause of AD is the cholinergic hypothesis. Biochemical studies in the late 1960s and early 1970s revealed decreased levels of choline acetyltransferase, the enzyme responsible for the synthesis of acetylcholine, as well as reduced levels of acetylcholine release, decreased choline uptake, and loss of cholinergic neurons in the basal forebrain and cholinergic transmission in the cerebral cortex [53]. These alterations were believed to lead to the cognitive decline in AD since they were present in the early stages of the disease.

Neurotransmitter dysregulation is not uniform across all classes of neurotransmitters, nor is it constant over time. Initially, only the cholinergic pathway, and to a lesser extent, the serotonergic and noradrenergic pathways are affected. GABA, dopamine and somatostatin remain unaltered in early disease stages [53]. Changes in the serotonergic pathway are thought to be more related to the behavioral changes seen in AD, whereas cholinergic changes are believed to be more related to cognitive decline. As AD progresses, the initially affected pathways are affected more, while the GABA and somatostatin pathway begin to be affected [123-124].

Given these recognized changes in neurotransmitter levels, particularly acetylcholine levels, cholinesterase inhibitors (Aricept, Exelon and Reminyl) are currently one of the only drugs available to treat AD. These drugs work by inhibiting the breakdown of acetylcholine by acetylcholinesterase, thus increasing the level of acetylcholine in the brain. The only other drug available to treat AD (Ebixa) blocks the release of glutamate and is supposed to prevent further damage to neuronal cells from glutamate excitotoxicity. Although these drugs are capable of lessening some of

the symptoms of AD, they are not able to stop or prevent AD pathogenesis. There are also some serious side effects related to their usage, often related to over-activity of the cholinergic pathway in the peripheral nervous system. Again, although there are some benefits to increasing the acetylcholine levels pharmaceutically, the cholinergic/neurotransmitter hypothesis fails to describe some of the observed pathology, such as increased $A\beta$ levels and decreased brain cholesterol.

Inflammation Hypothesis:

Neuroinflammation is a key characteristic of AD that leads to increased levels of cytokines, chemokines, complement proteins and free radicals, all of which are detrimental to the health of neurons [102-103]. Several groups of researchers have proposed that inflammation plays a significant, if not also a causative, role in AD pathogenesis [4-5, 34, 67, 82, 98, 127-128, 156, 161]. This hypothesis has been supported by several different studies. A relatively recent study by Cagnin et al used positron emission tomography (PET) and volumetric magnetic resonance imaging (MRI) in patients with mild to moderate cognitive dementia and found that microglial activation occurred at very early stages in the AD process [20]. Epidemiological studies have also shown that there is a reduction in the risk of AD if non-steroidal anti-inflammatory medication is taken [140-141, 151]. Lim et al provided data that demonstrated that treatment of AD transgenics with ibuprofen reduced the levels of interleukin-1β and glial fibrillary acidic protein, while simultaneously decreasing the total number and area of amyloid plaques [89]. It has also been shown that cognitive decline and suppression of long-term potentiation occur before observable plaques develop in the same models that show microglial and astrocyte activation.

Much of this data suggests that inflammation occurs early in AD pathogenesis. However, several questions still remain; in particular, even though inflammation occurs early in the AD process, it is not clear whether inflammation is the cause of neurodegeneration, what exactly triggers the inflammatory response, and whether it just helps to promote further neurodegeneration that has been started by a separate process. There is also insufficient understanding about how amyloid plaque deposits in cerebral blood vessels that disrupt the blood-brain barrier may influence the initiation of the inflammatory process.

LRP/RAGE Hypothesis:

More recent studies have started to focus on the interplay between cerebral amyloid angiopathy (CAA) and the influx/efflux of Aβ at the blood-brain barrier (BBB). Zlokovic et al have proposed a hypothesis that an increase in the blood-to-brain transport of Aβ, combined with a decrease in the brain-to-blood efflux of Aβ, leads to Aβ accumulation in the extracellular space, as well as accumulation in the basement membrane of vessels as CAA [164-165]. This accumulation leads to the activation of microglia, amyloid fibril formation, reduction of cerebral blood flow, localized ischemia, degeneration of the endothelial cell wall leading to accumulation of metabolic waste, changes in pH, electrolyte imbalance, and eventually, neuronal cell death when the capillary unit collapses [165]. The changes in BBB transport are believed to be due to two receptors: RAGE (the **r**eceptor for **a**dvanced **g**lycation **e**nd-products; responsible for Aβ influx) and LRP-1 (the low-density lipoprotein receptor-related protein; responsible for Aβ efflux).

Miller et al recently conducted a study using confocal microscopy of immunostained hippocampi to demonstrate that RAGE receptor levels on endothelial cells at the BBB are in AD patients when compared to controls, and that this increase is approximately a linear function of the severity of AD pathology [101]. Previous studies have confirmed this observation, noting the strong correlation between RAGE immunoreactivity in the microvasculature and low immunoreactivity in neurons [36-39, 43, 77].

LRP-1 expression levels have also been shown to be altered in AD. Donahue et al clearly demonstrated a decrease in LRP-1 expression levels in the cerebral microvasculature in AD hippocampi when compared to controls [43]. This data correlates well with Zlokovic's hypothesis, however, further studies are needed to ascertain whether the changes in LRP-1/RAGE expression levels are due to changes other than just aging (such as blood vessel abnormalities or atherosclerosis), whether cerebral amyloid deposition occurs before expression changes take place, whether there is a correlation between changing receptor expression levels and cholesterol, and whether decreased LRP-1 receptor levels affects ApoE binding and delivery of cholesterol to neurons and other cells.

Cerebrovascular Hypothesis:

One of the more recent areas of focus in AD research is studying the connection between lipid metabolism, cerebrovascular dysfunction and onset of AD [95]. Epidemiological studies have shown that several cardiovascular risk factors overlap with AD risk factors, including diabetes, hypertension, high cholesterol and having the apoE4 allele [159]. Ischemic white matter lesions and severe

38

atherosclerosis of the circle of Willis that lead to reduced cerebral blood flow are also often found in individuals with AD [122, 133]. Hemorheologic abnormalities have also been observed with a relatively high frequency in individuals with AD, including an increase in whole blood viscosity and significantly higher markings on a severity index for vasculopathy [132]. It is interesting to note that the apoE4 allele is one of the genetic links between atherosclerosis and AD [51]. An initial study into the relationship between AD pathology and hypercholesterolemia found that diet-induced high cholesterol led to an increase in the Aβ plaque load in the CNS, as well as an increase in the density and size of plaque deposits [118-119], however no one has crossed an AD transgenic mouse with a mouse strain prone to atherosclerosis. All of this data seems to indicate that the large overlap between AD risk factors and atherosclerosis risk factors implicates the need for further study to determine if there is an underlying similarity in pathogenesis.

Cholesterol Hypothesis:

Lipid metabolism, particularly processing of cholesterol, has come to the forefront of AD research in the past decade. As mentioned previously, cholesterol has important roles in the maintenance and survival of neurons in the CNS. Recent studies have demonstrated that cholesterol levels help to regulate the generation and clearance of Aβ [63, 113]. The belief here is that an increase in cholesterol, which is seen in the blood plasma of many individuals with AD, causes an increase in the production and deposition of amyloid beta peptides [72, 113]. However, there is contradictory evidence on this matter.

A recent study by Liu et al demonstrated that increasing the level of APP, particularly the γ-secretase cleavage product AICD, led to a decrease in LRP-1 expression levels, an increase in apoE levels and a decrease in cholesterol [90]. Further studies have shown that decreased brain levels of cholesterol are found in both apoE4 knock-in mice and in AD brains [64, 86-87]. The Framingham study which tracked 1894 individuals over the course of 16-18 years found that low or normal levels of cholesterol were correlated with lower cognitive performance levels [48]. This apparent contradiction between different studies may be due in part to the fact that under normal circumstances, the BBB prevents the transport of lipoprotein-bound cholesterol from leaving circulation and entering the brain [12]. However, once plaques form in the basement membrane of cerebral blood vessels, the integrity and protective function of the BBB may dissipate. Likewise, the presence of this contradiction highly recommends the need for further study and understanding of the interplay between changes in brain cholesterol levels and AD.

One treatment method that is currently being studied by researchers is the use of cholesterol-lowering drugs (statins) to prevent and possible reverse damage done by Aβ buildup and deposition. Several studies on the effects of cholesterol lowering drugs (statins) have been completed in the last few years. Fassbender et al studied the effect of simvastatin and lovastatin on primary hippocampal neurons and mixed cortical neurons and found that this led to decreased levels of Aβ40 and Aβ42 [51]. They also observed similar results using a guinea pig model. Refolo et al expanded on this by studying the effects of cholesterol-lowering drug BM15.766 on transgenic

mice expressing an AD phenotype and saw that plasma cholesterol levels, brain Aβ peptides and Aβ load were all decreased [119].

These and other studies are serving as the basis for the current movement to treat AD with statins. Nevertheless, one of the most interesting studies to recently come out clearly demonstrates that reducing the levels of brain cholesterol may not prevent AD pathogenesis, as is suggested by previous studies. In this study, Halford and Russell crossed transgenic AD mice with cholesterol 24-hydroxylase knockout mice, creating a mutant strain that was prone to AD, as well as had a 50% reduction in brain sterol synthesis to find that Aβ plaque deposition did not vary statistically between the mutant and AD control strains [63]. Another recent study by Kölsch et al measured the levels of cholesterol and cholesterol precursors in the CSF and plasma and found that these levels were significantly decreased in AD patients when compared to control patients, suggesting that *de novo* synthesis of cholesterol by astrocytes within the CNS might be reduced [81].

More recent studies of the effects of statin treatment on AD pathology have shown a different picture. Long-term treatment with atorvastatin in aged beagles did not lead to a change in Aβ levels [105]. In a similar experiment with beagles, long-term atorvastatin treatment did not change Aβ levels, although protein oxidation and lipo-peroxidation were decreased [9]. Long-term statin treatment has also been shown to decrease CoenzymeQ10 levels significantly, leading to impairment in energy metabolism in the heart, liver and skeletal muscles [13]. Additionally, lipophilic statins, such as simvastatin, have been shown to increase oxidative stress via nitric oxide and other reactive oxygen species [109]. Several recent clinical

studies have shown that statins did not improve cognitive function in the elderly or had only a very weak improvement on mild cognitive impairment [10, 68, 136]. Recent epidemiological studies have also had similar outcomes. The PROSPER study showed that treatment with pravastatin did not improve cognitive function; similar studies with atorvastatin and simvastatin showed similar results (no significant improvement with statin treatment; 52, 152, 155]. Only one recent study has shown that long-term treatment with atorvastatin led to improvement in cognitive functioning [137], though the constraints that were placed on the analysis were somewhat biased and may have altered results.

Statin treatment is also known to have several significant side effects, including decreased levels of isoprenylation, decreased pro-inflammatory cytokines (which could be good or bad depending on the condition of the body), and decreased ability to learn and remember in long-term treatment [18]. Levels of farnesyl pyrophosphate (FPP) and geranylgeranyl pyrophosphate (GGPP) are also decreased in statin treatment. Both FPP and GGPP are necessary for correct subcellular localization and trafficking of intracellular proteins. FPP is also the precursor for dolichol, a major membrane-anchoring molecule, and coenzymeQ10, which is necessary for energy metabolism. Given all of these results, caution should be used when treating AD patients with statins and further studies are needed to determine the efficacy and safety of using statins.

Drug/Dosage/ Sample	Length of Treatment	Results	Reference
Simvastatin, 40 mg/day, humans	12 weeks	No change in Aβ, decreased 24SHChol	Serrano-Pozo et al 2010
Simvastatin, 40 mg/day, humans	4 months	No changes in CSF levels of Aβ or τ	Carlsson et al 2008
Simvastatin, 40 mg/day, humans	14 weeks	Decreased phosphor-τ in CSF, no changes in sAPP,	Riekse et al 2006

		Aβ	
Simvastatin, 20 mg/day, humans	1 year	No change in CSF or plasma Aβ	Hoglund et al 2005
Simvastatin, 5 μM, human neuroblastoma & primary astrocytes	2 days	No change in APP levels, decreased τ on astrocytes, increased τ on neuroblastoma cells	Dong et al 2009
Simvastatin, 4 μM, primary hippocampal neurons from rats	2-3 days	Decreased Aβ in cell culture medium	Fassbender et al 2001
BM15.766, 250 mg/kg/day, APP/PS1 transgenic mice	5 weeks	Reduced amyloidogenic processing	Refolo et al 2001

Table 4: *Review of statin treatments on markers for AD:* Short review of some of the recent studies that have looked at the effects of statins on markers for AD pathology. The most recent reviews in humans suggest that treatment with simvastatin leads to no changes in AD pathology and would be unbeneficial as a treatment option.

Chronic stress is generally considered a causal factor in a wide variety of diseases, from cancer, to cardiovascular disease, to diabetes and metabolic syndrome. Stress is also known to play a negative role in neurological and psychiatric diseases, worsening symptoms or inducing the appearance of new symptoms. Chronic stress is also believed to be a negative modulator of learning and memory, decreasing the ability of hippocampal neurons to form and maintain long-term potentiation (LTP). Clinical studies of those with AD have shown that affected individuals have increased plasma cortisol levels when compared to controls [3]. Epidemiological studies have expanded on this and shown that individuals who are stressed or are more prone to being stressed have a significantly increased chance of developing mild cognitive impairment (MCI) and AD over non-stressed controls [76, 138-139, 150]. Furthermore, both clinical and animal model studies have shown that glucocorticoids, the main effector molecule of stress in the brain, play a role in the regulation of APP levels in the brain [59, 125, 135, 154].
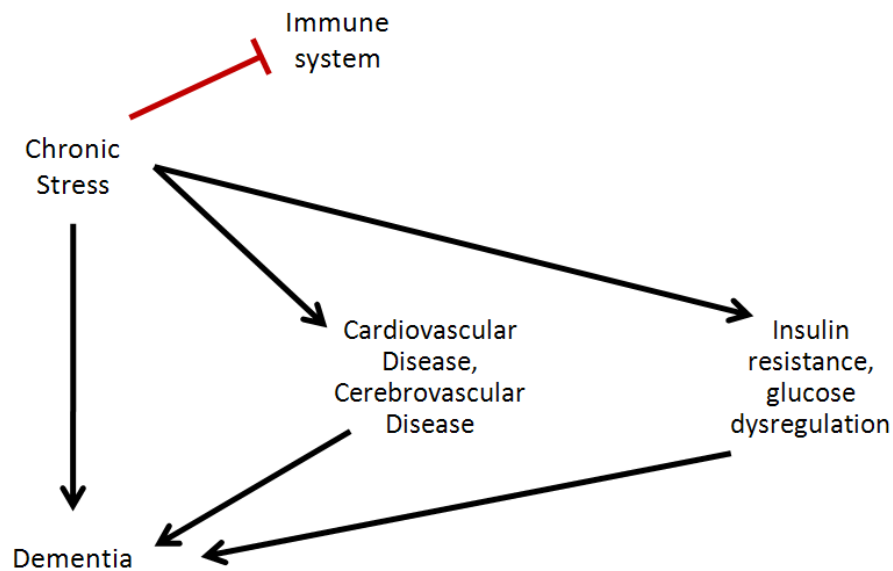
Figure 9: *Role of chronic stress in Dementia and related disease processes:* Chronic stress is known to play a major causal role in cardiovascular disease, cerebrovascular disease, insulin resistance (type II diabetes), and glucose dysregulation. Chronically high levels of cortisol (the main marker for system stress state) lead to the suppression of the immune system, increasing the risk of individuals to acquire an illness. Recent evidence has started to suggest the role of chronic stress in the pathogenesis of AD and other types of dementia.

Steroid hormones have unique and important roles in everyday functioning of the body. Steroids are produced both in relation to circadian rhythms, as well as in response to external cues. Adrenal steroids, produced by the adrenal gland, are secreted in response to an experience, such as fear, stress, aggression or sexual encounter. This includes glucocorticoids such as cortisol. The response of these steroids is often reversible; however, over time and with repeated exposure, adaptive effects resulting from repetitive stress do appear. These adaptive changes include: alterations in synaptic vesicle proteins, high-affinity GABA (γ-amino butyric acid) transport, neurotransmitter-stimulated cyclic AMP formation, and central serotonin and noradrenergic sensitivity [97]. In all cases, activation of the hypothalamic-pituitary-adrenal (HPA) axis occurs, which leads to increased secretion

of glucocorticoids into the blood. Neural, neuroendocrine and neuroendocrine-immunological mechanisms are activated, with cortisol and epinephrine acting as the main mediators.

Under most circumstances, allostasis is advantageous to the organism, since maintaining homeostasis and stability during change is a necessary precursor to survival. Adaptive brain response via allostatic loading, however, comes at a price, since constant or fluctuating levels of cortisol and epinephrine leads to 'wear and tear' and eventual damage to neurons. Allostatic loading can be caused by several different events:

1) Repeated activation by many stressful events;

2) Failing to shut off after the challenge is removed;

3) Or, the inability to be adequately activated, allowing other systems that are normally counter-regulated to become overactive (such as the inflammatory system).

Allostatic loading is necessary for adaptation in the short term for maintaining survival and homeostasis. However, in the long-term, this leads to significant changes and imbalances in the CNS, neuroendocrine and immune systems, affecting plasticity, brain structures, and hormonal functioning. Allostatic loading due to chronic stress is particularly damaging to the hippocampus because it is the only region of the brain that contains glucocorticoid receptors. Chronically high levels of cortisol lead to changes in synaptic vesicle proteins, high-affinity GABA transport, neurotransmitter-stimulated cAMP formation, and sensitivity of serotonergic and noradrenergic pathways (steroid hormone action in the brain book). Neurons also

begin to atrophy, especially those in the CA3 region of the hippocampus. This atrophy may be caused by excitatory amino acids, such as glutamate and can be blocked by NMDA receptor antagonists. This is an interesting paradox: in the short-run, adrenal steroids exert neuronal protection; in the long-run though, neuronal damage occurs if the allostatic response is not properly managed. Though little data is currently available to support this as the main cause of AD, it is well established that stress can play contributory factors to many diseases, and further research is needed to determine what role chronic stress may play in development of AD.

Summary:

This section has discussed the majority of theories about AD pathogenesis, covering everything from the initial theories (cholinergic hypothesis and amyloid cascade hypothesis), to the more recently developed theories (LRP, cholesterol and inflammation hypotheses). Though each theory looks at a specific set of symptoms or changes in protein or lipid expression, no current theory links all of these ideas and observations together, or looks at the role of lifestyle factors like chronic stress, in the development of AD. By bringing each of these perspectives together, the hope is that a new hypothesis that takes into account the role of inflammation, changes in protein expression, changes in neurotransmitter levels, changes in lipids and the role of stress and cerebrovascular disease can be formed that also appropriately maps the timescales of such changes, allowing for a clear understanding of AD pathogenesis and development of effective therapeutic treatments. One of the goals of the systems biology math model developed in this thesis is to bring together all of the information that is known about AD to come up with a more complete theory looking at the

disease from various aspects and attempting to figure out the interconnections between interacting pathways, be they cellular, molecular or regulatory, beginning this process. The following table summarizes the current theories for AD.

Theory	Evidence for:	Evidence Against:
Amyloid Cascade Hypothesis	- High concentrations of Aβ are toxic to neurons & lead to synapse loss - Aβ activates inflammation & reactive astrocytes	- Unable to account for why beta amyloid is increased - Increased beta amyloid is seen in non-pathological controls
Neurotransmitter Hypothesis	- Decreased levels of acetylcholine & serotonin observed - Alterations in enzymes related to acetylcholine processing	- Unable to describe why Aβ is increased and why cholesterol is also dysregulated in the brain - Acetylcholinesterase inhibitors are unable to stop progression of disease
Inflammation Hypothesis	- Microglial activation observed early in AD - NSAIDs help reduce risk of developing AD - Abnormal increase in activated microglia	- Does not explain why Aβ forms plaques in the parenchyma and the walls of cerebral blood vessels - NSAIDS cannot stop progression of AD
LRP Hypothesis	- RAGE expression levels increase with aging - LRP1 expression levels are reduced in both normal aging & in patients with CAA and AD	- Aβ found in the brain is produced by neurons; only minor fractions are thought to be derived from the blood - Increases in RAGE expression levels are not unique to AD
Cerebrovascular Hypothesis	- Overlapping risk factors between AD & cardiovascular disease - Hemorheologic abnormalities seen frequently in AD	- Having these risk factors does not mean an individual will get AD definitively
Cholesterol Hypothesis	- Epidemiological & experimental studies demonstrate that altered cholesterol metabolism occurs in AD - Cholesterol is able to modulate levels of Aβ - Cholesterol is an important molecule within the brain, as well as an important precursor molecule for neurosteroids - Interacts with the inflammatory pathways	- Statin treatment is not efficacious in preventing AD - Having altered cholesterol levels, either in plasma or in the brain, cannot be used as a definitive marker for AD

Table 5: *Review of current hypotheses for AD pathogenesis:* There are a variety of pathogenesis theories that have been developed for AD. Many of these theories look only at one perspective of the disease, failing to recognize that AD is a complex disease affecting a multitude of pathways on various time scales. A unified hypothesis that looks at AD from this aspect is needed to truly understand pathogenesis and to create effective treatments.

Over the last few hundred years, much of biology has been studied using the reductionist method; that is, taking apart the entire system and focusing on one or two components of interest. Reductionism offers several advantages, including ease of studying function of individual proteins or other small molecules and reduction in system complexity to better help control for undesired system changes, there are however, several significant disadvantages. One of the main problems with reductionism is that it has a tendency to oversimplify a complex, interconnected system of network such that the actual network connectivity and interacting nodes may be lost in the process, thus stifling the ability of researchers to fully grasp the overarching impact that specific proteins or molecules may have on a multitude of interacting networks. This mindset, of looking at subsystems in isolation, prevents fully understanding system level interactions.

For many years, the main hindering block in studying data across a wider scale has been the lack of methods and technologies to accurately control for cross-system variables, as well as a minimal number of methods to accurately analyze biological data, which contains a relatively large amount of experimental noise and variation. With the advance of technology, newer methods have become available for studying large amounts of data across a system –level model such as microarrays, ELISAs and optimized Western blotting methods, opening up the avenue for a new form of biology, systems biology.

Systems biology, a branch of science that combines systems-level biology with mathematical biology, aims to study biological organisms from a systems-level

approach. The main goal of systems biology is to develop mathematical models to study various aspects of a single system function (for example, the interaction of molecules that individually have been known to lead to inflammation), or to develop models for disease processes, such as diabetes and cancer. As of yet, very few systems biology models have been applied to neurodegenerative and neurological disorders, perhaps owing to the fact that the available methods to study the brain and its metabolic networks in real-time are fairly limited. As imaging technologies advance and new assays are developed, this drawback may dissipate in the near future.

Advantages of modeling

Systems biology offers several advantages over pure biology or pure math. By developing models that look at the interactions between various molecules and networks, a more complete picture of how the system works can be defined. This, in turn, will help researchers develop more effective treatments for diseases and other ailments. Through the enmeshed interaction between model development, network definition, and parameter estimation from obtained data, detailed network architectures can be developed.

Systems biology also offers several advantages over conventional biological techniques. One of the most commonly used techniques in biology to study the effect of different compounds or try to understand regulation is cell culture. Although cell culture is simple and easy to test many hypotheses, the results fail to allow researchers to view the interaction of one cell type with other cell types, and thus, the validity of such results is called into play in complex disease states, such as AD.

Drawbacks

One of the main drawbacks to systems biology is the complexity of networks that are often obtained from data analysis require significant understanding of a variety of metabolic and regulatory networks, a task that is not easy to achieve for many people and at times, may seem overwhelming. Another drawback is that data obtained from microarrays, ELISAs and Western blots carries a very high margin of noise, often with the signal-to-noise ratio approaching one [6]. This can lead to development of inaccurate network topologies or incorrect parameter estimation, which would severely affect downstream model estimations. Further work on the development of mathematical tools to analyze such data would help to prevent this. A final drawback is that many networks contain dozens to hundreds of nodes, and an order or more number of interacting edges, which makes most models computationally intensive to model and require significant computing resources to achieve relevant model simulations without simplification of network topology.

Previous models pertaining to AD

Although a relatively new approach to studying AD, several models have been developed to study various aspects of the AD disease process. The earliest models studied the kinetics of beta amyloid fibril formation using data and rate constants obtained from experimental work [91, 107]. Later models started to look at the interactions between genes that have been linked with AD, such as ApoE, and the interactions between different cell types. Macdonald and Pritchard developed a detailed Markov model that uses epidemiological data to derive rate constants for transitions between no disease, disease, institutionalization, and death, in relation to

an individual carrying the ApoE gene. The main goal of this model was to determine the expected long term care costs associated with patients having AD.

More recent models have started to look at the roles of microglia in the AD disease process. Edelstein-Keshet and Spiros developed a model that studied the development of Aβ plaques *in silico,* which included the involvement of inflammation by microglia, effects of cytokines on neurons and a role for astrocytes in the disease process [46]. Luca et al developed a model describing the aggregation of microglia in AD in response to increased levels of Aβ, performing a stability analysis on their system of equations and suggesting that stochastic differences in cells may lead to the development of senile plaques [92]. Only one recent paper, which has some striking similarity to our work, has been published that uses a network model to study the role of cross-talk between neurons, microglia and astrocytes [114]. A literature review showed no systems biology models had been developed to study AD. Thus, the network systems biology model described herein is the first such model of its kind.

Chapter 3: Starting Point: A systems biology model of Alzheimer's disease incorporating spatial-temporal distribution of beta amyloid

Introduction and Model Goals:

As described in the background section, AD has many possible causative culprits: Aβ, cholesterol, ApoE, LRP-1, amongst several other contenders. To study the role of each of these molecules, an initial model was developed to simulate the spatial-temporal distribution of beta amyloid within a region of the brain. The model looked at generation rate of beta amyloid by neurons within the hippocampus and mapped the change in beta amyloid distribution with respect to time and location. A McCulloch-Pitts model was modified to study how neuron number changed over time dependent on the Aβ concentration level. A network that describes the interaction between astrocytes and neurons during cholesterol synthesis in the brain was also modified from one found in the literature to include possible interactions of cholesterol with APP processing. The initial goal of this model was to study the relationship between APP, Aβ and cholesterol processing in the brain, with particular emphasis on the effects of low brain cholesterol and LRP-1 expression levels in the initiating phases of AD and neurodegeneration. Although this was not accomplished with this version of the systems biology model, the framework was laid for the development of future model versions. This was the only model developed that studied the spatial distribution of beta amyloid; it was later decided that spatial

distribution was rather trivial if we were focusing on the hippocampus and more specifically, the CA1 region.

Local Network for Aβ & Cholesterol Processing in the Adult Brain:

As discussed in the background, beta amyloid is believed to be the causative factor in AD given its increased concentration levels in the brain in individuals with AD, as well as it's predominant presence in amyloid plaque deposits in both the brain parenchyma and cerebral vasculature. The amyloid precursor protein is cleaved in a two-step cleavage process by β-secretase and subsequently γ-secretase to form Aβ. Alternatively, APP is cleaved by α-secretase to form non-amyloidogenic sAPPα. Both sAPPα and Aβ are expressed during normal conditions and are believed to play key roles in neuronal excitability, enhanced synaptic plasticity, learning/memory and development, response to neuronal injury, and synapse formation, respectively.

In the adult brain, cholesterol is produced by *de novo* synthesis by astrocytes, with subsequent transport via lipoproteins and uptake by neurons. Oligodendrocytes are also capable of producing their own cholesterol, but were not studied in this model. Astrocytic cholesterol synthesis proceeds through the same pathway that is seen in other cell types, proceeding through an energy-intensive process that starts with Acetly-Coenzyme A and finishes with cholesterol. Cholesterol is then packaged into ApoE, the main lipoprotein in the brain, transported out of astrocytes via the ABCA1 receptor and shuttled to neurons.

At the neuronal membrane, cholesterol-laden ApoE binds to LRP-1 and releases cholesterol to the neuron. It is not well understood whether or not

cholesterol plays a role in APP processing. Excess cholesterol or aged cholesterol is degraded via action of the CYP46 cytochrome, which processes cholesterol to form the brain-specific end product, 24S-hydroxycholesterol (24SOH). 24SOH is transported out of the brain and can then be transported across the BBB to the blood to be cleared from the brain. It has also been suggested that a portion of the 24SOH is transported back to astrocytes to help modulate cholesterol synthesis, since tight regulation over neuronal cholesterol levels is absolutely necessary for normal neuronal function. The following figure describes this process in visual detail.
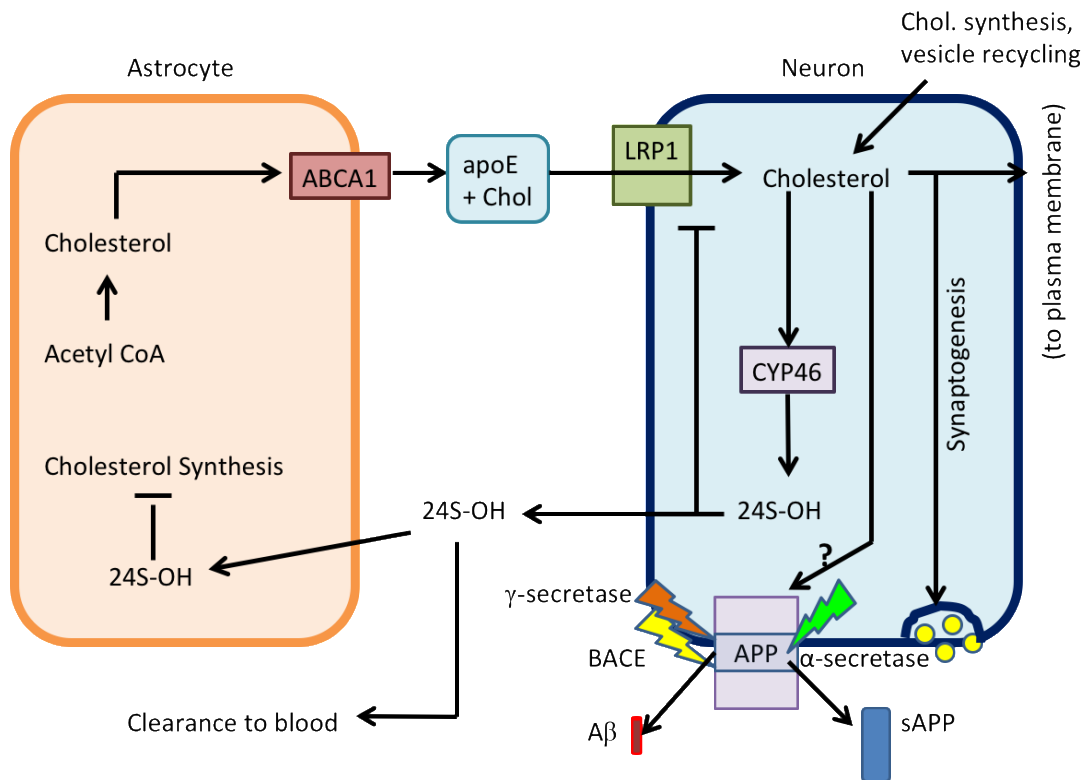

Figure 10: *Cholesterol processing in the adult brain*.

Derivation of the Reaction-Diffusion Equation for Aβ Distribution:

In AD, the most severely affected regions of the brain are the hippocampus, the amygdala and the cerebral cortex. Given that the hippocampus is the initially

affected brain region and is also known to play a role in memory, this model focuses on the distribution of Aβ in the hippocampus. A deterministic model was chosen following calculation of the number of beta amyloid molecules within both healthy individuals and individuals with AD. Briefly, the volume of the hippocampus can be approximated as 6 cm^3 [22]. Assays of the total brain beta amyloid in healthy and diseased individuals were found to be 0.6 μM and 8.8 μM, respectively, which corresponds to 2.2×10^{15} and 3.2×10^{16} molecules of Aβ. Thus, for the case of a single neuron or small group of neurons, a statistical model would be adequate, however, in the case of larger sections of the hippocampus, such as the CA1 region which we are interested in studying, a statistical model becomes intractable given the inefficiency of simulation. This potential difficulty was overcome by using a reaction-diffusion equation (RDE) to model Aβ distribution:

$$\frac{\partial c}{\partial t} = D_{AB} \left(\frac{\partial^2 c}{\partial x^2} + \frac{\partial^2 c}{\partial y^2} + \frac{\partial^2 c}{\partial z^2} \right) + R_i$$

where c is the concentration of beta amyloid, D_{AB} is the diffusion coefficient of Aβ and R_i represents the reactions that occur within the control volume. The reaction term, Ri, can be expanded to account for beta amyloid production by neurons, degradation by proteases, fibril formation and uptake by microglia respectively as:

$$R_i = \sum \beta \delta (x - x_n, y - y_n, z - z_n) - \alpha c [IDE] - \gamma_1 c c_n - \gamma_2 c^2 - \sum \varepsilon c \delta (x - x_n, y - y_n, z - z_n) - \Psi$$

The first term represents beta amyloid production, which occurs only in the cell body of neurons. The location of each neuron is represented by a delta function (point source), while the production rate of beta amyloid, β, is given by a Poisson distribution whose mean is a function of:

$$\beta = f(APP, cholesterol, BACE, PS1)$$

Beta amyloid production if also dependent on: the extent of inflammation, the general stress level, and on whether neurons are recovering or remodeling. Degradation by proteases depends on the reaction rate, α, the Aβ concentration and the concentration of insulin-degrading enzyme (IDE). A simplified model for Aβ fibril formation is described where the two rates constants, $\gamma1$ and $\gamma2$, represent the attachment of beta amyloid monomers onto an oligomer or fibril and the initial formation of an oligomer, respectively. The rate of uptake by microglia, given by ε, is dependent on the beta amyloid concentration. The location of microglia is defined by a delta function for simplicity in modeling.

A key player in the overall dynamics of the model is the flux rate of beta amyloid across the blood-brain barrier (BBB). Clearance of Aβ from the brain occurs either by direct transport of beta amyloid via the LRP-1 receptor, or more commonly, by the transport of ApoE-bound beta amyloid. Net flux is given as the sum of active and passive transport across the BBB, where active transport requires some source of energy (ATP, GTP, etc) to transport a substance, while passive transport often occurs down a concentration gradient or by molecules that are easily diffusible through cell membranes (lipophilic molecules). A simplified version of the Kedem-Katchalsky equations were used to model passive transport of beta amyloid; physically, passive transport of Aβ can be likened to leakage across a semi-permeable BBB. Passive transport occurs only in late stages of AD beta amyloid plaque deposition (cerebral amyloid angiopathy, CAA) or inflammation of the neurovascular unit leads to localized breakdown of the BBB. Thus, during the initiating stages of the disease that

we are trying to study, passive transport contributes only a trivial amount of Aβ clearance from the brain.

Active transport has been modeled as the major contributor to Aβ clearance during the initial stages of AD. To model this interaction, we assume that Aβ must first be bound to the ApoE molecule, then diffuse through the brain parenchyma before reaching the BBB. At the BBB, Aβ-ApoE molecule must bind to the LRP-1 receptor, which will subsequently transport the Aβ across the BBB, while ApoE is recycled to the cellular surface for re-use. Binding kinetics between the Aβ-ApoE complex and LRP-1 have been modeled using Michaelis-Menten kinetics:

$$R_s = \frac{R_{max} c(x - x', t)}{K_M + c(x - x', t)}$$

where R_{max} is the maximum rate of reaction, K_M is the Michealis constant and c represents the concentration of Aβ within a narrow boundary region around the BBB. The net reaction rate is also dependent upon the rate at which Aβ binds to apoE to be transported and on the density of LRP1 receptors along the BBB:

$$R_{max} = f([LRP1], [apoE], [apoE * Aβ])$$

For our model, the role of LRP1 to the reaction rate will be written as a ratiometric coefficient, L, where L ranges from 0 to 1 as follows:

$$L = \frac{[LRP1]}{[LRP1]_{avg}}$$

The rate at which apoE and Aβ bind is defined macroscopically as:

$$[apoE * Aβ] = σ[Aβ][apoE]$$

The total flux of Aβ across the BBB is described by the reaction rate (R_s) and the total cross-sectional area of BBB that we are studying:

$$Ψ = R_s A_{BBB}$$

Experimental values for the Michaelis constant and the R_{max} for Aβ40 were derived by Shibata et al to be 15.3 nM and 70-100 nM, respectively [131]. Values for Aβ42 are not necessary since LRP-1 predominantly transports the 40 amino acid length protein as opposed to the 42 amino acid form of Aβ. Additionally, Aβ40 is the form found in cerebrovascular plaques, so we have assumed that this will be the form localized near LRP-1 receptors.

Derivation of Aβ Diffusion Coefficient:

The diffusion coefficient for Aβ (D_{AB}) moving through brain tissue is not a readily available parameter due to the difficulty in obtaining accurate measurements. To overcome this, D_{AB} was calculated using a combination of the Stokes-Einstein equation and a previously described method [70]. The effective diffusion coefficient through brain tissue can be given by:

$$D_{AB} = \frac{D}{\lambda^2}$$

where D is the theoretical value for the diffusion coefficient given by the Stokes-Einstein relationship in a fluid medium free of any obstacles and λ is the tortuosity, or the average hindrance of a complex medium relative to an obstacle-free medium. In the brain, λ is typically ~1.6, though this value can increase during insult or stress to the brain, decreasing the effective diffusion. The Stokes-Einstein relationship is:

$$D = \frac{k_B T}{6\pi\eta r}$$

where k_B is the Boltzmann constant (1.38e-23 J/K), T is the temperature in Kelvin (310.15 K), η is the effective viscosity (0.7-1 mPa·s, [14], and r is the effective radius

of Aβ (estimated as 2 nm, [30]). Substituting these values into the given equations gives an effective diffusion coefficient of $D_{AB} \sim 1.14 \times 10^{-6}$ cm^2/s.

Modeling Microglial Movement through the Brain and Uptake of Aβ

As discussed previously in the background section, the CNS maintains it's own immune system separate from that of the rest of the body, partially due to the presence of the BBB. CNS macrophages, known as microglia, are distributed relatively uniformly throughout the brain during healthy, resting states. During disease, microglia become activated, take on a ramified form and migrate towards the site (or sites) of infection, releasing pro-inflammatory cytokines and phagocytosing invading cells or material.

The movement of microglia within the brain has been modeled parametrically and depends on whether the microglia are activated or ramified (resting). Ramified microglia are modeled using a simple random walk along a continuous plane:

$$x_{c,i,t+1} := x_{c,i,t} + \xi(t)$$

where x_c is a matrix that tracks the position of the center of mass of each of the ith microglia at time t, and $\xi(t)$ is Gaussian white noise with the constraint that the center of mass of two microglia cannot be less than 2R (R=microglial radius) distance from each other at the same time point (microglial aggregation only occurs in the activated state). Microglia are assigned initial positions prior to running the simulation. Ramified microglia have several other constraints: microglia do not traverse the BBB and are confined to brain tissue; and under extreme circumstances, macrophages in the blood may cross into the brain and differentiate into microglia. Microglia can switch to the activated state once a specified threshold difference has been exceeded.

When the local concentration of Aβ in the brain reaches 200 nM or greater,

microglia become activated and migrate up the concentration gradient towards the main source of Aβ. Experimentally, this has been shown to occur near neurons or near the basement membrane of blood vessels. The directed movement of microglia towards a chemoattractant (chemotaxis) has been modeled using the Langevin equation of motion:

$$\dot{x}_{c,i}(t) = \xi(t) + \kappa\alpha\nabla\phi(x_{c,i},t)$$

where x_c represents the position of the ith microglia at time t, $\nabla\phi$ represents the Aβ concentration gradient, ξ represents Gaussian white noise that the microglia would experience during chemotaxis, α is a positive constant that describes the strength of chemotaxis ($\alpha = 1$ for our simulations), and κ describes whether it is positive chemotaxis ($\kappa = +1$; value used for our simulations) or negative chemotaxis ($\kappa = -1$).

Neural Network Model for Neurons:

Neurons were modeled using a modified McCulloch-Pitts model previously developed by Butz et al [19]. The network is defined by several variables: N, NE, C, θ, Φ and β. N represents the number of logical neurons, NE is the number of excitatory neurons (1 to NE are excitatory, while NE to N are inhibitory), C is the NxN matrix of connections between neurons, θ is the common threshold of all neurons, Φ is the relative weight of inputs from inhibitory neurons, and β is the noise level in the threshold function. The state of the network at any given time, t, is defined by the vector z^t:

$$z^t = (z_1^t, \ldots, z_N^t), z_i^t \in \{0,1\}, 1 \le i \le N, t \ge 0$$

The network connectivity matrix is defined as:

$$C = \begin{pmatrix} c_{1,1} & \cdots & c_{1,NE} & \cdots & c_{1,N} \\ \vdots & \ddots & \vdots & \ddots & \vdots \\ c_{N,1} & \cdots & c_{N,NE} & \cdots & c_{N,N} \end{pmatrix}$$

where $c_{i,j}$ is the strength of the connection from neuron j onto neuron i. From a biological standpoint, C represents the probability for synaptogenesis between two neurons (Butz 2006). The membrane potential for neuron *i* is:

$$MP_i^t = \sum_{j=1}^{NE} c_{i,j} z_j^t - \Phi \sum_{j=NE+1}^{N} c_{i,j} z_j^t$$

The probability of neuron *i* being active in the next time instant is governed by the threshold potential (θ), the actual membrane potential (MP), the noise level (β), and the percentage afference (α) as:

$$Prob(z_i^{t+1}) = \frac{1}{1 + e^{(MP_i^t + \alpha - \theta)/(-\beta)}}$$

The percentage afference models the shift in the probability of firing, and is related to the relative levels of Aβ. Changes in network connections are modeled by updating the connectivity matrix at each time step with respect to changes in pre- and post-synaptic elements. Decay of pre- and post-synaptic elements is proportional to the strength of existing connections and the relative level of Aβ. Pre-synaptic elements that are connected to a post-synaptic element that is lost are able to recombine and form a new synapse in future time steps, whereas the 'lost' post-synaptic element is removed from the post-synaptic pool. Free pre- and post-synaptic elements are updated to account for synaptic losses, recombinations, and strengthening of existing contacts. The number of possible contact offers is dependent on the number of free contacts that a neuron contributes to the network.

The number of neurons in the network is varied during the simulation depending on the neuronal activity level, as well as the local concentration of beta amyloid. Neuron loss is modeled by the calcium set-point hypothesis in combination

with apoptosis occurring above a maximal beta amyloid concentration. Calcium previously determined that a neuron's activity level should remain between $0.25 < s_i < 0.85$. The neuron number in the system at a given time point is defined by a vector of N elements given as:

$$cells_i := \begin{cases} 1, & if\ neuron\ exists, 0.25 < s_i < 0.85 \\ & and\ \phi(x,t) < A\beta_{max} \\ 0, & if\ the\ neuron\ does\ not\ exist, \\ & or\ above\ conditions\ are\ not\ met \end{cases}$$

Chapter Conclusion:

In this chapter, we have discussed the initial approach that was used to model pathogenesis of AD. A reaction-diffusion equation was used to model the spatial-temporal aspects of Aβ distribution within the CA1 region of the hippocampus. No effect of geometry was studied, aside from the total volume of CA1. A deterministic method was chosen since the expected number of beta amyloid molecules, even in a healthy brain, is greater than 10^{15}. Equations for the diffusion coefficient and key reaction rates were derived. Movement of microglia was modeled as a random walk along a continuous plane, while the number of neurons was described by a modified McCulloch-Pitts model. Simulations of this model were not run for several reasons: difficulty of implementing an appropriate algorithm across such a variety of modeling modalities; lack of pertinent rate constants or values needed to iteratively solve the RDE; and the subsequent belief that the spatial distribution of Aβ was relatively trivial in the actual initiation of the disease process. To overcome these issues, a network model was developed that looked at this problem from a more systems level approach. The following chapters will discuss this model in further detail.

Chapter 4: What do Networks Have to do with AD? An Initial Network Model for AD

Introduction & Model Goals

AD is a multi-faceted disease most likely caused by the interaction of several simultaneous dysfunctions. In recent years, a large interest has been put on understanding the possible role of cholesterol in AD pathogenesis. Neuroinflammation has also been suggested to play a key role in disease progression. Although several experimental trials with statins and epidemiological trials measuring plasma and brain cholesterol have been undertaken, results have been relatively inconsistent. Some of these inconsistencies may be due to hidden factors: biological pathways that may be interacting in previously unsuspected manners. Given the inherently high-connectivity and cross-reactivity and regulation existing between many biological pathways, a network-based mathematical model would help to elucidate some of these underlying interactions, not only by helping to visualize and fully list the entirety of all known and suspected interacting pathways, but to also provide a method to discover how pathways currently thought to be unrelated may contribute or play a role in disease progression, as well as to study how these interactions change over time as the system moves from a healthy state to a disease state.

Systems biology provides a nice format to develop such a proposed model, bringing together data from biological experiments and simulation results from mathematical models that are based on understanding the system as a sum of

interacting parts at multiple levels of interaction (molecular, cellular, tissue, organ, body). To achieve this notion, an initial network describing the interactions between the metabolic, lipidomic and proteomic networks was developed. One of the main goals of this model, and all subsequent models, was to study the role of cholesterol in AD pathogenesis since a growing body of literature has suggested the cholesterol levels in both the brain and plasma may play roles in disease progression. Within the plasma, experimental results generally seem to concur that high plasma levels of cholesterol is a risk factor for developing AD; however, the exact role of cholesterol in the brain with respect to Aβ production, transcription of other proteins, metabolic pathways and induction of inflammation are not well understood.   The following figure describes the possible regulatory interactions between Aβ and cholesterol.
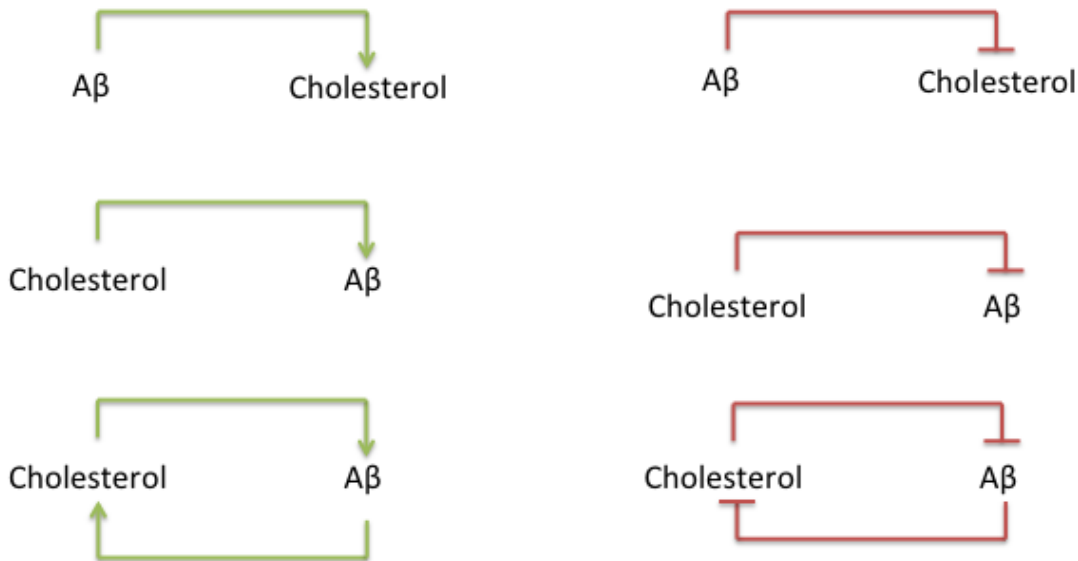

Figure 11: *Possible regulatory interactions between cholesterol and beta amyloid.* Green arrows correspond interactions that increase the production rate, while red lines with the blunted end correspond to inhibitory interactions.

This simple network model represents the first known attempt to study AD from a systems biology approach. The network derived here consists of 6 high level

nodes: 5 nodes representing the various cell types present in the brain and a single node representing the brain extracellular matrix. Each cellular node contains an interconnected sub-network representing the biomolecular pathways specific to that cell type. Sub-networks are capable of interacting and influencing each other, leading to changes in the weights of sub-network nodes. Basic simulations were run using Matlab, demonstrating a key role for regulation of beta amyloid generation by cholesterol inhibition. Further simulations also looked at the role that LRP-1, apoE, cholesterol transfer rate between astrocytes and neurons, and the effect of sinusoidal cholesterol inputs on the concentration of APP and Aβ.

Hierarchies of Networks in Biological Systems

One way of quantitatively thinking about diseases is to view them as aberrant networks. In this manner, any given organism can be represented as a hierarchy of interacting networks, from the biomolecular-level all of the way to the organism-level. Networks interact within their respective hierarchal level, and can also interact with other levels. Take, for example, energy production in multicellular organisms. At the cellular level, mitochondria are responsible for producing sufficient ATP to keep cellular processes running smoothly (biomolecular to cellular level interactions). In turn, mitochondrial output is also controlled by the local environment (whether the cell is being attacked by pathogens, whether local oxygen and nutrient levels are normal, etc); by usage demands (whether the cell is resting or in an active state, such as a muscle cell during exercise); and by cross-talk between other organs or the external environment via release of hormones, other signaling molecules and epigenetic and RNA regulatory control mechanisms.

These hierarchies are important to understand and take into account when modeling biological systems. One of the key properties that hierarchal network structures convey to a system is a time delay between input signal at one level and response at another level, analogous to that seen in control systems with feedback loops. This is an important feature that is indeed observed in biological systems. For example, if one were to look at what seems to be a relatively simple system process to model such as ingesting a meal, it would quickly become obvious that many different organs are involved *and* affected. Simply the thought of having food when one is hungry causes salivation (activation of salivary glands in response to "hunger sensations"). Downstream, muscles in the face and throat are used, enzymes are released by the salivary glands, pancreas and liver to digest food, hydrochloric acid is produced and released by cells lining the stomach, sodium bicarbonate is released by cells in the small intestine, receptors all along the intestines absorb broken down nutrients and water, the kidneys and liver filter absorbed nutrients to remove wastes or unnecessary nutrients, intestinal smooth muscle is activated to maintain peristalsis, and finally, the anal sphincter is contracted to expel solid waste (liquid wastes pass through the urethra). This very simple process activates a multitude of system levels in the body, from cellular to organ, all working in unison to achieve a final goal, but uniquely to achieve their specific part in the process, while also initiating several time delays between different levels to maintain the proper feedback regulation and control.

In essence, many biological processes encompass a basic pattern of interaction between biochemical networks, proteomic networks and genomic networks. The genome provides the basic outline for what proteins are transcribed and translated, while epigenetic material (RNA, histones, DNA methylation) controls the finer details of how the organism responds to the environment through modification of protein transcription. It has been suggested that genetic networks can be modeled with Boolean or digital logic approaches, with switches and multi-input gates leading to convergence along key regulatory pathways. In turn, the proteins produced interact with other cellular structures to maintain the biochemical pathways necessary to keep the cell alive and functioning via enzymatic reactions, catalysis, transport of precursors from the extracellular space into the intracellular space via transporters, receptors to respond to the environment, and cytoskeletal proteins. Proteomic networks can be modeled with a combination of Boolean logic, network theory, and
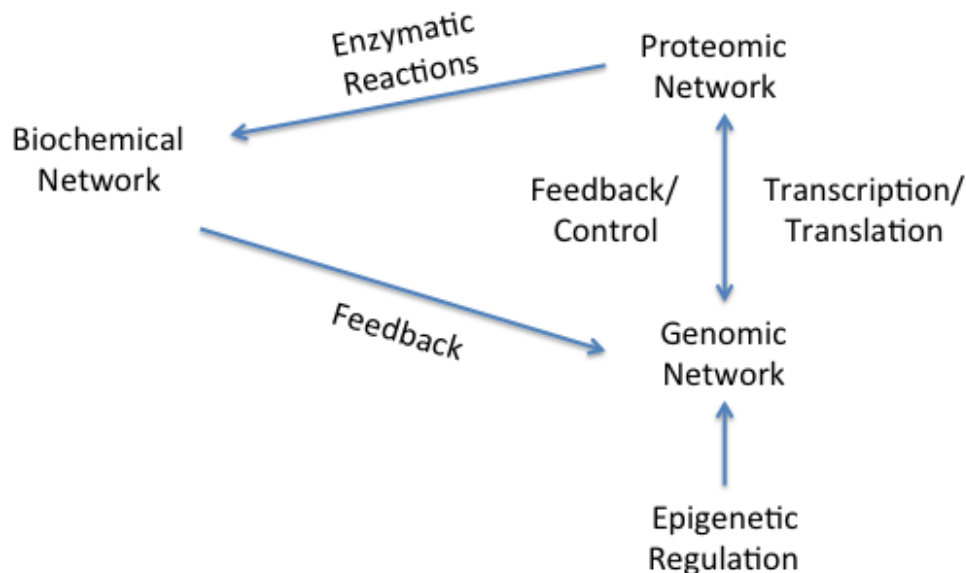

Figure 12: *Basic Interaction Pattern Between Heirarcheal Networks*: The three basic pathways that interact within any given cell are genomic, proteomic and biochemical networks. Each network can be modeled using a variety of approaches, though most commonly, genetic networks are modeled using Boolean logic, while proteomic networks are modeled using a combination of network theory and chemical rate kinetics.

chemical rate kinetics. Biochemical networks, running in the background, form many of the basic components necessary for the formation and function of a cell: ATP, lipids, cholesterol, carbohydrate side groups, and specialty molecules. Chemical rate kinetics and Michaelis-Menten kinetics are two of the most commonly used methods to model biochemical networks. With all of these networks and processes running simultaneously, one could easily imagine that the cell is like a mini-computer and the different interacting pathways are the run-time stack, microprocessor and bus.

Diseases as System States

If we look at the many biological processes 'running' in a given organism, a unique idea that comes to mind is the convolution of each of these processes into an overall net process, or *state* of the system. That is, the state of a biological organism can be described by the sum total of the various genomic, proteomic and biochemical pathways that are currently being expressed by that organism. This varies from phenotype, which has more to do with how the genetic and proteomic pathways interact to form certain physical or behavioral characteristics, with little regard to the role that biochemical pathways can provide feedback and indirectly modulate the phenotype (ie. environmental or nutritional factors).

The concept of an organismal state can be expanded to help differentiate more quantitatively the differences present during health and disease. Assume that initially, each organism starts in a healthy state i, where all pathways are interacting as expected and expression levels are also at the expected values. Over time, external influences, responses to the environment, oxidative stress and other stimuli cause the system to shift from state i -> state j, which represents one of the many possible states

of a perturbed network that is operating less efficiently. There is a range of healthy states that are possible for a single organism to take one; that is, small deviations in the expression level or interaction between pathways lead to only minor changes in the system, which, as a whole, can adjust to such a perturbation. However, as enough of the networks become perturbed, expression and concentration levels slowly begin to deviate from the expected range, which leads to downstream consequences in other network topologies. This is the suggested beginning of many disease processes. The system may attempt to compensate initially, but if the external stimulus (environment, stressor, etc) is not removed or its effect ameliorated, the system converges to an alternative steady state, where pathways are running non-optimally, alternate pathways may be activated, and eventually networks must adapt and concentration levels change.

From a mathematical standpoint, the state of the system can be represented using two matrices: one matrix which represents the current concentration levels of all molecules of interest (MOI), and a second matrix which represents the level of interaction between two given MOI. MOI can be protein products, enzymes, lipids, cytokines or any other molecule involved in a proteomic, lipidomic or metabolic pathway. To simplify our model here, genomic data has not been included, though future models will look at this to be more accurate. The interaction matrix can change over time to reflect inherent changes in the system interaction and changes in network topology that may occur.

This setup is very similar to a Markov process and in many ways, the state of many interactions in a biological system can be thought of as a Markovian finite state

space. The state is Markovian because the future state of a complex biological network depends only on the current state. It does not matter how the system reached the current state, only that it is at the current state; that is, the current state is pathway independent. This implies that various, differing inputs can lead to a similarly convergent output or end result.

Logically, this follows closely to what is seen in biological systems. Take, for example, the activation of beta cells in the pancreas (responsible for producing insulin). When these cells receive the appropriate input stimulus (high blood glucose levels), they begin producing and releasing insulin. Assuming that there is not a malfunction in the control system regulating this as in diabetes, beta cells will not have any *memory* of previous times that they were stimulated to produce insulin. Another logical point to make here is that the Markovian memoryless property fails when the frequency of input signals passes a threshold. In this case, there is not a sufficient time delay to allow the system to recover from the applied input and input signals begin to 'merge' with each other, causing the system to shift states.

Alternatively, the interactome of a biological system can be represented by a set of differential equations that describe the interactions between various molecules. This is somewhat easier to model over well-defined time steps, however, the main drawback is the need for having rate constant data and other parametric constants available to make the model results most accurate. A system of differential equations is also a direct application of graph theory and can be expanded to include a bipartite structure; in effect, this graph theoretic approach represents the interactome of different cell types within the brain.

The networks described in the last section have been simplified and normalized to those that would be expressed across the various cell types within the brain.   At the cellular level, networks in neurons, astrocytes, microglia, oligodendrocytes and brain endothelial cells are important to model, as well as their interaction with the brain extracellular space.
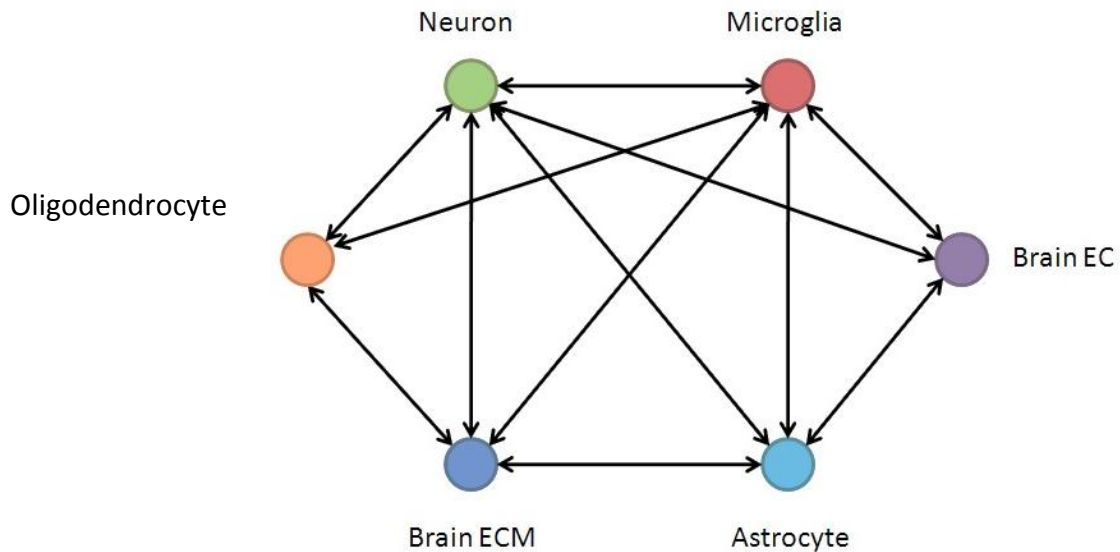

Figure 13: *Interaction Graph Between Different Cell Types in the Brain:* Directed graph describing the interactions present between different cell types in the brain.

In deriving the system of equations to describe the network topology that we have given, several key assumptions were made. Abstracting the network to the higher hierarchy (from intracellular to cellular level), we see that each cell of a given cell type (neuron, microglia, astrocyte or brain endothelial cell) has a similar biochemical and proteomic network to neighboring cells of the same cell type, with minor variations existing between cells within a local vicinity. This is true because all cells have the same genetic background, and cells of the same type exposed to the

71

same local environment should have similar epigenetic material, as well as activation of similar proteomic and biochemical pathways. This implies that single or small groups of aberrant cells do not have a distinct effect on the system as a whole, and are often removed via apoptosis. Within the brain, it is reasonable to assume that besides synaptic transmission and paracrine signaling of hormones from the HPA axis, there is minimal, direct chemical cross talk between metabolic pathways (glycolysis, lipid metabolism, etc) in neurons. This implies that the biochemical network between neurons is independent from each other, allowing us to represent each cellular node within the cellular network as a sum of all biochemical pathways being expressed by that cell type. This sum can be described by a sample distribution given by:

$$X(node) \sim Normal(\mu_{j,k}, \sigma_{j,k}/\sqrt{n_{j,k}})$$

$\mu_{healthy}$ μ_{AD}
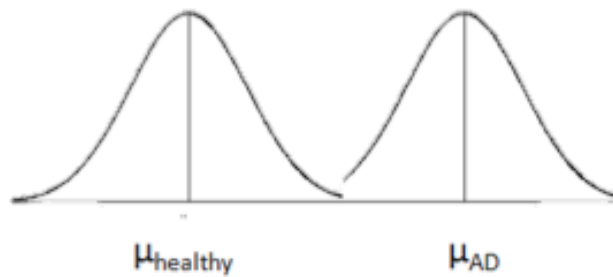
Model Goals

Taking these ideas into account, two unique systems biology models were developed to study the role of cholesterol in AD. The first model was developed to study the role of negative feedback regulation in the mixed lipidomic-proteomic-metabolic pathway, while the second model was developed to help ask several questions: (1) What are the key nodes and regulatory points in the described network? (2) Does inhibition of BACE activity by cholesterol fit with the known data? (3) How does varying the expression levels of LRP-1 alter steady state levels of Aβ?

A topological network describing the interactions between the simplified proteomic, lipidomic and metabolic pathways has been derived for both models (Figure 13). The network was simplified to include only those molecules that are most relevant from a biological standpoint and directly relevant to the questions that we were trying to ask. In the first network, there are 10 molecules of interest in the network and 11 rate constants associated with the model. There is no compartmentalization of the model equations into different cell types, and limited data exists for the rate constants. Therefore, the rate constants were approximated as fractions of molecules that would interact within the defined time step.

The second model includes compartmentalization and thus an increase in the number of molecules and rate constants; there are 15 rate constants and a total of 17 molecules in this network. The degree of each major node was calculated and is listed in Table 6. All molecules are assumed to reside in one of two compartments: the brain (limited concentration levels) and blood (infinite sink for any molecule being transported across the BBB). Within the brain, the cholesterol was subdivided between astrocytes and neurons, while the ApoE pool was subdivided into astrocytic and free ApoE. Rate constants in this model were also approximated as the fraction of molecules interacting per time step and fitted to maintain a stable simulation environment.

Model 1 Network & Equations

A simplified network encompassing the molecules pertinent to cholesterol and Aβ production was developed. The network consists of 10 molecules (only 8 molecules are simulated and change with time; pyruvate is modeled as a constant and

fatty acid levels are not tracked), 7 reaction edges and 3 regulatory edges (negative feedback). The following figure represents the model that is being studied here.
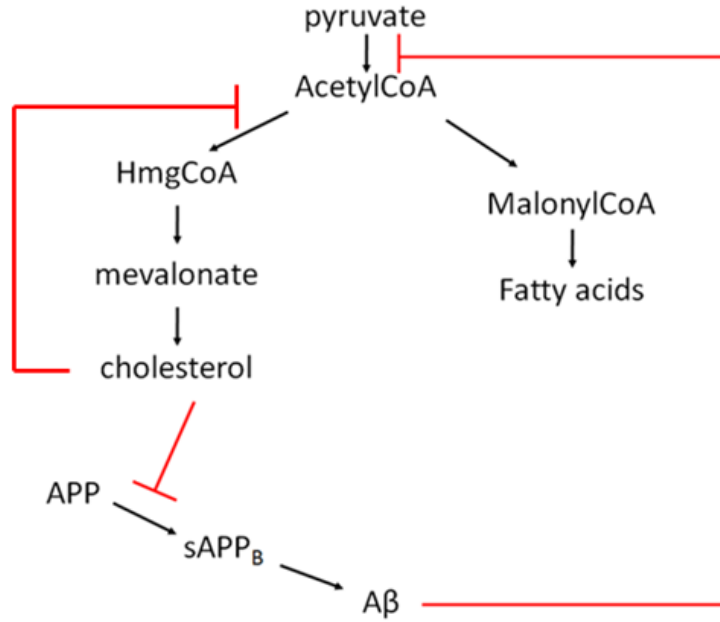

Figure 14: *Network topology for model 1 network* demonstrating the interactions that exist between the cholesterol production and Aβ generation pathways. This model was developed to study the role of negative feedback inhibition in the level of Aβ, particularly by cholesterol since this exact regulation is not well understood. No compartmentalization was added.

Acetyl coenzyme A (AcetylCoA) is produced from the action of pyruvate dehydrogenase (PDH) on pyruvate, and is itself the precursor to both the cholesterol and fatty acid synthesis pathways (HmgCoA and MalonylCoA respectively). AcetylCoA generation is believed to be at least partially inhibited by beta amyloid [66].

$$\frac{dACoA}{dt} = k\left(\frac{1}{1+k_\beta[A\beta]}\right)[PDH][pyruvate] - k_5[ACoA] - k_{chol}k_T\left(\frac{1}{1+k_\gamma[chol]}\right)[ACoA]$$
$$- k_{FA}k_T[ACoA]$$

where k_β is the strength of inhibition and is dependent on the concentration of beta amyloid, k_5 is the rate of AcetylCoA degradation, $k_{chol}k_T$ is the ratio of AcetylCoA

that is converted to HmgCoA, k_γ is the strength of inhibition provided by cholesterol on own synthesis (end-product inhibition), and $k_{FA}k_T$ is the ratio of AcetylCoA that is converted to MalonylCoA and other fatty acids. From AcetylCoA, both HmgCoA and MalonylCoA are produced. The rate of this production is dependent on several factors, of which the concentration of both cholesterol and fatty acids is accounted for when the system decides to choose one pathway over the other:

$$\frac{dHmgCoA}{dt} = k_{chol}k_T\left(\frac{1}{1+k_\gamma[chol]}\right)[ACoA] - k_2[HmgCoA]$$

$$\frac{dMCoA}{dt} = k_{FA}k_T[ACoA] - [MCoA]$$

The cholesterol pathway is then simplified to include only mevalonate and cholesterol production. The rate limiting step in cholesterol production is HmgCoA to mevalonate, which is regulated by the current level of cholesterol in the cell via the SREBP/SCAP pathway. For simplification sakes, it has been assumed that all HmgCoA is converted to mevalonate, as well as all mevalonate is converted to cholesterol.

$$\frac{dmev}{dt} = [HmgCoA] - [mev]$$

$$\frac{dchol}{dt} = [mev] - k_D$$

Lastly, beta amyloid levels were modeled as a function of APP concentration, with inhibition from cholesterol:

$$\frac{dA\beta}{dt} = k_{BACE}\left(\frac{1}{1+k_\alpha[chol]}\right)[BACE][APP] - k_{DA}$$

The second model presents the first-ever systems biology model used to study the role of cholesterol in AD. This model was developed to help ask several questions: (1) What are the key nodes and regulatory points in the described network? (2) Does inhibition of BACE activity by cholesterol fit with the known data? (3) How does varying the expression levels of LRP-1 alter steady state levels of Aβ?

A topological network describing the interactions between the simplified proteomic, lipidomic and metabolic pathways have been derived (Figure 14). The network was simplified to include only those molecules that are most relevant from a biological standpoint and directly relevant to the questions that we were trying to ask. There are 15 rate constants and a total of 17 molecules in the network. The degree of each major node was calculated and is listed in the table. All molecules are assumed to reside in one of two compartments: the brain (limited concentration levels) and blood (infinite sink for any molecule being transported across the BBB). Within the brain, the cholesterol was subdivided between astrocytes and neurons, while the ApoE was subdivided into astrocytic ApoE and free ApoE.

A system of non-linear differential equations was developed to represent the described network. The majority of metabolic reactions were described by direct conversion rates from precursor to product molecule. Inhibitory interactions within metabolic reactions or between metabolic, proteomic or lipidomic sub-networks were described by Michaelis-Menten-like rate kinetics. Neuronal cholesterol levels were maintained at a constant value throughout simulations via feedback control. This feedback mechanism also affected cholesterol levels in astrocytes, the level of ApoE in both astrocytes and in the interstitial space, and synthesis levels of HmgCoA by

76

astrocytes, demonstrating the highly interdependent nature of cholesterol and ApoE concentrations in different cell types within the brain. The following sections describe these equations in further detail.
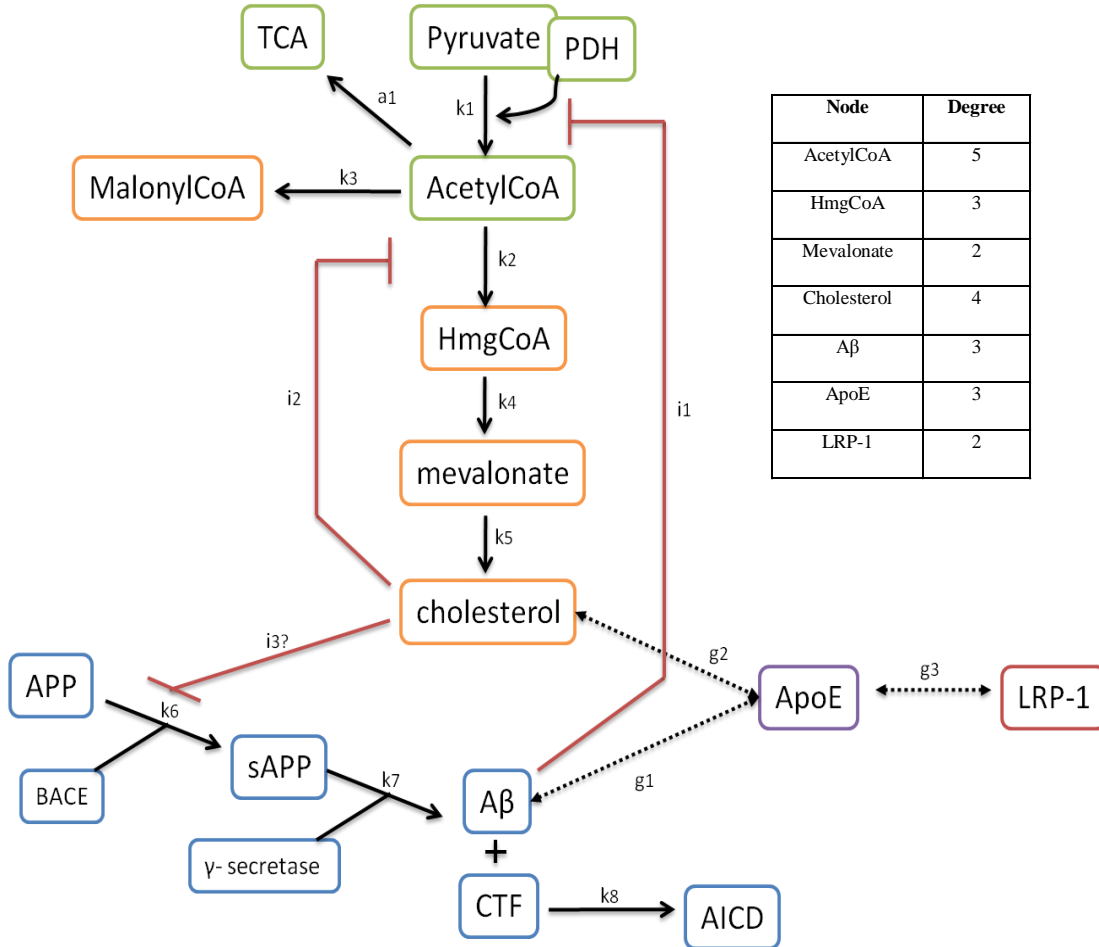

Node	Degree
AcetylCoA	5
HmgCoA	3
Mevalonate	2
Cholesterol	4
Aβ	3
ApoE	3
LRP-1	2

Figure 15: *Network topology for mixed proteomic-lipidomic network to study AD.* Precursor molecules (green boxes), lipidomic molecules (orange), and proteomic molecules (blue, purple and red) are described. Inhibitory interactions are given by a red line with a blunted bar, metabolic reactions between precursor and product are described by solid black lines, and binding interactions between molecules are given by dotted, black lines. **Table (right inset): Degree of Key Nodes.** AcetylCoA has the highest degree, followed by cholesterol. **Acronyms used: APP**: amyloid precursor protein; **ApoE:** apolipoprotein E; **AICD:** APP intracellular domain; **Aβ:** beta amyloid; **CTF:** C-terminal fragment; **HmgCoA:** 3-hydroxy-3-methylglutaryl-coenzyme A; **LRP-1:** low density lipoprotein receptor-related protein; **PDH:** pyruvate dehydrogenase; **TCA:** the citric acid cycle

Metabolic Interactions:

Metabolic interactions encompass all interactions represented by green boxes in Figure 14. AcetylCoA is generated from pyruvate via action of pyruvate dehydrogenase (PDH). The rate of this reaction has been shown to be influenced by the concentration of Aβ [66]. Since the concentration of PDH is believed to be constant during AD, the rate equation was modified to be independent of PDH concentration:

$$\frac{dACoA}{dt} = k_1 \left(\frac{1}{1 + \alpha[A\beta]}\right)[pyruvate] - k_2[ACoA] - a_1[ACoA]$$

A small fraction of this AcetylCoA (k_2) will be converted to HmgCoA. Conversion of HmgCoA to mevalonate is the rate-limiting step in cholesterol synthesis, and is negatively inhibited by cholesterol (negative feedback loop). When neuronal cholesterol (cholN) is below the threshold value, all HmgCoA that is synthesized is used to make mevalonate:

$$\frac{dHmgCoA}{dt} = k_2[ACoA] - k_4 \left(\frac{1}{1 + \gamma[cholN]}\right)[HmgCoA]$$

When neuronal cholesterol levels are normal, there is relative excess of HmgCoA, which can then be used for other metabolic processes or degraded:

$$\frac{dHmgCoA}{dt} = k_2[ACoA] - k_4 \left(\frac{1}{1 + \gamma[cholN]}\right)[HmgCoA] - d_6[HmgCoA]$$

Lipidomic Reactions & Interactions:

Mevalonate is the precursor to cholesterol; the cholesterol synthesis pathway actually has 19 steps between mevalonate and cholesterol, however, these steps have been considered trivial for the goals of this model and the average production rate for cholesterol has been used:

$$\frac{dmev}{dt} = k_4 \left(\frac{1}{1 + \gamma[cholN]}\right)[HmgCoA] - k_5[mev]$$

All cholesterol synthesis occurs in astrocytes. This cholesterol must then be bound to ApoE and transported from astrocytes to neurons, at a rate t_1. Astrocytic cholesterol is also degraded at an extremely slow rate (half-life of 5 years):

$$\frac{dcholA}{dt} = k_5[mev] - t_1[ApoE_A] - d_2[cholA]$$

Proteomic Interactions:

When neuronal cholesterol is at or above the threshold value, there is no need to transport cholesterol to neurons; in this case, the middle term is trivial. The concentration of ApoE in astrocytes would also vary similarly (birth minus death minus amount transported):

$$\frac{dapoE_A}{dt} = b_a - t_1[ApoE_A] - ([apoe_A] - [cholA])$$

Neuronal cholesterol levels vary depending on the amount of cholesterol being transferred from neurons; cholesterol also degrades very slowly (same half-life as astrocytic cholesterol):

$$\frac{dchol_N}{dt} = t_1[ApoE_A] - d_2[cholN]$$

The ApoE that is used to transport cholesterol from astrocytes to neurons is often recycled back to the cell surface and, in combination with ApoE that is generated by neurons, can be used to transport Aβ from the brain to the blood in a two-step process of Aβ binding to ApoE, followed by transport across the blood-brain barrier via LRP-1:

$$\frac{dapoe}{dt} = b_n - k_{f1}[Abeta][apoe]$$

$$+ \left(\frac{k_{f2} + k_{f3}}{\left([Abeta] + \left(\frac{k_{f2} + k_{f3}}{k_{f1}} \right) [LRP] \right)} \right) [LRP][Abeta][apoe]$$

$$+ t_1[ApoE_A] - d_5[apoe]$$

When neuronal cholesterol levels are above threshold, there is only trivial amounts of cholesterol-laden ApoE being transferred to neurons, and thus, very minimal recycling of ApoE back to the surface to be part of the free ApoE pool. The amount of total LRP in the system is assumed to stay at a constant value.

APP Processing:

APP is processed into Aβ via a two-step process by action of beta-secretase, followed by cleavage by gamma-secretase. No difference has been made between the 40 and 42 amino acid length forms. Beta-secretase activity is believed to be regulated by levels of neuronal cholesterol. In this model, we have used the evidence presented by Crameri et al to introduce an inhibitory effect of cholesterol on beta-secretase activity:

$$\frac{dAPP}{dt} = b_1[APP] - k_6[APP]\left(\frac{1}{1 + \beta[cholN]} \right) - d_3[APP]$$

Beta amyloid is produced from this cleavage, but is also degraded via endocytosis or binding and removal by ApoE/LRP-1:

$$\frac{dAbeta}{dt} = k_7[sAPP] - endo[Abeta] - k_{f1}[Abeta][apoe] - k_t[Aeta][LRP]$$

Rate constants for generation and degradation of most key molecules were approximated using data from the literature. Forward binding rates, interaction rates

and the strength of inhibition were all approximated and fitted to create a stable simulation environment. All rates have units of x/day^{-1}. Table 6 describes the rate constants that were used in the model.

Rate	Value (day^{-1})	Rate	Value (day^{-1})	Rate	Value (day^{-1})
k_1	0.9	b_n	2000	t_2	0.5
k_2	0.05	b_a	750	k_{f1}	0.005
k_3	0.05	d_1	0.8	k_{f2}	0.001
k_4	1	d_2	1/1825	k_{f3}	0.005
k_5	1	d_3	0.8336	α	0.001
k_6	1	d_4	8000	β	0.01
k_7	0.8	d_5	1	γ	0.8
a_1	0.9	d_6	0.9	endo	0.25
b_1	1	t_1	1824/1825	k_t	0.00025

Table 6: *Values used for Rate Constants*. Rate constants were derived from the literature or estimated as a fraction of where the output would go. All rate constants were estimated except for the degradation rate of cholesterol (t_1).

Simulation Methodology

The system of equations was solved numerically using ODE45 solver in Matlab. Initial conditions, rate constants, magnitude and frequency of input, and expression levels of different proteins were varied to study their effect on the system and more specifically, on the beta amyloid levels (though increased beta amyloid levels does not inherently imply that the system has shifted to a disease state, simply that the system being modeled is behaving similarly to what is seen in a disease model). The time step for each simulation was a single day. The model was initialized with values that would be found in an average 20 year old and run for a total of approximately 55 years (final age 75 years) to correspond to the time period

when cognitive changes begin to be apparent in individuals who will have Alzheimer's disease or dementia in late life.

Simulation Results

A simulation using all rate constants as described in Table 6 was run as a reference. Convergence was reached for all simulated molecules within the first 6000 days of the simulation. Only APP continued a slowly upward trend during the entirety of the simulation, increasing from an initial value of 1000 to a final value of 1183. Not shown is AcetylCoA levels, which converged from 10,000 to 8845.
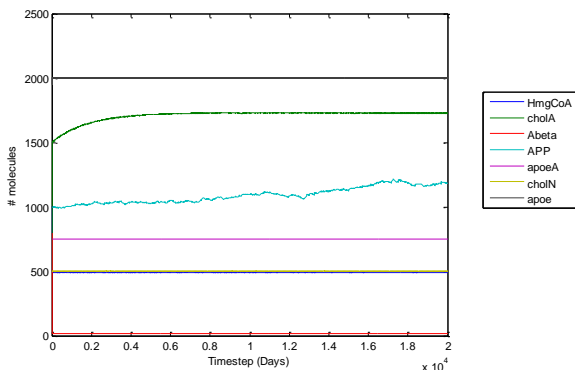
Figure 16: *Reference simulation*. Standard simulation showing a subtle increase in the levels of APP. Only trivial increases in Aβ are noticed.

Effect of increased APP and Aβ generation

Several simulations were run to study the effect that increased initial concentrations of APP or increased generation of Aβ have on the system as a whole. In two cases (increased initial APP concentration and 25% increased Aβ generation rate) led to significant increases in the concentration of APP, and subsequently increased levels of Aβ.
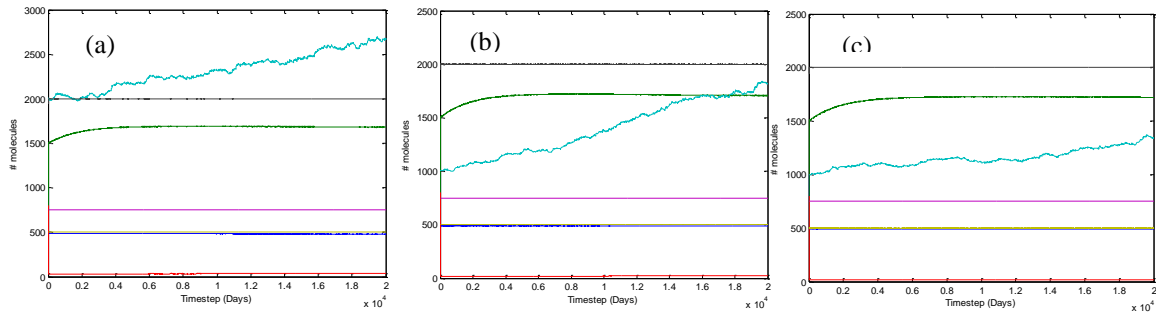
Figure 17: *Effect of Increased Initial APP concentration or increased Aβ cleavage.* (a) Initial APP levels were doubled, leading to a significant increase in the amount of APP and Aβ present in the system. HmgCoA levels began to drop slightly as Aβ levels started to increase. Final APP level: 2672; final Aβ level: 40 (b) Aβ generation rates were increased by 25%, leading APP levels to nearly double. Ironically, Aβ levels did not change significantly. Final APP level: 1821; final Aβ level: 27 (c) Aβ generation rates were increased by 12.5%, leading APP levels to increase slightly. Aβ levels did not change significantly. Final APP level: 1345; final Aβ level: 20

Effect of sinusoidal input functions

Steroids and other molecules derived from cholesterol often have a sinusoidal generation rate related to circadian rhythms. To study the possible effect of oscillatory cholesterol input on the system, we varied cholesterol generation by introducing a periodic generator function. The period of the sinusoid was approximately one day, while the magnitude of the function was varied from 0 to 1 (normal range), 0.25 to 1 (assumes a basal generation rate), and 0 to 2 or 4 (assuming an increase in the cholesterol production). Figure 17 displays simulation results.

Effect of decreased LRP

LRP-1 levels have been shown to be decreased in individuals with AD. To study this, we varied the LRP levels from 25% to 75% of levels used in the reference simulation. Figure 18 displays these results.
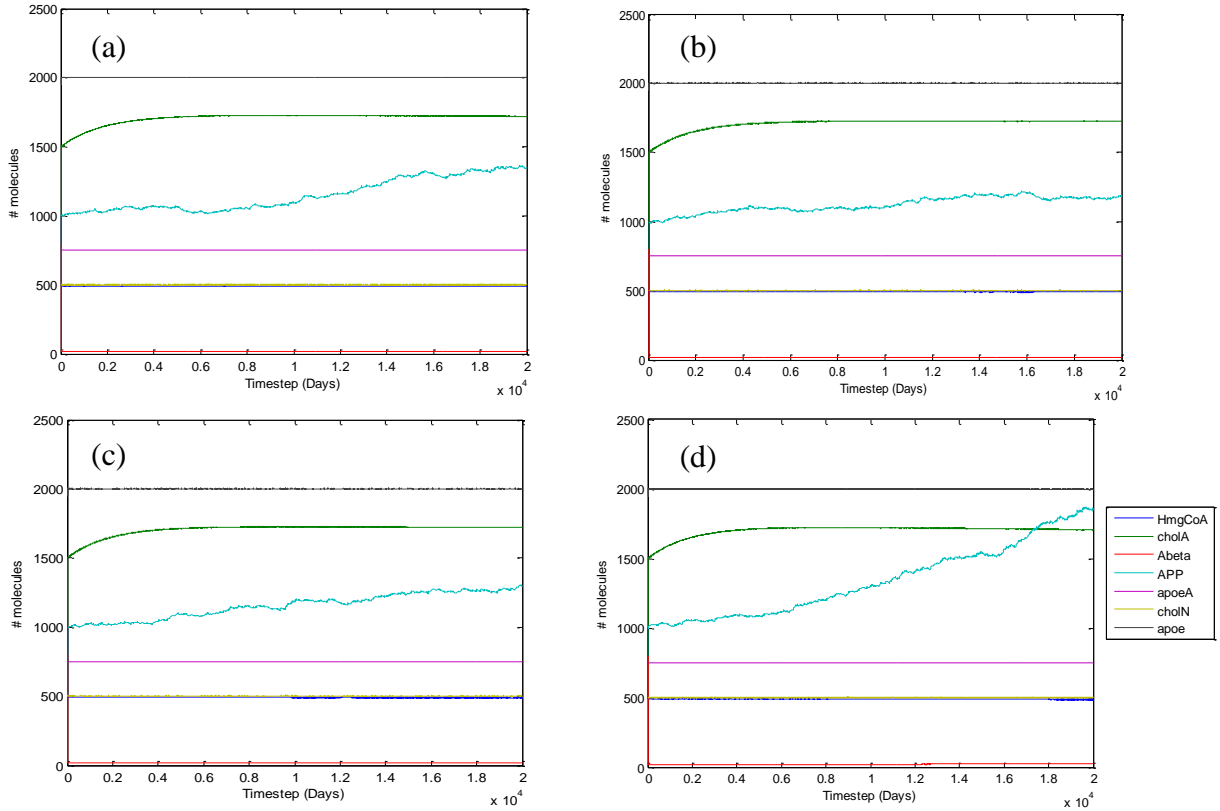
Figure 18: *Effect of Periodic Cholesterol Generation.* (a) Sinusoidal generation of cholesterol assuming a basal generation rate. Magnitude of generation rate varies from 0.25 to 1. $k_5 = 0.375*\sin(2\pi t-\pi/2)+0.625$. Final APP: 1349; final Aβ: 20. (b) Magnitude of generation rate varied from 0 to 1. $k_5 = 0.5\sin(2\pi t-\pi/2)+0.5$. Final APP: 1187; final Aβ: 18. (c) Magnitude of generation rate varied from 0 to 2. $k_5 = \sin(2\pi t-\pi/2)+1$. Final APP: 1297; final Aβ: 19. (d) Magnitude of generation rate varied from 0 to 4. $k_5 = 2\sin(2\pi t-\pi/2)+2$. Final APP: 1858; final Aβ: 27.

Effect of decreased Neuronal Cholesterol

Recently, a lot of interest has been paid to the effect of cholesterol on APP processing and Aβ levels in the brain. Although treatment with a statin is now being studied as a possible treatment paradigm, there are a multitude of conflicting results. In these simulations, the effect of decreased neuronal cholesterol on the system was studied. Specifically, the effect of decreased initial cholesterol concentration, as well as a decrease in the transfer of cholesterol from astrocytes to neurons, was studied. Results are presented in Figure 19.
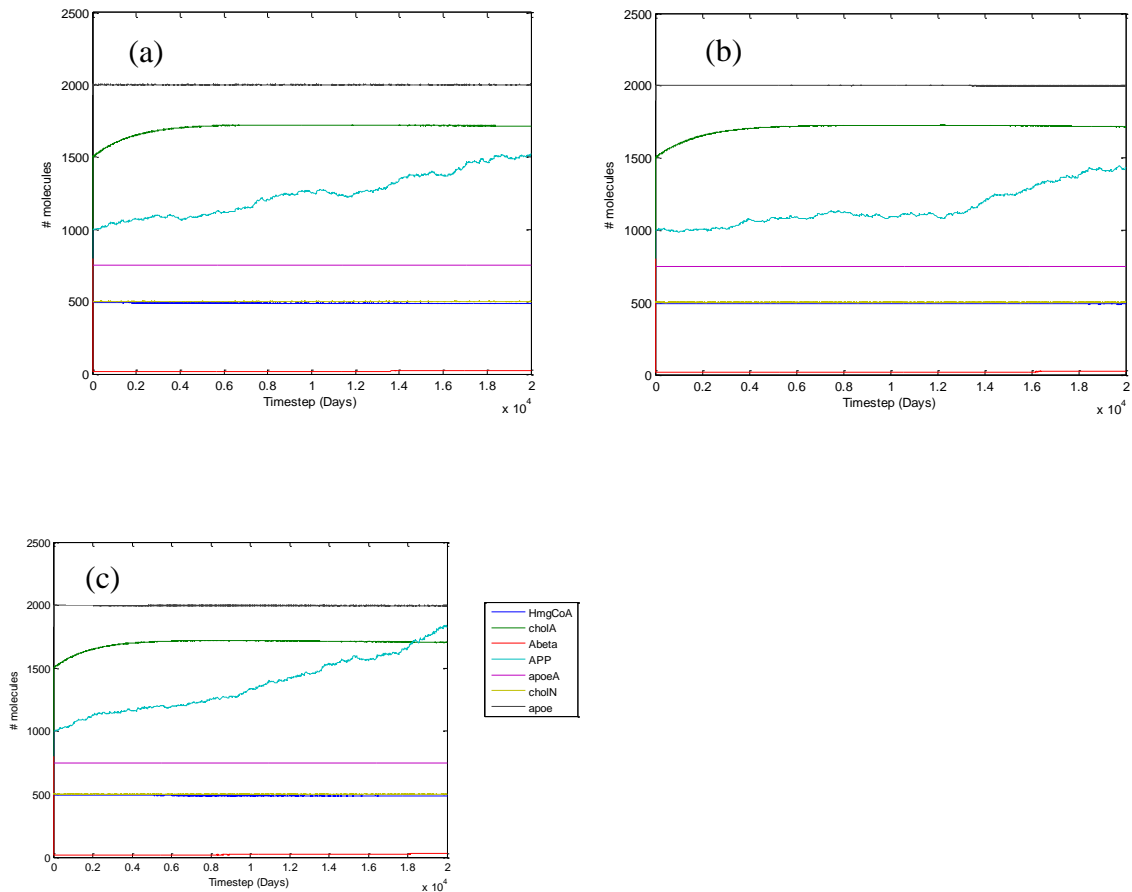

Figure 19: *Effect of Decreased LRP*: (a) LRP levels decreased by 25%. Final APP: 1520; final Aβ: 23. (b) LRP levels decreased by 50%. Final APP: 1431; final Aβ: 22. (c) LRP levels decreased by 75%. Final APP: 1828; final Aβ: 29.
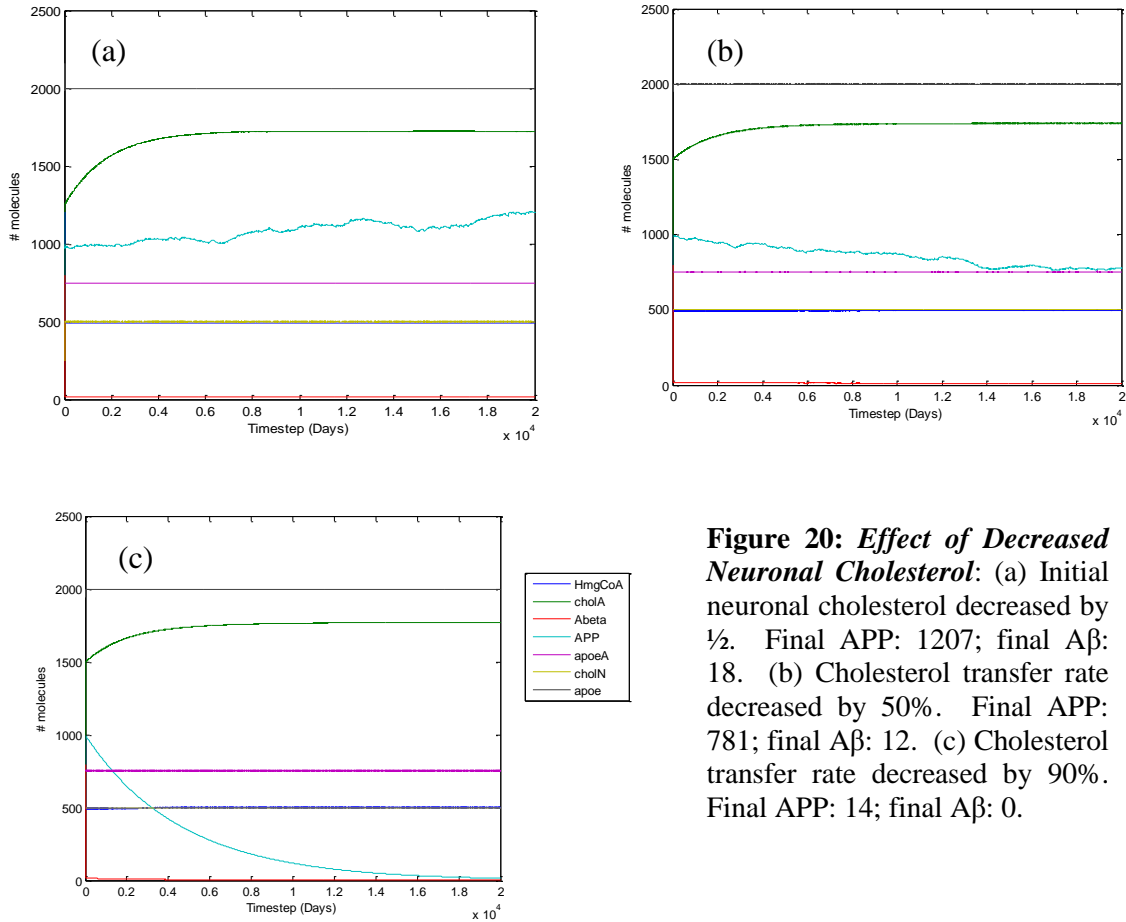
Figure 20: *Effect of Decreased Neuronal Cholesterol*: (a) Initial neuronal cholesterol decreased by ½. Final APP: 1207; final Aβ: 18. (b) Cholesterol transfer rate decreased by 50%. Final APP: 781; final Aβ: 12. (c) Cholesterol transfer rate decreased by 90%. Final APP: 14; final Aβ: 0.

Discussion:

Effect of increased APP and/or Aβ generation:

Increasing the initial concentration of APP led to a significantly increased concentration of APP in the long-term (2672 versus 1183), as well as a nearly double increase in Aβ (40 versus 18). This seems to imply that, at least in this model, there are few mechanisms keeping the APP levels in check, and if a significant increase in APP occurs during the formative years, it may have significant negative consequences years later.

Increasing the generation rate of Aβ by 25% led to a significant increase in the amount of APP in the system. However, the levels of Aβ only increased moderately

(27 versus 18). It is a bit unexpected that the APP levels would increase so dramatically without an equally significant increase in Aβ levels. This could be explained by the fact that Aβ cleavage is a relatively uncommon event in the first place, and that a critical level of APP must be achieved before significant changes in Aβ are also observed. This seems to be a bit counterintuitive and not necessarily in agreement with biological data, since APP levels are not significantly increased in AD, and increases in Aβ are thought to be due more to decreased clearance rather than increased generation. Further studies on this effect, as well as refinement of the model to prevent the increase in APP that is seen over time even in the standard reference simulation.

Effect of sinusoidal input functions:

Oscillatory generation of astrocytic cholesterol led to significant changes in the system output only in the case where the magnitude of the generation rate constant was varied from 0 to 4. This would correlate to 'uncalibrated' generation of cholesterol by astrocytes. This increased level of cholesterol in astrocytes led to an increase in the amount of APP and a moderate increase in Aβ, which was unexpected given the inhibitory regulation that is supposed to exist between cholesterol and APP processing by beta-secretase. Since neuronal cholesterol levels stay approximately constant, and it is these levels that effect APP processing, it may be possible that the increased APP may be due to other factors that have not been directly studied here. It is also interesting to note that the degradation rate for APP was highly sensitive and even small changes from the chosen value could lead to chaos (data not shown). This

in itself may provide some insight into why APP levels may respond to such small changes in other molecules in the system.

Effect of Decreased LRP:

Decreasing LRP-1 levels led to an increase in APP as well as Aβ. This was the expected result since LRP-1 is necessary to clear Aβ from the brain. Future computational models should further subdivide the LRP into neuronal and endothelial to make an even more accurate model.

Effect of Decreased Neuronal Cholesterol:

Decreasing the initial value of neuronal cholesterol did not change the outcome of the system for any of the molecules studied. This was expected, given that a strong feedback loop was used to keep neuronal cholesterol within tight bounds. Future simulations should study the effect of this feedback to get a better idea of its importance in maintaining the system within the realm of stability. Decreasing the rate of transfer of cholesterol from astrocytes to neurons significantly decreased the levels of APP and Aβ. Such a situation might arise if ApoE did not carry cholesterol as well, or if fewer LRP receptors were present on neurons. However, it is interesting to note that even with a decreased efficiency of transfer, neuronal cholesterol levels were maintained at approximately constant levels. Just as in the study of the effects of oscillatory cholesterol production by astrocytes, the sensitivity of the APP reaction may be the cause of the observed increase in APP and Aβ.

Conclusion:

In this section, we have presented one of the first systems biology models for Alzheimer's disease. We have studied in computational detail the interactions between cholesterol, ApoE, LRP-1 and Aβ. Simulation results showed several unexpected phenomena, including a decrease in APP and Aβ when the transfer rate of cholesterol between astrocytes and neurons is decreased. These results show that cholesterol and LRP levels play significant roles in the development of increased Aβ levels in the brain, one of the key markers for AD. Future models should study these effects in further detail and incorporate aspects of inflammation that are believed to play a role in AD pathogenesis.

Chapter 5: Biological Experiments

Simvastatin Treatment:

C57BLK mice on a mixed background (n= 44, donated by Dr. Mary Ann Ottinger), as well as B6C3-Tg(APPswe, PSEN1dE9)85Dbo/J mice (n=13, Jackson Laboratories) were used in experiments. These mice contained a double transgene for APP/PS1, which has been shown to lead to plaque development by 6 months of age, and cognitive impairments soon after. An equal number of age-matched controls were also obtained. Mice were treated with 100 mg/kg/day of simvastatin (Fisher Scientific) for either 2 or 8 weeks, in addition to normal chow and free-range water. Mice were weighed initially to ascertain that the correct dosage per weight was being given. Simvastatin was diluted into 40% Tween-20 to ensure accurate dosage in each mouse, and mixed with peanut butter to be more palpable (Giant brand natural peanut butter, Greenbelt, MD). Control mice received peanut butter loaded only with the 40% Tween-20 daily for the duration of the trial. The same control animals were used for both the 2 week and the 8 week trials.

Group	Treatment (with simvastatin)		# in each group
Control (wild-type) mice	Short (2 weeks)	No treatment	N = 2 for WB
		100 mg/kg	N = 10 for WB N = 2 for IHC
	Long (8 weeks)	No treatment	N = 4 for WB N = 2 for IHC
		100 mg/kg	N = 5 for WB N = 2 for IHC
APPswe;PS1ΔE9 transgenic mice	Short (2 weeks)	No treatment	N = 1 for WB
		100 mg/kg	N = 7 for WB N = 2 for IHC
	Long (8 weeks)	No treatment	N = 2 for IHC
		100 mg/kg	N = 6 for WB N = 2 for IHC

Table 7: *Treatment table summarizing mice usage in simvastatin trial*. Distribution of mice into specified treatment groups and breakdown of numbers used for the Western blotting (WB) and immunohistochemistry (IHC).

Measurement of serum 24S-hydroxycholesterol:

Blood from terminal mouse bleeds was collected from mice, separated using a serum separation tube and stored at -80C until further processing. To isolate the sterol components of the serum, a previously developed protocol was modified. Briefly, serum was thawed to room temperature and 50 μL of serum was spiked with 24S-hydroxycholesterol- d_7 internal standard (Avanti Lipids) at a concentration of 4 ppm. Samples were saponified for 1 hour at 37°C after addition of 200 μl of 0.9 M sodium hydroxide (diluted in 90% ethanol in water). The saponification product was diluted into 100 μl of aqueous sodium chloride and the organic layer was extracted using 700 μl of hexane and dried by applying light flow of nitrogen gas. Prior to being running through HPLC, the dried product was dissolved into 10 μl of the mobile phase (methanol at a 14:1 ratio with deionized water).

An AccuTOF-CS ESI-TOF (electrospray ionization time of flight) mass spectrometer equipped with an atmospheric pressure chemical ionization (APCI) source was used to run HPLC samples. The protocol used here was modified from a previously developed protocol for detecting 24S-hydroxycholesterol from plasma samples [40]. The ionization interface was operated in the positive mode using the following settings: desolving chamber temperature, 350 °C; oriface temperature, 100 °C; corona discharge current, 4kV; chamber pressure, 49 barr; flow rate, 0.250 ml/min. The LC-MS system was composed of an in-line auto-sampler and HPLC pump. Oxysterols were separated using a C18 RP-HPLC column. The HPLC column temperature was room temperature (25 °C). The mobile phase consisted of methanol/water (14:1 by volume), delivered at a flow rate of 0.25 ml/min. A 20

minute column wash was included. The injection volume was 10 ul in mobile phase. A single pole MS system to monitor for specific elution times in reference to the standards elution time, as well as m/z of 305, 329, 330, 367, 373/374 and 385. The 385 and 367 mass-to-charge ratios were barely detectable in the majority of samples, so are not included in the final data set that was analyzed.

Measurement of total serum cholesterol:

Blood from mice (50-100 μL/mouse) was taken prior to initiation of treatment via saphenous vein bleeding. Initially, bi-weekly bleeding was done for several mice, though bleeding was stopped when a few mice (n=2) became infected and ill. Terminal blood was collected immediately after sacrifice to determine the value of the final cholesterol concentration. Blood was collected into serum separator tubes (Becton Dickinson, Franklin Lakes, NJ, US) to separate serum from red blood cells, and spun on a table-top centrifuge kept at 4°C for 10 minutes at 4000 rpm. Samples were then stored at -80°C until further usage.

Serum cholesterol levels were measured using the Amplex Red Cholesterol Assay (Invitrogen, CA). Briefly, standard cholesterol solutions were prepared using the supplied cholesterol stock solution and used to create a standard curve (Range: 0-25 μg/μL). Sample serum was diluted 1:100 in reaction buffer and mixed with the Amplex Red solution, before being incubated for 30 minutes in a hot water bath kept at 37°C. Detergents in the reaction buffer (Triton-X) prevented the formation of large aggregates of lipid-soluble molecules. Following incubation, fluorescence intensity of samples was measured using a plate reader with fluorescence reading abilities

(Molecular Devices SpectraMax5 microplate reader, Sunnyvale, CA, US; excitation/emission: 540/580 nm).

Western Blotting:

Western blotting was performed using standard procedures to assay for the approximate expression levels of several proteins of interest: *synaptophysin* (Sy38, pre-synaptic marker); *post-synaptic density 95* (PSD95, post-synaptic marker, used with Sy38 to quantify if changes in synaptic density occur); *apolipoprotein E* (ApoE); *glial fibrillary acidic protein* (GFAP, astrocytic and inflammatory level marker); l*ow density lipoprotein receptor-related protein* (LRP-1); *amyloid precursor protein* (APP) and *beta amyloid* (Aβ). These levels were assessed to study how they changed during simvastatin treatment, as well as to gather key data for development of more realistic concentration ratios and constants used in the systems biology math model.

Samples were prepared using the following protocol. Briefly, six hours following the final treatment, mice were sedated using isoflurane and sacrificed via decapitation. Immediately following sacrifice and terminal bleeding, brains were excised and the hippocampus was isolated. Both the hippocampus and the whole brain (minus the cerebellum and meninges) were transferred to a pre-chilled centrifuge tube and frozen at -80^0C until further usage.

To prepare samples for Western blotting, brain tissue was thawed to room temperature and 500 μL of ice-sold lysis buffer containing 10 U/ml protease inhibitor was added (Sigma). Samples were then sonicated to homogenize tissue, followed by centrifugation at 1,000 rpm for 10 minutes at 4^0C to remove unhomogenized tissue. Protein content of the supernatant was assayed by mixing 10 μL of sample with 500

μL of Coomassie reagent and measuring the absorbance at 595 nm. Bovine serum albumin protein standards (0-2 mg/ml) were also assayed to calculate the approximate protein concentration in samples. Samples were then mixed with 1x GSB and normalized to 1-3 mg/ml of protein.

Several different gels were used to run the Western, depending on which protein was being assayed. Higher molecular weight proteins (APP, LRP) were run on 6% gels, lower molecular weight proteins (Sy38, PSD 95, ApoE, GFAP) were run on 10% gels, and beta amyloid Westerns were run on 4-20% gradient gels (Bio-Rad, Hercules, CA). All gels were run in triplicate using one of three loading schema to account for possible variations in running or transfer conditions due to instrumentation or other factors associated with the gel boxes.

Twenty micrograms of protein was loaded into each sample lane (30 μg for Aβ gels); a standard ladder was also loaded onto each gel (ECL-Plex ladder, GE Healthcare, Piscataway, NJ, US) and the appropriate standard for each protein. Beta amyloid gels were run at 100 V for 40 minutes in MES buffer (2-[morpholino]ethanesulfonic acid buffer, 20x, Fisher Scientific, Pittsburgh, PA, US). Samples were specially prepared to contain 100 mM DTT (dithiothreitol) as a reducing agent (1.54 μl of 1 mg/ml stock DTT into 100 μl of sample). Blots were transferred using standard transfer buffer (3 g Tris base, 14.4 g glycine, diluted into 1600 ml ddH2O, brought up to 2 L with methanol) at room temperature kept under ice for 60 minutes. All other gels were run at 100 V for 75 minutes using standard running buffer (25 mM Tris base, 250 mM glycine, 0.1 % w/v SDS, pH 8.3) and transferred using standard transfer buffer for 75 minutes kept under ice. In both

cases, gels were transferred to nitrocellulose membranes that had been pre-wet in methanol.

Following transfer, blots were incubated in blocking solution (1% bovine serum albumin, 0.1% Tween-20 into 1x phosphate buffer solution) for 1 hour at room temperature, agitated gently on a shaker. Blots were then incubated in primary antibody overnight on a shaker at 4°C. After primary incubation, blots were rinsed 3 times for 5 minutes each in blocking solution, incubated for 1.5 hours in the appropriate secondary antibody (mouse Cy3/Cy5, rabbit Cy3/Cy5, AlexaFluor 555 goat-anti-chicken secondary, or AlexaFluor 633 donkey-anti-goat secondary) and rinsed 3 additional times for 5 minutes each in blocking solution before being imaged with a blot scanner (Typhoon Scanner, GE Healthcare, Piscataway, NJ, US). The following table describes in further detail the primary and corresponding secondary antibodies that were used.

Analysis of Western Blot Data

Data was analyzed using ImageQuant software (GE Healthcare, Piscataway, NJ, US). Briefly, scanned gel images were loaded into the software program, lanes were manually created, the background was thresholded to remove noise, and the intensity of the band in each lane was measured. Values were tabulated and saved in an Excel file for further statistical analysis.

Immunohistochemistry

Immunohistochemistry was performed to determine the cellular localization of ApoE in astrocytes in response to simvastatin treatment; the relative density of LRP-1 in cerebral blood vessels in treated and untreated mice; and the extent of Aβ plaque

load. All protocols described below were approved by the University of Maryland IACUC committee (protocol #R10-21, renewed March 2011). Briefly, mice were anesthetized using isoflurane, the thoracic cavity was accessed and 20 ml pre-warmed PBS was injected into the left ventricle following puncture of the right atrium to clear blood from the vessels and allow for a better perfusion. Terminal blood was collected in serum separator tubes prior to pumping of the pre-warmed PBS and stored as described previously.

Protein	Primary Antibody	Dilution	Secondary Antibody	Dilution
Synaptophysin	Sy38 (*mouse monoclonal, Abcam, ab8049*)	1:500	Mcy5	1:2500
Post-synaptic density marker	PSD95 (*rabbit polyclonal, Abcam, ab18258*)	1:500	RCy3	1:2500
ApoE	apoE (*rabbit polyclonal, Santa Cruz Biotech, M-293*)	1:200	RCy5	1:2500
GFAP	GFAP (*chicken polyclonal, Abcam, ab4674*)	1:5000	AlexaFluor555 goat anti-chicken (*Invitrogen*)	1:1000
LRP	LRP (*goat polyclonal, Santa Cruz Biotech, N-20*)	1:200	AlexaFluor633 donkey anti-goat (*Invitrogen*)	1:1000
APP	APP (*rabbit polyclonal, Abcam, ab2072*)	1:1000	RCy5	1:2500
Aβ	6E10 (*Covance*)	1:1000	MCy5	1:2500

Table 8: *Summary of antibodies used in Western blotting*.

After completion of injection of PBS, mice were fixed with 4% paraformaldehyde (PFA; Fisher Scientific), decapitated and the brain was removed. The cerebellum was removed and the remaining portions of the brain were placed into 4% PFA overnight to ensure complete fixation. Brains were then sunk in 30% sucrose (diluted in 0.1 M phosphate buffer) overnight at 4˚C. The following day, brains were rinsed in 30% sucrose, extraneous material was removed, and the brain

was mounted on a freezing microtome with a sucrose stand. Twenty μm slices were obtained and stored in cryoprotectant at -20˚C until further usage.

On the day of primary incubation, 20 slices from each treatment group (10 slices per mouse; n =2 for each immunohistochemistry group) were thawed at room temperature briefly before being rinsed 4 times for 5 minutes each in 1x PBS at room temperature. Sections were then permeabilized by incubating in 2% Triton-X in sodium phosphate buffer for 1 hour at room temperature. Following permeabilization, slices were incubated in ice cold methanol for 10 minutes to quench background signal. Slices were then rinsed again 4 times for 5 minutes each in 1x PBS on a gentle rotator and incubated for 1 hour in blocking solution (10% normal donkey serum, 1% Triton-X, 4% BSA in 1x PBS) at room temperature. Finally, sections were incubated in primary antibody overnight, either at room temperature or at 4˚C. All primary antibodies were diluted into the same blocking solution consisting of 1.5 ml normal donkey serum, 0.5 ml 20% Triton-X, and 6 ml of 10% BSA into 7.35 ml of 1x PBS.

Following primary incubation, slices were rinsed 4 times for 5 minutes each in 1x PBS to remove excess primary antibody, incubated in the appropriate secondary antibody in blocking solution (1.5% normal donkey serum in 1x PBS) for 2 hours at room temperature on a gentle rocker, protected from light, and rinsed again after incubation (4x for 5 minutes each time). Slices were incubated for ten additional minutes prior to being mounted on superfrost slides (Fisher Scientific, Pittsburgh, PA; pre-cleaned with 70% ethanol) and air-dried overnight protected from light. DAPI (1:100 dilution, Invitrogen, Carlsbad, CA, US) was added to beta amyloid slices 10

minutes prior to the secondary antibody incubation ending. The next day, slices were cover-slipped with mounting solution (ProLong Gold Anti-fade mounting solution, Invitrogen), excess mounting solution was removed with Kimwipes, and allowed to dry overnight. Cover-slipped slides were sealed with clear nail polish. The following tables describe in further detail the antibodies that were used for each set of slices and the incubation conditions.

Purpose of Staining	Primary Antibody	Dilution	Incubation Conditions	Secondary Antibody	Dilution
Label ApoE in neurons and astrocytes	apoE GFAP NeuN	1:50 1:500 1:100	Overnight, 25°C	Donkey anti-rabbit 488 Goat anti-chicken 555 Donkey anti-mouse 450	1:500 1:200 1:200
Label LRP-1 levels in cerebral blood vessels	LRP CD31 NeuN	1:50 1:50 1:100	Overnight, 4°C	Donkey anti-goat 633 Donkey anti-rabbit 488 Donkey anti-mouse 450	1:200 1:500 1:200
Quantify Aβ plaque density	6E10 DAPI	1:500 1:100	Overnight, 4°C (DAPI for 10 minutes)	Donkey anti-mouse 450	1:200

Antibody	Clonality	Vendor/Catalog #	Antibody	Clonality	Vendor/Catalog #
GFAP	Chicken polyclonal	Abcam/ab4674	CD31	Rabbit polyclonal	Abcam/ab28364
ApoE	Rabbit polyclonal	Santa Cruz Biotech/M-293	Aβ	Mouse monoclonal	Covance/6E10
LRP	Goat polyclonal	Santa Cruz Biotech/N-20	NeuN	Mouse monoclonal	Millipore/MAB377

Table 9: (Top) Details on dilution and incubation conditions used for immuno-histochemistry. (Bottom) Clonality and suppliers for antibodies that were used.

Imaging Acquisition & Analysis

Immunohistochemistry sections (n= 360, ~120 per group) were imaged using a Zeiss LSM confocal microscope (Zeiss, Germany). ApoE and LRP sections were imaged with a 40x oil objective, while Aβ sections were imaged with a 10x objective. The CA1 region of the hippocampus was identified with the visual view and

subsequently imaged. Images were taken with Zeiss software program, at 1024 x 1024 bits set at speed 6 to optimize the resolution of the image. Overall image area was 212.3 x 212.3 μm. pixel size was set to 0.21 μm. Images quantifying the levels of LRP used the 405, 488 and 633 lasers at the following settings: **405:** laser power was set to 4.0, pinhole was 47.6, gain was 626, offset was -7 and digital gain was 1.1; **488:** laser power was set to 1.8, pinhole was 47.6, gain was 790, offset was -1 and digital gain was 1.2; **633:** laser power was set to 15.0, pinhole was 47.6, gain was 727, offset was -8 and digital gain was 1.0. For GFAP images, laser settings were as follows: **405:** laser power was set to 4.0, pinhole was 57.7, gain was 556, offset was -7 and digital gain was 1.3; **488:** laser power was set to 1.8, pinhole was 57.7, gain was 597, offset was -8 and digital gain was 1.3; **555:** laser power was set to 1.5, pinhole was 57.7, gain was 431, offset was -5 and digital gain was 1.2. For beta amyloid images, only the 405 and 633 lasers were used: **405:** laser power was set to 4.0, pinhole was 47.6, gain was 735, offset was -6 and digital gain was 1.1; **633:** laser power was set to 15.0, pinhole was 47.6, gain was 660, offset was -7 and digital gain was 1.0.

Images were analyzed using the software program Volocity (PerkinElmer, Waltham, MA, US). For ApoE and LRP slices, image stacks were loaded into Volocity, images were split into their corresponding z stacks by channel, and the four images with the highest signal intensity for ApoE and LRP were selected and re-merged. A protocol was then created to identify all regions of that image where astrocytes (stained by GFAP; red channel) and cerebral blood vessels (stained by CD31; green channel) were. The protocol computed the intensity the opposing

99

channel within the identified region (red and green channels for both ApoE and LRP sections), and the sum of this intensity was calculated for each image. The total volume of the image was also calculated and used to determine the overlapping intensities between the two channels per volume (effective "co-localization" density).

Cholesterol & 24S-hydroxycholesterol levels in plasma

Data from the cholesterol assay was tabulated and analyzed using Excel. Cholesterol values derived from brain samples were normalized against the µg of protein in the sample, while plasma samples were simply measured in µg/ml of plasma. A standard control curve was obtained and all sample fluorescence values were normalized to this curve and the concentration adjusted to account for differences in dilution.

Data from the brain cholesterol assay was analyzed using Excel. Normality of data sets was assessed using the histogram function. Bar graphs were used to visualize data. Brain cholesterol levels were analyzed using a single factor ANOVA for each genotype of mice. There was no statistically significant difference in the brain cholesterol levels for APP mice, regardless of treatment regime. Conversely, WT mice had statistically significant differences at 90% confidence levels (F=3.013, p-value = 0.072). This was further verified by t-tests, which showed that the differences between both the 2 week treatment and 8 week treatment groups were statistically significant at 90% confidence (for 2 week: t = 1.82, p-value<0.056; for 8 week: t= 1.48, p-value<0.087). This seems to suggest that treatment with simvastatin affected the WT mice differently than the transgenic APP mice, leading to decreased

levels of brain cholesterol in WT mice. An increased sample size in future

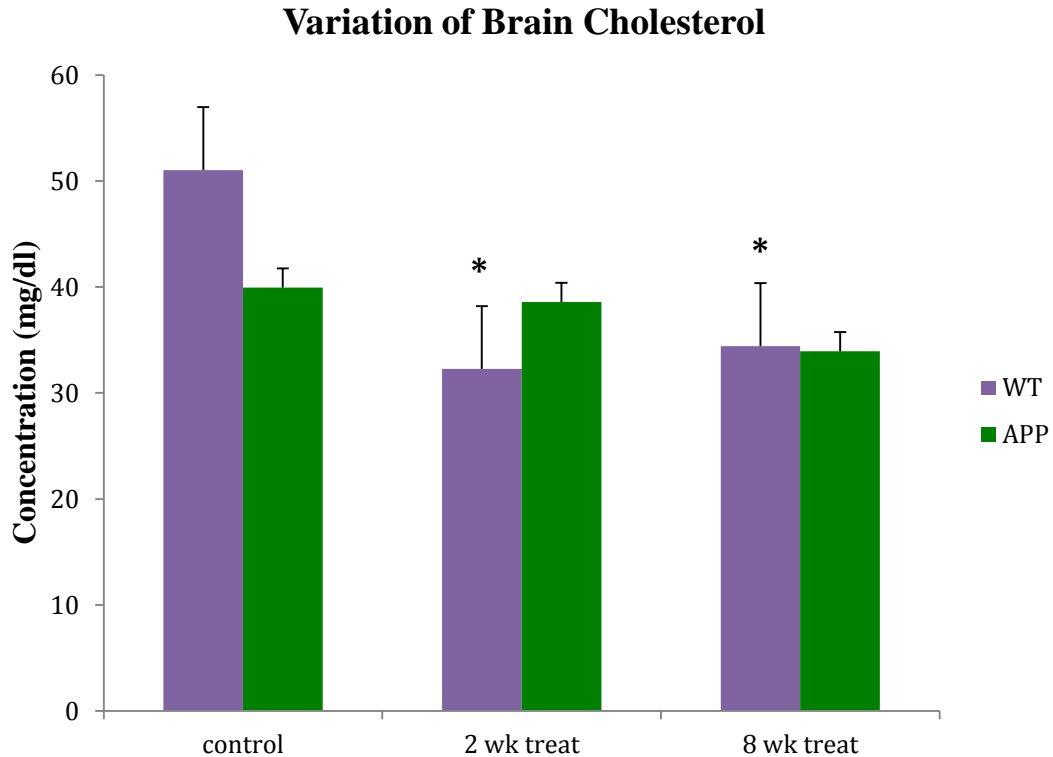experiments will help to elucidate this role further.

Variation of Brain Cholesterol

Figure 21: *Variation of Brain Cholesterol Levels*. Cholesterol assay data was visualized using histograms to check whether or not the data was normal and could be analyzed using ANOVA and other parametric tests. Only wild-type mice treated with simvastatin for 2 or 8 weeks showed a statistically significant decrease in brain cholesterol levels (for 2 week: t = 1.82, p-value<0.056; for 8 week: t= 1.48, p-value<0.087). No statistically significant variation was observed in APP transgenic mice. Simvastatin treatment appears to decrease the overall variability in the brain cholesterol level across both wild-type and transgenic mice. Long-term treatment with simvastatin does not appear to lead to substantial and maintained changes in APP transgenic mice.

A single factor ANOVA done on wild-type and transgenic groups separately

demonstrated that both pre-treatment groups had no statistical difference between the

mean values across any treatment group (for WT: F = 0.435, p-value = 0.655; for

APP: F = 0.49, p-value = 0.622). This implies that all groups of mice started out with

approximately the same level of total plasma cholesterol. Single-factor ANOVA on post-treatment WT and APP groups demonstrated that means across the three treatment groups varied with 95% and 90% confidence, respectively (for WT: $F = 6.53$, p-value = 0.009; for APP: $F = 3.307$, p-value = .057). Further analysis with t-tests showed that only the 2 week APP treatment group was statistically different from the control APP group ($t = 2.609$, one-tail P-value=0.0114, 95% significance). All other control versus treatment group t-tests showed no statistical significance; the control versus 2 week WT treatment group was statistically significant at 90% significance ($t = 1.898$, P-value=0.0532) but not at 95% significance. One reason for the statistical indifference in our data set is the small sample size that was used. Increasing the sample size will help to minimize the variation and is suggested for future experiments.

The differences between the mean pre- and post-treatment values were also analyzed using ANOVA and t-tests. In this case, differences in means across the APP transgenic group were statistically significant ($F = 5.177$, p-value < 0.022), whereas differences across the WT groups were not ($F = 2.34$, p-value < 0.167). Only the 2 week APP treatment group showed statistical significance in differences in mean pre- and post-treatment plasma TC values ($t = 3.522$, p-value < 0.012), suggesting that treatment with simvastatin for 2 weeks in transgenic mice was able to prevent the observed increase in plasma total cholesterol (TC). All other groups were statistically insignificant. Although a similar trend is observed in the WT data set in terms of a decreased mean post-treatment TC at 2 weeks, due to the relatively large variability in this dataset it was not statistically significant.
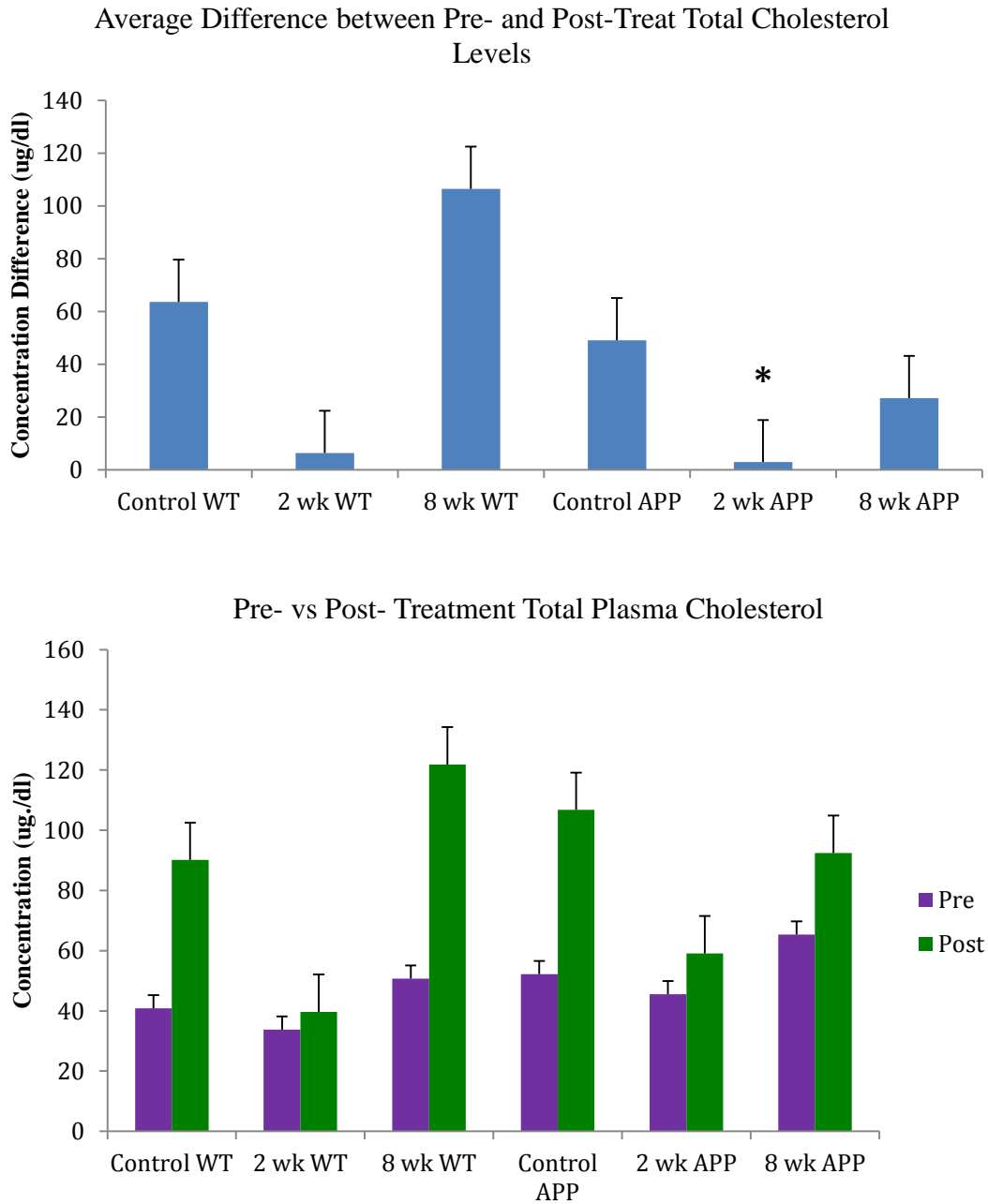
Average Difference between Pre- and Post-Treat Total Cholesterol Levels

Pre- vs Post- Treatment Total Plasma Cholesterol

Figure 22: *Differences between Pre- and Post-Treatment Plasma Cholesterol*. Plasma cholesterol levels (mg/dl) were measured at an initial time point before treatment was started, and then again terminally to study how cholesterol levels changed over the course of treatment. In all groups studied, the cholesterol levels increased between the initial and the final measured time points. This could be due to the high fat content of peanut butter. Although there is an increase in plasma cholesterol in all groups, the magnitude of this difference in statistically significant in the APP transgenic mice ($F = 5.176$, p-value $= 0.022$, $\alpha = 0.05$), and more specifically, this difference exists between the control and 2 week treatment group ($t = 3.522$, p-value $= 0.0122$, $\alpha = 0.05$).

Correlation between total plasma cholesterol and total brain cholesterol levels, as well as between total plasma cholesterol levels and age of the mice during treatment was investigated. No significant correlation existed between pre- and post-treatment plasma cholesterol levels (linear regression, $R^2 = 0.1784$). Plotting total plasma cholesterol versus total brain cholesterol for all samples that could be matched revealed only a very weak positive correlation between total plasma cholesterol levels and total brain cholesterol levels ($R^2 = 0.2002$), indicating that increased plasma total cholesterol levels were associated with a minor increase in brain total cholesterol levels across all groups.

Correlation between Pre- and Post-Treatment Total Cholesterol Levels

Correlation between Plasma TC and Brain TC
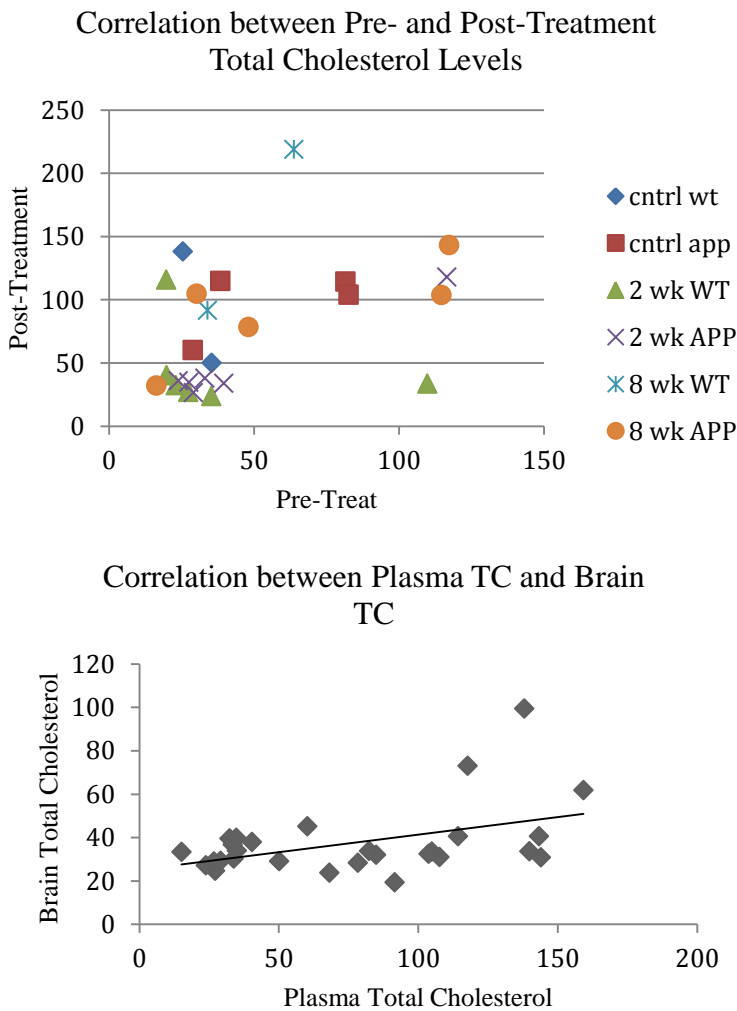
Figure 23: *Correlation between Plasma Cholesterol and Brain Cholesterol Levels*. (top inset) Pre- and post-treatment total plasma cholesterol levels were plotted to determine if any correlation existed between the pre- and post- treatment values. A weak positive correlation was found ($R^2 = 0.1784$), suggesting that higher values of pre-treatment cholesterol led to a more significant increase in post-treatment cholesterol levels. (bottom inset) Correlation between post-treatment plasma cholesterol levels and brain cholesterol levels also showed a weak positive correlation ($R^2 = 0.2002$), suggesting that increased plasma cholesterol levels may affect brain cholesterol levels. However, removing the few data points that appear to be outliers (n=2), this correlation all but disappears and is therefore more an artifact of relatively small sample size.

Correlation analysis was also completed by separating the data by treatment group (WT and APP grouped together). It can be seen that the majority of the 2 week treatment group is clustered in the lower left corner, indicating that the data has the least variation of the three treatment groups, as well as a limited range of values. In this sense, treatment of either WT or transgenic mice with simvastatin seemed to normalize the effect between plasma cholesterol and brain cholesterol. Analogously, the 8 week treatment group had a wide range for possible plasma total cholesterol values, but a very limited range on the corresponding brain cholesterol values, demonstrating that simvastatin treatment provides a normalizing or convergent effect on brain cholesterol levels. Although the means in total brain cholesterol were not statistically different between the treatment groups for either the WT or the APP transgenic groups, the variability between measurements was decreased. Correlation data showed weak positive correlation: control: $R^2 = 0.2848$; 2 week treat: $R^2 = 0.248$; 8 week treat: $R^2 = 0.3631$. In the future, a larger sample size would help to possibly eliminate some of the variability that is seen here, as well as in other data sets. The regression data also seems to suggest that as plasma cholesterol increases, total brain cholesterol increases mildly, though more sample data is needed to draw such a statistical conclusion.

Lastly, age versus cholesterol levels was studied. To determine whether the observed increase in post-treatment plasma cholesterol in the control and 8 week treatment groups was due to increasing age, a scatter plot of the data was done for both pre- and post-treatment cholesterol as a function of age, as well as scatter plots for pre-treatment only and post-treatment only. Correlation analysis revealed no
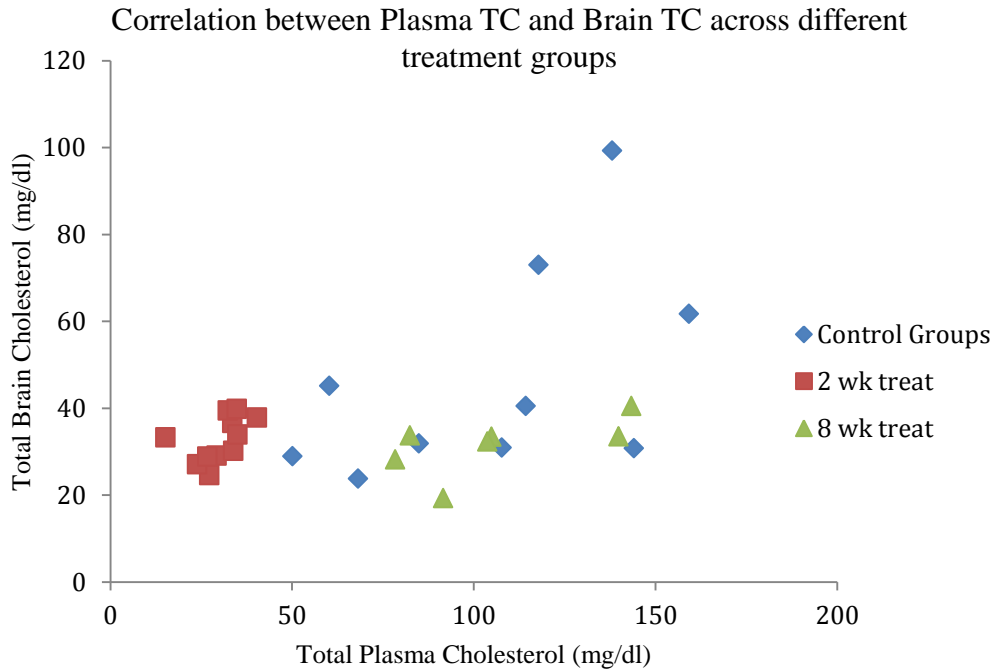
Figure 24: *Correlation between Plasma and Brain Total Cholesterol*. Brain cholesterol levels (mg/dl) were plotted as a function of post-treatment total plasma cholesterol levels. Very weak correlation was found between plasma cholesterol and brain cholesterol levels (***control***: $R^2 = 0.2848$; **2 week treat**: $R^2 = 0.248$; **8 week treat**: $R^2 = 0.3631$), which, upon removal of outliers, disappeared. This suggests that the correlation seen here between plasma cholesterol levels and brain cholesterol levels is quite weak and would need a larger sample size to verify its accuracy. The data here do show though that treatment of mice with simvastatin appears to decrease the variability in the brain cholesterol levels when compared to control treated mice.

linear correlation between age and total plasma cholesterol levels in either the pre- or post-treatment groups (for pre: $R^2 = 0.0113$, negative correlation; for post: $R^2 = 0.0012$, positive correlation), suggesting that plasma TC levels are independent of mouse age. This independence of age from plasma TC is most apparent in the pre-treatment group, where mice of the same age at starting have significant variability in their plasma TC levels (41 weeks in the pre-treatment scatter plot is a good example of this). This variability in plasma TC levels also appears to be independent of genotype. Looking at the post-treatment TC by treatment group, the correlation between age and TC levels seems to be mixed. Control WT, 2 week APP, 8 week

APP have mild negative correlations (R^2 = 0.054, 0.0086 and 0.1664, respectively), while control APP, 2 week WT, and 8 week WT have positive correlations (R^2 = 0.3706, 0.1499, and 0.3784, respectively). The only statistically relevant correlations are control APP and 8 week WT. This implies, like the net data analyzed above, that there is no distinct correlation between age of the mouse and level of brain total cholesterol.

Other confounding factors may also have been at play. For example, there were some issues with the 8 week treatment mice that they adjusted to the peanut butter with drug and refused to eat duped peanut butter samples. Although this was overcome by dosing the mice briefly with drug in baby food, this may have had an unexpected effect on our outcomes for this group. The increase in cholesterol may have been due to an age-dependent effect, as has been suggested; however, there is not statistically relevant data in this sample to make that conclusion. Another factor that may have been at play is the fact that peanut butter, due to its high fat content, is expected to increase cholesterol over long term treatment. Within the shorter time periods, this increase in fat in the mouse's diet should not have had an effect on the plasma cholesterol values. The exact time point when this mild increase in fat to the mice's diet would lead to increased cholesterol levels has not been investigated for the mice that were used here. Also, although mice were age-matched for final time points, the initial blood draw occurred immediately before the group was started on treatment (either 2 or 8 weeks before treatment finished). This may have led to different rates of changes in the plasma cholesterol depending on the age of the animal. There are several data points in the control samples (n=4 in WT; n = 2 in

APP) that were treated as control (peanut butter plus Tween-20 only) for 2 week periods of time. These samples show a normal pre-treatment value for TC, with a qualitative increase in final TC levels equal to or greater than mice that had been on treatment for the entire 8 week period. Finally, the increased cholesterol in the 8 week treatment group may have been caused by a 'rebounding' effect often seen in human subjects treated with statins longer than 12 months [50]. Previous studies have also shown that a similar simvastatin dosage does not actually lead to decreased plasma cholesterol, and in apoE null mice, actually leads to an increase in plasma cholesterol after only 4 weeks of treatment [29].
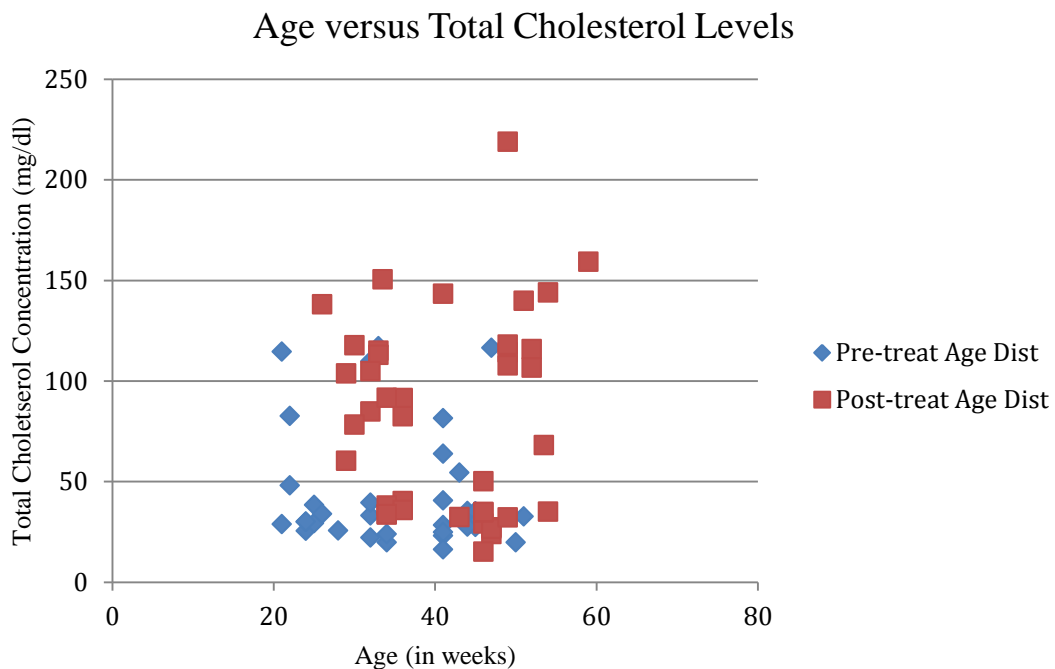
Figure 25: *Average Cholesterol as a Function of Age*. Brain cholesterol levels (mg/dl) were plotted as a function of the age of mice before and after treatment. No correlation was found between age and total post-treatment plasma cholesterol levels (for pre: R^2 = 0.0113, negative correlation; for post: R^2 = 0.0012, positive correlation), suggesting that plasma cholesterol levels are independent of age and that the observed increases in plasma cholesterol seen in mice are due to treatment with peanut butter, as opposed to an increase associated with aging in mice.
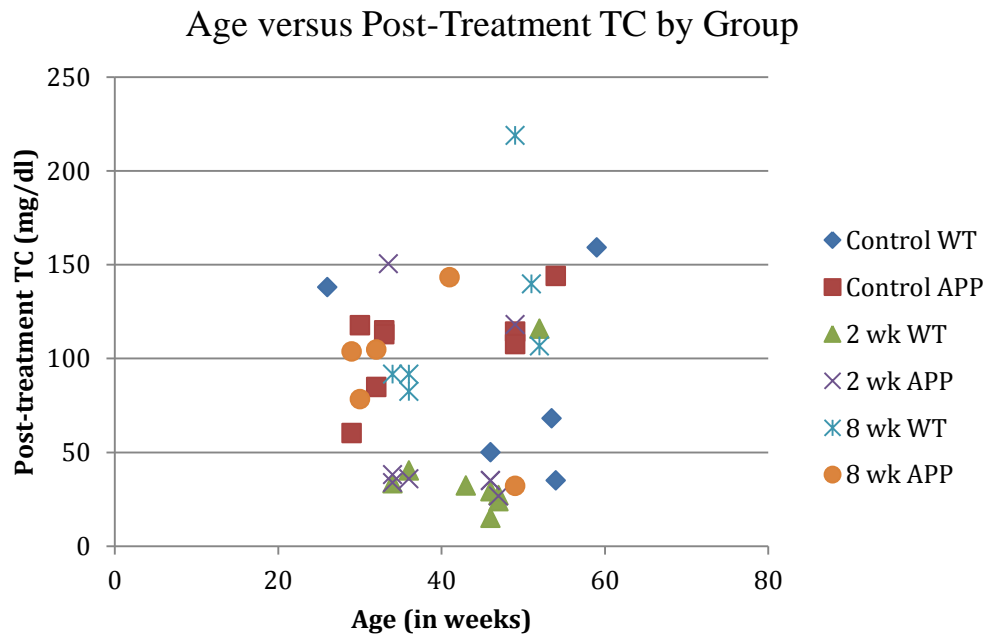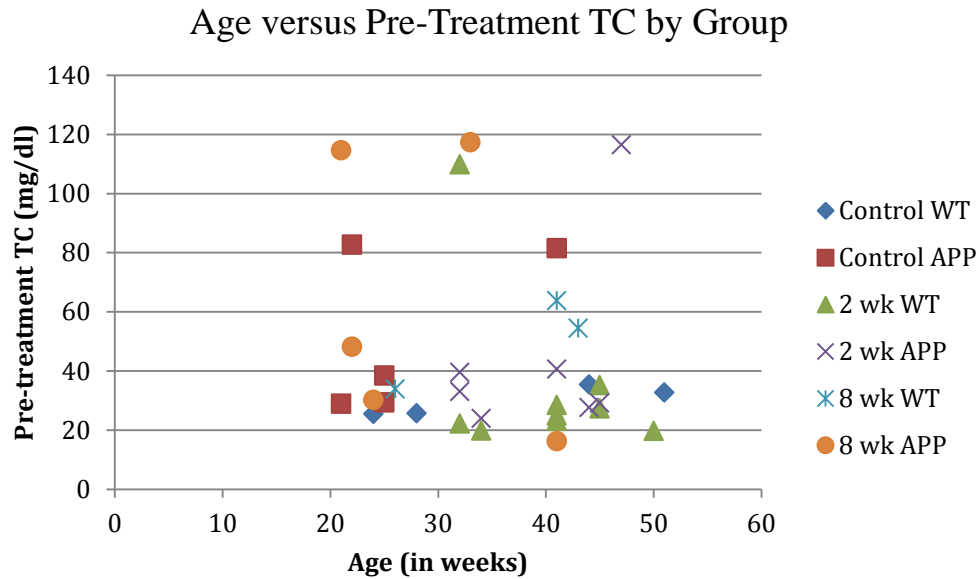
Figure 26: *Average Cholesterol as a Function of Age*. Brain cholesterol levels (mg/dl) were plotted as a function of the age of mice before and after treatment on separate plots. No correlation was found between age and total pre-treatment plasma cholesterol levels. Weak correlations were seen in two groups in the post-treatment plot: control APP ($R^2 = 0.3706$) and 8 week WT ($R^2 = 0.3784$), while no correlation was seen in other groups (both positive and negative correlations were seen). This suggests that plasma cholesterol levels are independent of age and genotype.

Western blots were used to assess protein levels semi-quantitatively to determine whether statistically significant changes or relevant trends were apparent in the data following treatment with simvastatin. Of particular interest was how ApoE, LRP and Aβ changed in response to simvastatin so results could be compared to the immunohistochemistry results. Although n=15 blots per group were performed (more blots were run in many cases), many groups did not have more than 12 blots with usable data, thus sample size was somewhat lacking. However, trends in the data could still be seen, as discussed further here, though they are not statistically significant.

APP & Aβ Results:

Western blot results for APP and beta amyloid are shown in the following figure. No statistically significant level of beta amyloid expression was observed between treatment group ($p < 0.288$; two-way ANOVA). There was also no interaction between genotype or treatment group ($p<0.118$). There was a noticeably increased expression of beta amyloid by the transgenic group as compared to the wild-type group, however, this difference was not statistically significant ($p<0.123$). It is also important to note that there were three main bands that were observed on the beta amyloid westerns: a large band at ~100 kDa representing APP, a medium-sized band at ~52 kDa representing C-terminal fragments that had been cleaved from APP, and a small band at ~31 kDa representing oligomeric beta amyloid. Monomeric or small oligomeric beta amyloid was not detected in samples, though the Aβ42 monomeric form was detected in the sample standard lane. This suggests that only
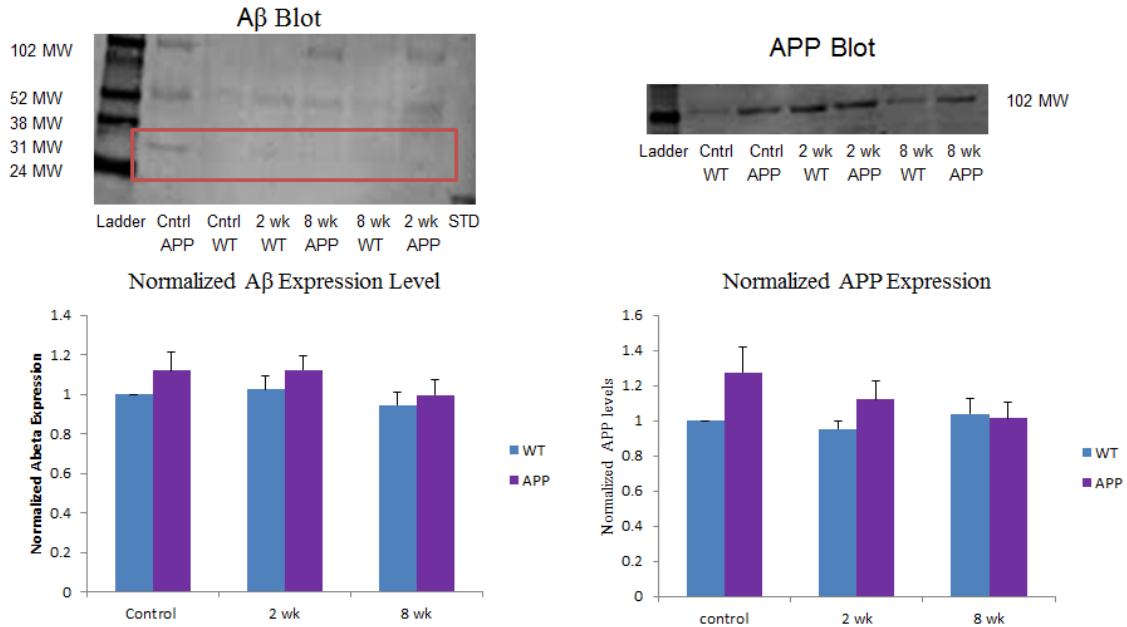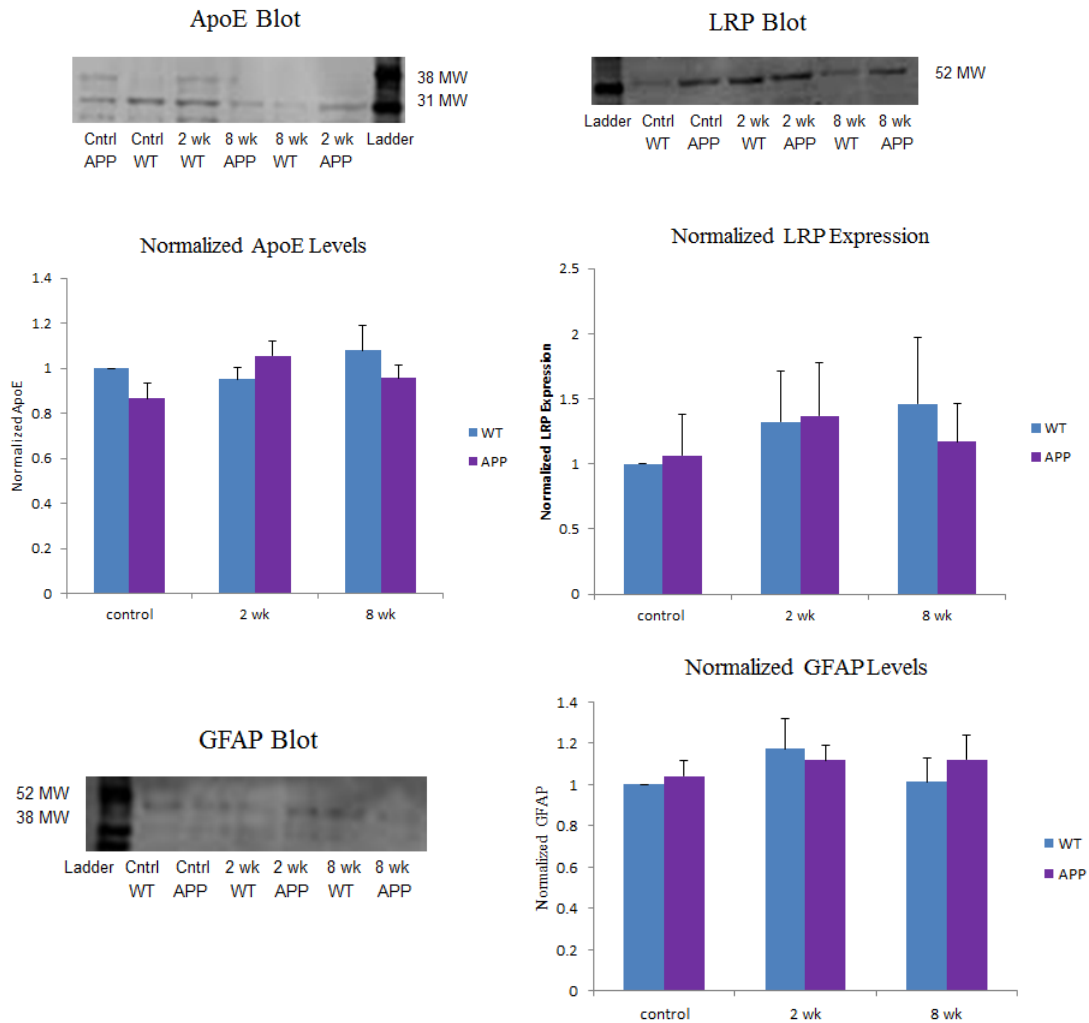
Figure 27: *Western Blot Results for APP & Aβ:* Western blots for APP and beta amyloid showed no statistically significant changes in expression levels of either protein. There was a decreasing trend for APP expression amongst the treated transgenic group, though.

non-detectable levels of oligomeric beta amyloid were present in this sample (<10 µg/lane).

Within the APP western blots, a similar trend with no statistical significance between genotype or treatment was observed. There was a decreasing trend in the level of APP expression in the transgenic group treated with simvastatin, though the change was only very minor ($p < 0.063$ and 0.399, respectively, for between genotype and between treatment groups; two-way ANOVA).

ApoE, GFAP & LRP Results:

Again, there were no statistically significant differences between genotype or treatment group in the ApoE, GFAP and LRP Western blotting groups. Within the ApoE group, two-way ANOVA analysis revealed relatively high p-values for differences in genotype and treatment ($p < 0.368$ and 0.412, respectively). Within the

Figure 28: *Western Blot results for ApoE, GFAP & LRP:* Western blots for ApoE, GFAP and LRP showed no statistically significant changes in expression levels of either protein. There was a weak increasing trend in the LRP levels in the 2 week treatment groups for both WT and APP, whoever this increase was not statistically significant.

GFAP and LRP groups, p-values were also quite high ($p < 0.7$ and 0.45, respectively, and 0.84 and 0.62, respectively for LRP).

Sy38 & PSD95 Results:

Post-synaptic density 95 (PSD95) showed the only statistically significant difference ($p < 0.029$), suggesting that APP mice had a significant increase in PSD95 expression when compared to WT mice. This is an interesting result because AD is
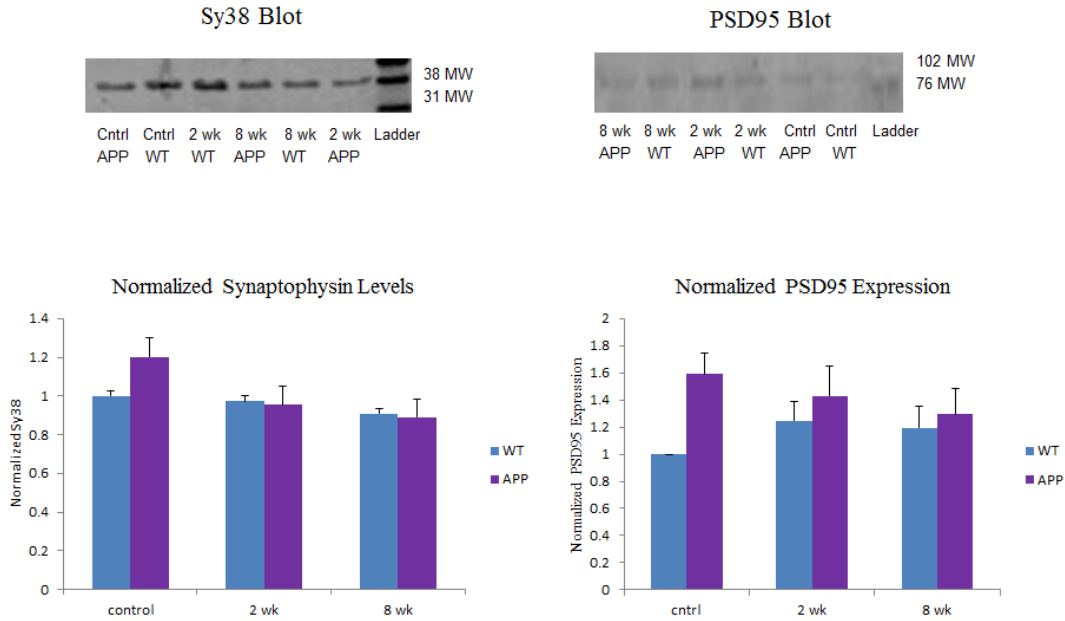
Figure 29: *Sy38 & PSD95 Expression Levels*: Expression levels of Sy38 and PSD95 had a decreasing trend in the APP transgenic group, though no trend was observed in the WT groups. PSD95 expression was significantly increased between WT and APP groups.

usually associated with a decrease in synaptic density; a similar trend is also seen in the Sy38 expression in the control group. PSD95 levels appear to have a decreasing trend with respect to treatment time, though this decrease is not significant ($p<0.845$). Ironically, WT mice show an increase in PSD95 expression in response to simvastatin treatment, suggesting that simvastatin may potentially affect transgenic mice differently than wild-type mice. Synaptophysin expression also appeared to have a decreasing trend between control and 2 week treatment groups in APP transgenics, suggesting that treatment with simvastatin may inhibit the maintenance of synapses, however, this difference was not statistically significant ($p<0.55$ and 0.19, respectively between genotype and treatment group, two-way ANOVA). This was the expected result since cholesterol is absolutely necessary for forming and maintaining synapses, and treatment with simvastatin would be expected to decrease cholesterol levels and subsequently decrease the synaptic density.

Immunohistochemistry Results & Quantification

Beta Amyloid Results:

Beta amyloid levels in the brain were measured semi-quantitatively by immunohistochemistry to study the density of plaques, as well as the localization of these plaques. Stained Aβ was divided up into two groups depending on the size of the stained region: large plaques (area > 5 μm^3) and small Aβ plaques (area < 5 μm^3). A plot of this data shows that mice treated with simvastatin, regardless of whether they are WT or APP transgenic, have an increased number of beta amyloid plaques.

Statistical analysis was performed using single factor ANOVA for both wild-type and APP transgenic mice, which showed that treatment of both WT and transgenic mice with simvastatin led to a statistical difference between the means of these groups (for WT: F=12.60115, p-value<0.0000323; for APP: F=14.01905, p-value<0.00000978).   Analyzing further with t-tests revealed that a statistically significant difference between control WT and control transgenic mice exists (t=5.805, p-value<0.000055), whereas no statistical difference exists between the 2 week treatment or 8 week treatment groups (p-value<0.163 and 0.090, respectively). A statistical difference between the means of the control-treated mice and the 2 and 8 week-treated mice also exists (for WT: p-value<0.00038 and 0.0029, respectively; for APP: p-value<0.028 and 0.000012, respectively). This seems to further suggest that treatment with simvastatin leads to an increase in the Aβ plaque density, regardless of whether the mouse is WT or APP transgenic. This is an interesting outcome which seems to suggest that treatment with simvastatin may actually lead to increased plaque load and worsening AD.
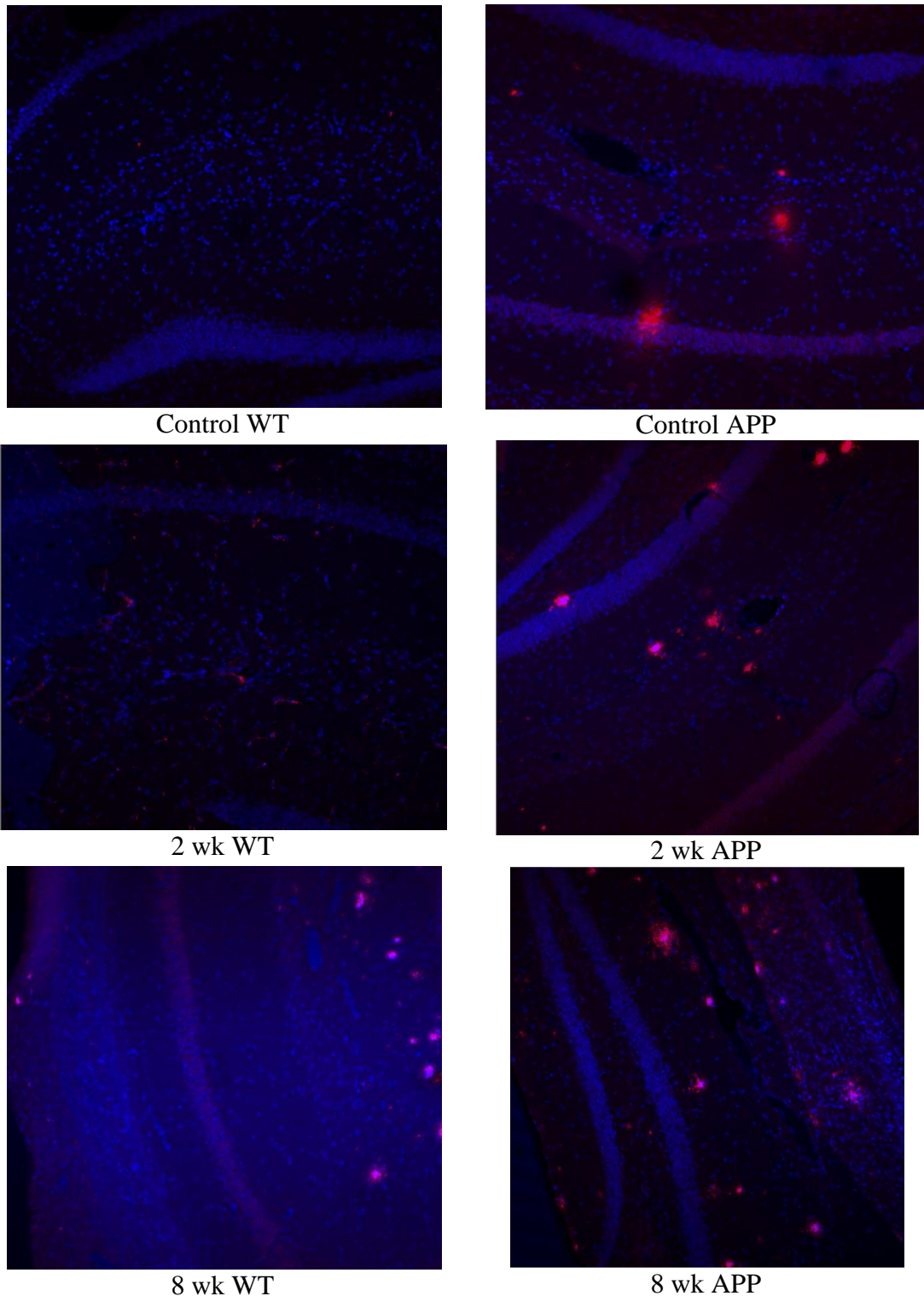
Control WT   Control APP

2 wk WT   2 wk APP

8 wk WT   8 wk APP

Figure 30: *Aβ Plaque Density in Mice across Different Treatments*. Beta amyloid plaque densities were assayed using immunohistochemistry (IHC). Dual staining was used to detect Aβ (6E10, magenta channel) and neurons (DAPI, blue channel). Increased levels of Aβ were seen in groups treated with simvastatin when compared to controls. Plaques were not identified as intra- or extracellular.

115

Additionally, this suggests that decreasing cholesterol levels may lead to an increase in Aβ expression, a relationship that has been suggested by others in the literature and also included in our mathematical model.

Aβ Plaque Density- Large Plaques

Aβ Plaque Density- Small Plaques
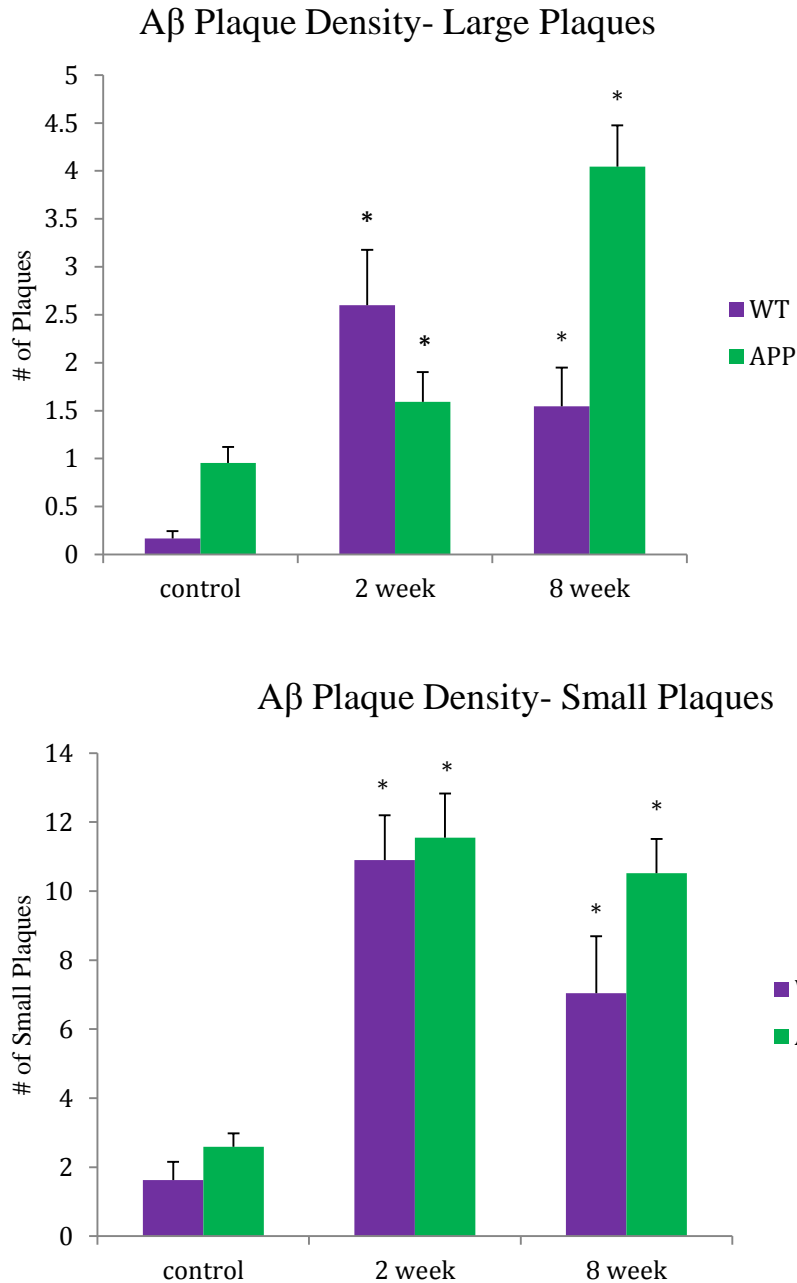
Figure 31: *Plaque Density in Mice across Different Treatments*. Beta amyloid plaque densities were measured for in control, 2 week and 8 week treatment with simvastatin. Treatment with simvastatin, regardless of group type (WT or APP) led to an increased plaque density.

Correlation analysis was completed to determine whether plaque density was dependent on the age of the mouse. All mice used for immunohistochemistry were greater than 6 months of age, which is the time when beta amyloid plaques have been shown to develop at an easily measurable level. Plaque levels were expected increase with age. Grouping both WT and APP transgenic mice into the same plot showed a weak positive correlation between age in plaque density ($R^2 = 0.0764$). Separating these out by group type showed a very weak negative correlation with age between the APP group ($R^2 = 0.0019$), while the WT group showed a weak positive correlation ($R^2 = 0.2219$).

Although there appears to be a no measurable correlation between age and plaque density, looking at the 6 possible data pairs of old mouse and young mouse for each treatment group, we see that in 4 of these 6 pairs, the older mouse has increased plaque density (the exceptions being the control WT and 2 week APP groups). This relative lack of correlation may be due again to the relatively small sample size that was used (n=2 for each group), which is quite small and can lead to skewed results.

It is also interesting that the WT mice that were treated with simvastatin showed increased Aβ plaque densities. These seems to suggest that treatment of mice with simvastatin, which significantly reduces plasma cholesterol in the 2 week treatment group, may have a negative effect on APP processing, leading to increased generation of the amyloidogenic processing pathway. There are several papers in the literature which describe a similar trend as well [1, 33], and points towards the role of cholesterol as an important modulator in APP processing. Recent research has also shown that decreased levels of membrane cholesterol can inhibit the degradation of

beta amyloid, thus leading to increased Aβ levels [144]. This also agrees with epidemiological studies that have shown that individuals with AD have decreased brain cholesterol, particularly in regions most affected by the disease [86]. Given the small sample size, however, it is not fair to put much backing in this result without further experimentation with a larger sample size.
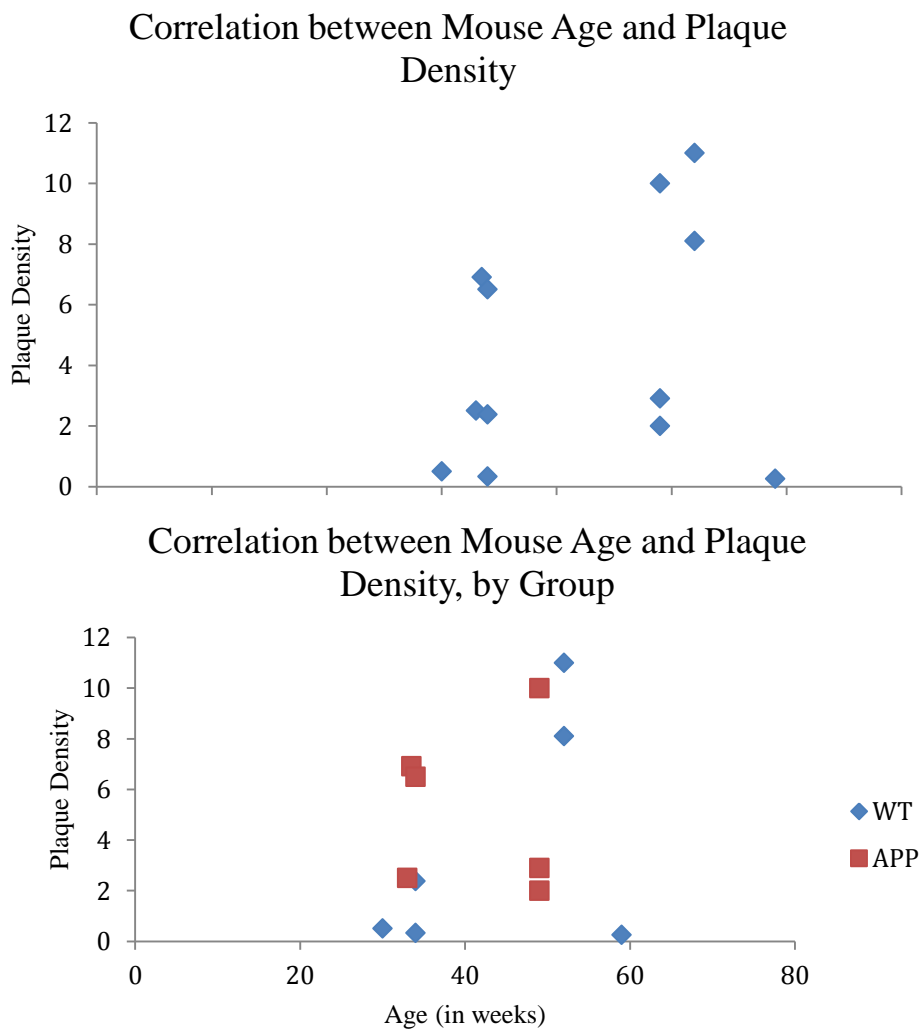

Figure 32: *Correlation between Mouse Age & Plaque Density:* No correlation was apparent between age and plaque density, suggesting that changes in plaque density were due to treatment and were not directly dependent on age.

Co-localization of ApoE with astrocytes:

The average density of ApoE 'co-localizing' with astrocytes was studied to determine if treatment with simvastatin altered expression levels of this key protein. The overlapping intensities between the red (astrocyte) and green (ApoE) channels was measured for each image in the set (n=15-20 per treatment group) and plotted in a bar graph. Data showed an increase in ApoE on astrocytes in the 2 week treatment group for both WT and APP transgenics, but a significant decrease in ApoE on the 8 week WT and APP transgenics.
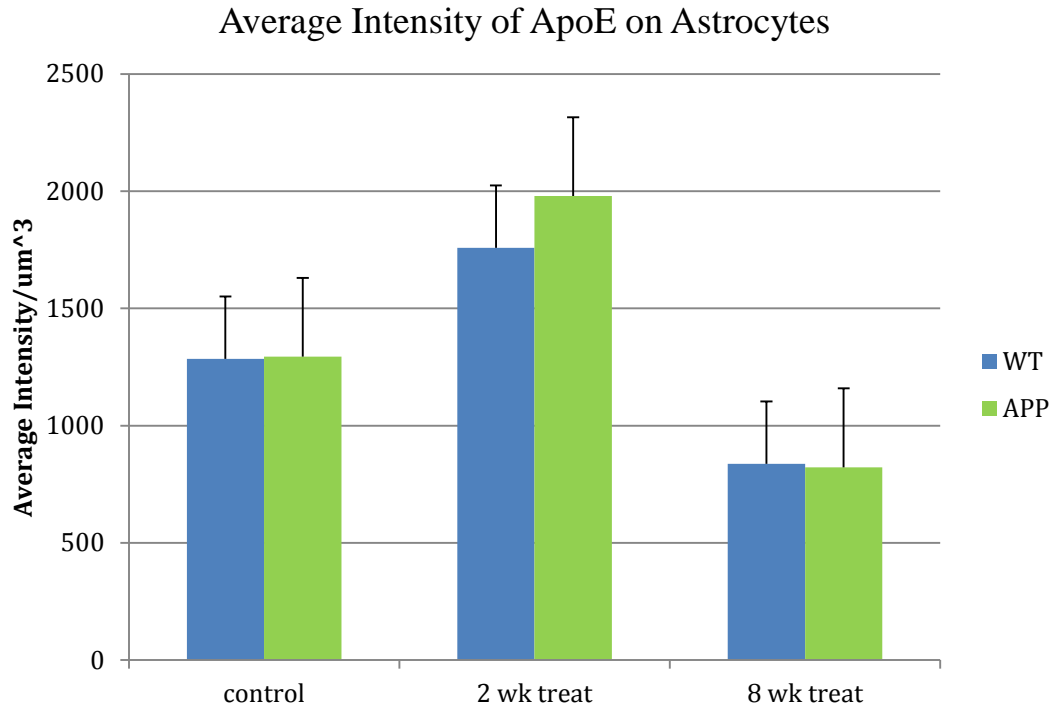
Figure 33: *Average ApoE Intensity of Overlap with Astrocytes in Mice across Different Treatments*. Average intensity of ApoE overlap on astrocytes was measured in control mice, and in mice treated for 2 and 8 week with simvastatin. Intensities were normalized to the total area of astrocytes in each image. Treatment with simvastatin for 2 weeks increased the average intensity of ApoE on astrocytes, while 8 week treatment significantly decreased the average intensity of ApoE, irrespective of genotype.

A single factor ANOVA was done separately for the WT and APP transgenic mice to study the statistical difference between the means of treatment groups in these samples. In WT mice, the means between control, 2 week treat, and 8 week treat were statistically difference (F=9.49, p-value<0.00031); in APP transgenics, the means between these three groups were also statistically significant (F=28.61, p-value<5.58e-9). It is important to note that there was considerable variability within each group, which can be seen by the relatively wide confidence intervals for each group/ relatively large standard deviations. This could be due to minor changes in the laser power at different imaging times, or relative differences in staining that are possible even for slices that are placed into the same well (due to folding, not exactly the same thicknesses, or relative placement within the well during primary incubation). Still, however, this data suggests that statistically different changes in the average intensities were obtained.

To further study these changes, t tests were performed between matched groups. No statistical difference between WT and APP controls, 2 week, or 8 week treated mice was observed for a two-tailed test (for control: t = 0.042, p-value<0.97; for 2 week treat: t = 0.995, p-value<0.327; for 8 week: t = 0.11, p-value<0.915). Amongst WT mice, a statistical difference was observed between control and 2 week treatment, and control and 8 week treatment (p-values<0.028 and 0.014, respectively, one-tailed test). A similar trend was observed in APP transgenic mice where there was a significant increase in ApoE in the 2 week treatment group, and a significant decrease in the 8 week treatment group (p-values<0.00026 and 0.0019, respectively, one-tailed test).
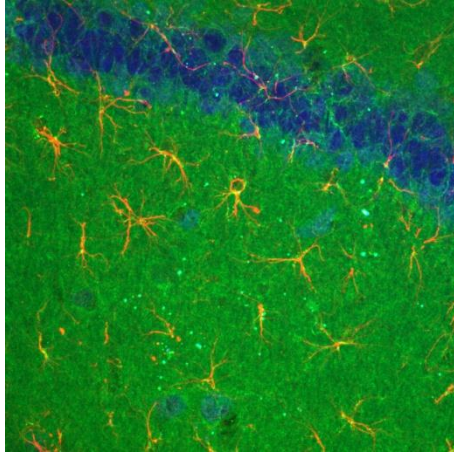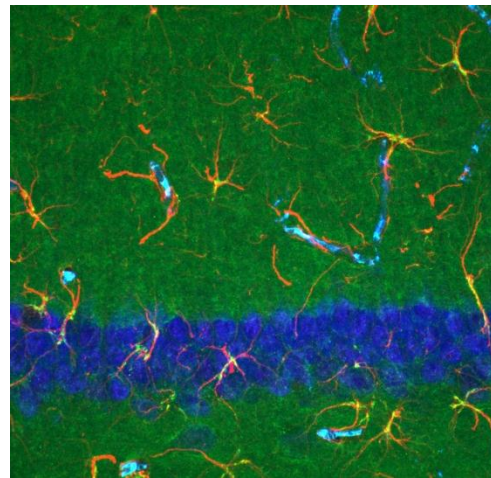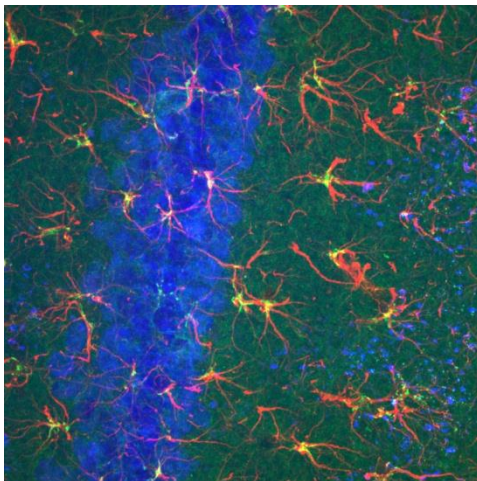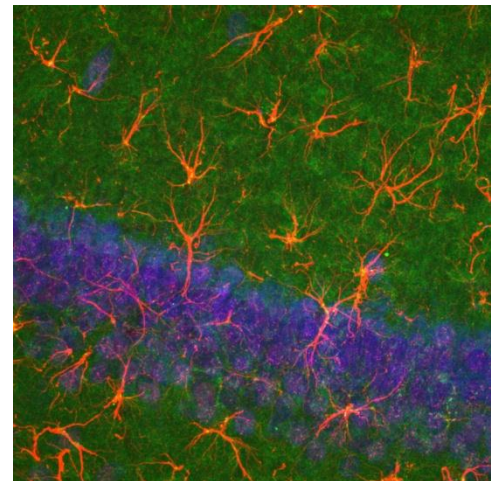
Control WT
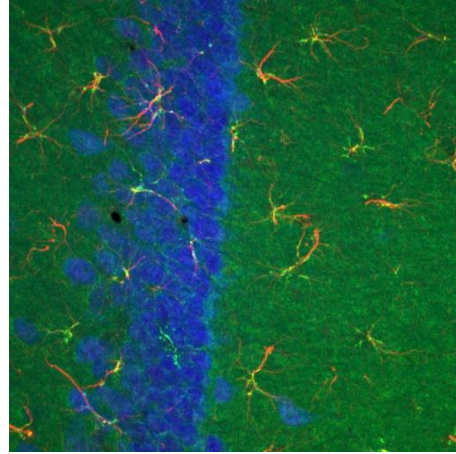
Control APP
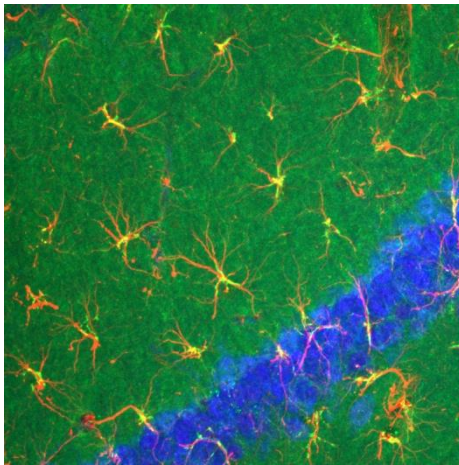
2 week WT

2 week APP

8 week WT

8 week APP

Figure 34: *GFAP IHC:* Hippocampal slices were triple-labeled with GFAP (red channel; glial fibrillary acidic protein; labels astrocytes), ApoE (green channel; labels apolipoprotein E) and NeuN (blue channel; labels neuronal cells).

The average number of astrocytes in each image was also measured to verify that the observed changes in ApoE were not due to changes in the number of astrocytes. The mean astrocyte number in across all groups ranged from 20 to 25 astrocytes per image. A single factor ANOVA for WT and APP groups, done separately, indicated that there was no statistical difference between these mean values (for WT: $F=1.12$, p-value < 0.3335; for APP: $F=0.803$, p-value<0.453). T tests done between control/2 week and control/8 week treat for both WT and APP samples showed no statistical difference between the mean astrocyte number per image (for WT: p-values<0.368 and 0.588; for APP: p-values<0.316 and 0.732, respectively; two-tailed test). This suggests that the observed differences in ApoE are more likely due to changes in protein expression rather than changes in astrocyte number.

Combining the result in this section for ApoE with the cholesterol assay results, it is reasonable to suggest that decreasing the plasma cholesterol levels leads to a decrease in the observed ApoE expression on astrocytes. This, in fact, agrees with some of the data in the literature (Liu 2007). The 8 week treatment results are a little bit more difficult to interpret, since cholesterol levels were at similar levels to the control treated group in both WT and APP mice. Since ApoE expression is increased when cholesterol levels are low and/or when IL-1 levels are high, the converse being true also, it is reasonable to suggest that cholesterol levels may have been sufficient enough, but inflammation low enough, to prevent an increase in ApoE expression. This would imply that the 8 week treatment of mice with simvastatin has no statistical effect on cholesterol levels, but does seem to normalize the level of

inflammation, and thus decrease the expression level of ApoE. However, the astrocytes in the 8 week treated groups do appear to be reactive state rather than in the resting state, suggesting that inflammation is actually not decreased. Further experiments measuring the level of inflammation by ELISA or Western blot analysis of IL-1 and TNFα would be needed to better determine whether inflammation is increased or decreased in treated mice.
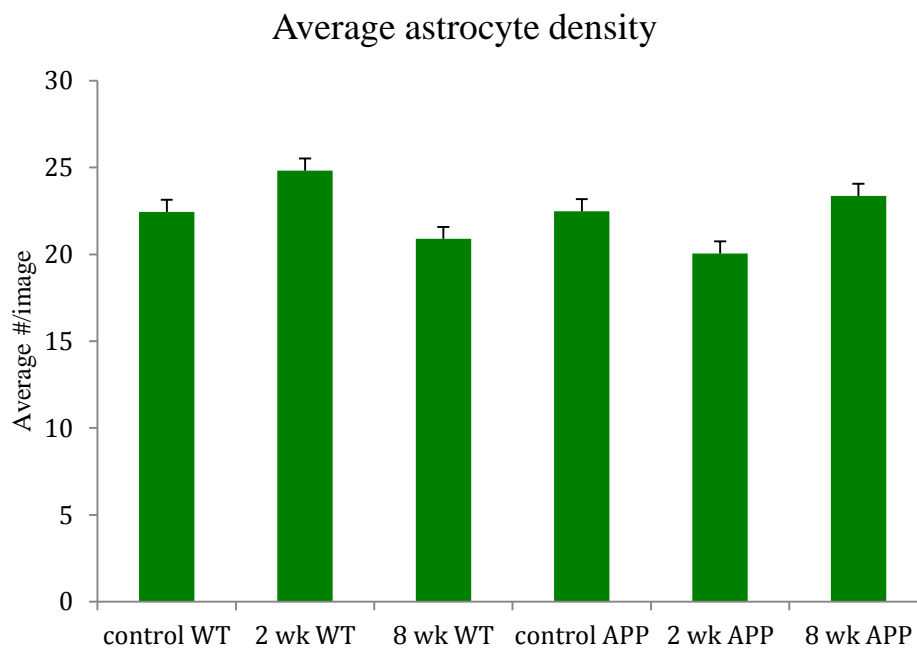
Average astrocyte density

Figure 35: *Average Astrocyte Density:* Average astrocyte density did not vary significantly across genotype or treatment group, ranging from 20-25 astrocytes per image field.

Co-localization of LRP on cerebral blood vessels & neurons:

The final set of immunohistochemistry experiments that was done studied the expression levels of LRP on both cerebral blood vessels and on neurons to determine whether these levels changed individually, and whether the ratio of LRP on cerebral blood vessels to that on neurons varied across genotype or treatment. Plotting the

data for LRP on cerebral blood vessels showed an increase in LRP in 2 week treated

WT and a mild increase in 2 week treat APP mice. Little change between the control

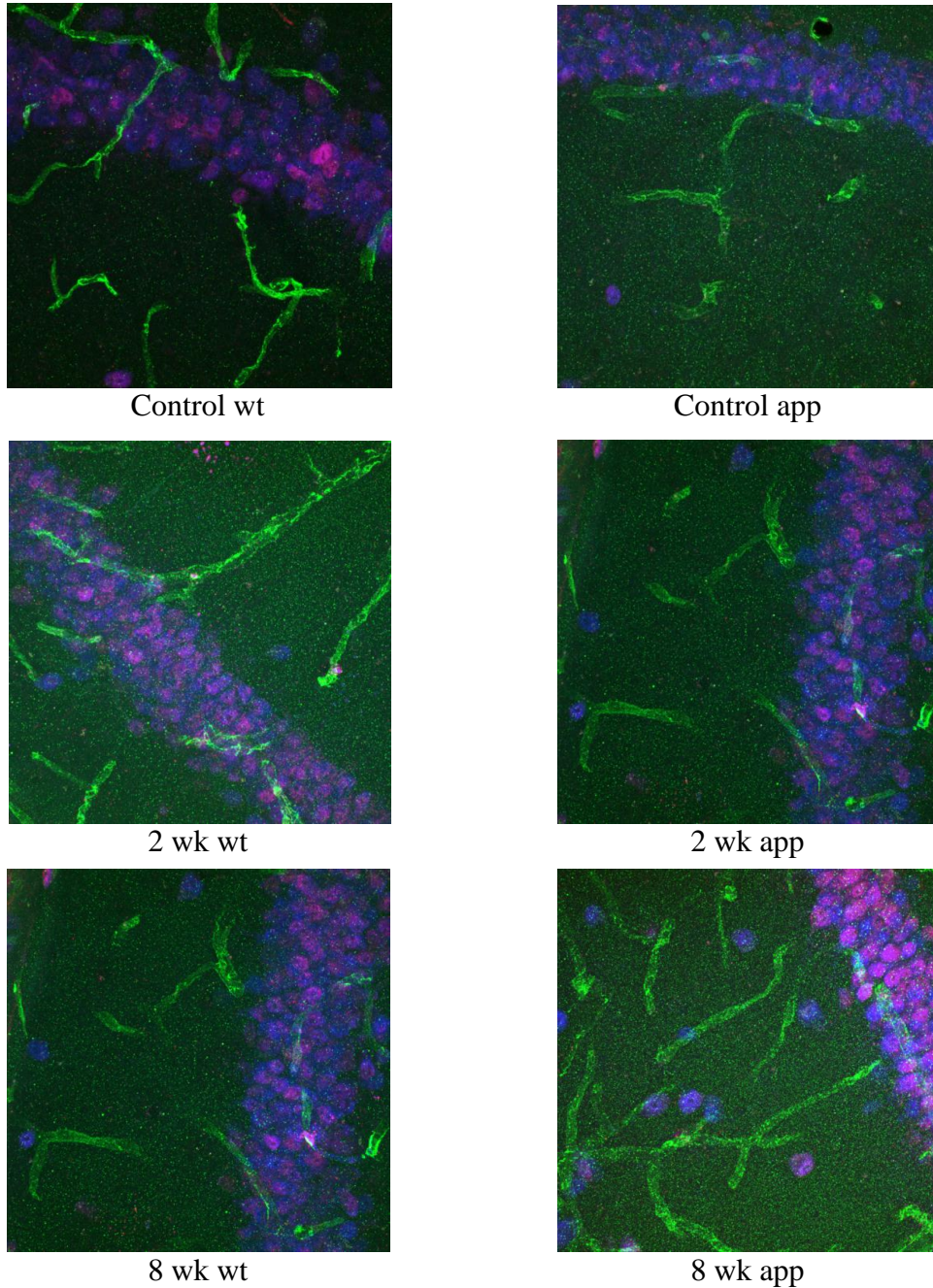and 8 week treatment groups were seen in either WT or APP transgenic mice.

Control wt	Control app
2 wk wt	2 wk app
8 wk wt	8 wk app

Figure 36: *LRP IHC:* Hippocampal slices were triple-labeled with LRP (red channel; labels LRP protein), CD31 (green channel; labels blood vessels) and NeuN (blue channel; labels neuronal cells).

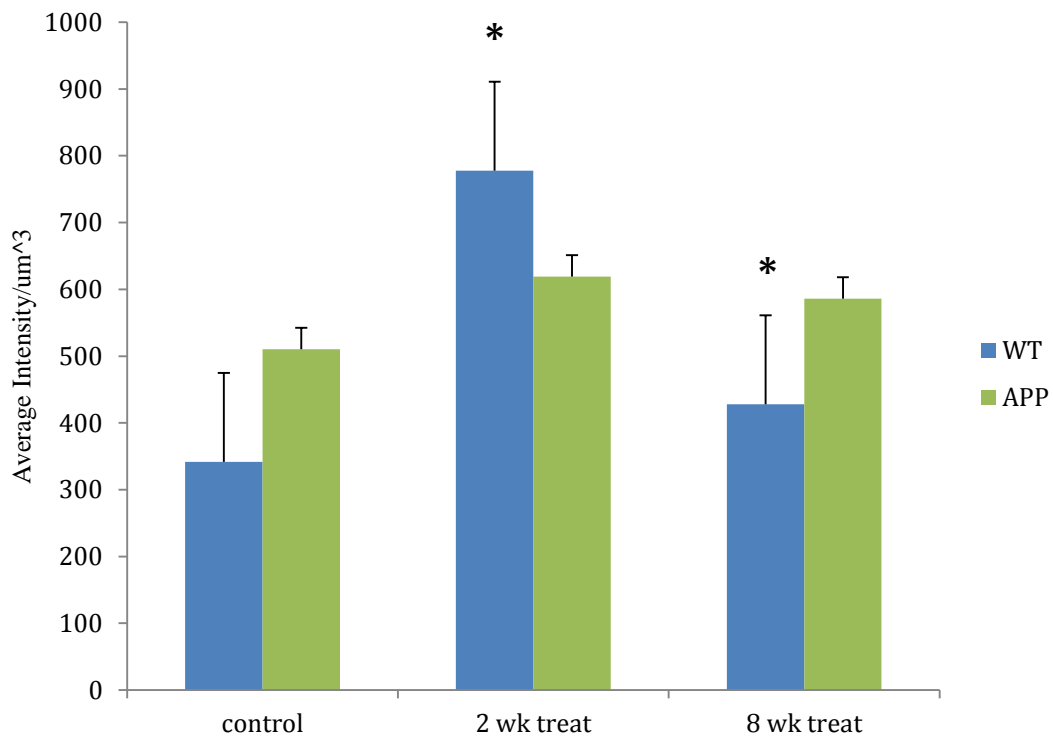## Average Intensity of LRP signal in Cerebral Blood Vessels

Figure 37: *Average LRP Intensity on Cerebral Blood Vessels:* Average LRP intensity on cerebral blood vessel was increased significantly only in the 2 week and 8 week WT groups (*), although all treatment groups showed an increase with respect to the control group. There was no significant increase in either treatment group for APP mice. The difference in LRP intensity in the control and 8 week treatment groups between WT and APP was also statistically significant (p-values<0.017 and 0.023, respectively).

Single factor ANOVA for all treatment groups with the WT genotype revealed statistically different values in the means (F=11.86, p-value<3.55e-5). There was no statistical difference between the means in the APP transgenic group (F=0.744, p-value<0.48). Further analysis with one-tailed t tests showed that the average intensities of LRP between control WT/control APP and 8 week WT/8 week APP are statistically different (p-values<0.017 and 0.023, respectively), though there is no statistical difference between the 2 week treatment WT and APP groups (p-

value<0.135). One-tailed t tests between treatment groups with the same genotype demonstrated that LRP was increased significantly in both the 2 week and the 8 week treatment WT groups (p-values<0.00023 and 0.043, respectively); there was no statistical difference in the increased LRP that were observed for the APP group (p-value<0.124 and 0.139, respectively).
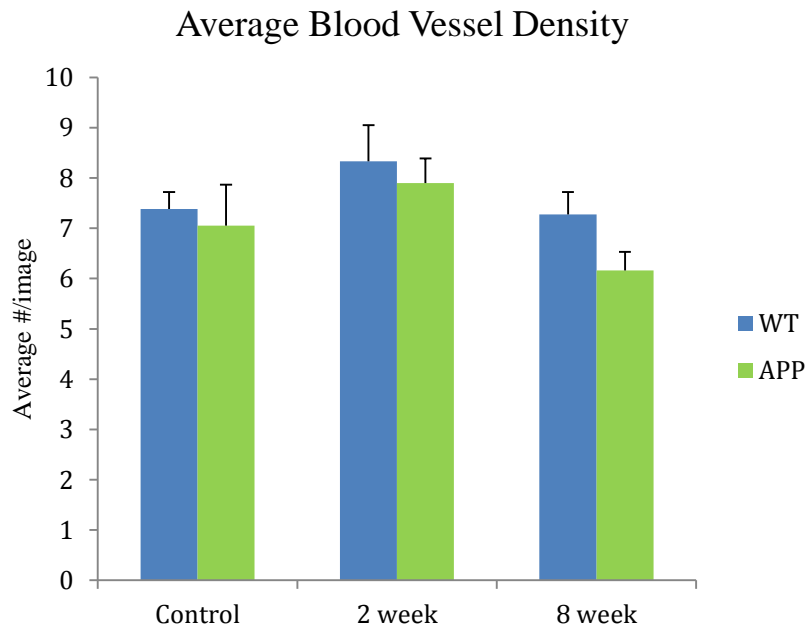
Average Blood Vessel Density

Figure 38: *Average Blood Vessel Density:* Average cerebral blood vessel density did not vary significantly across genotype or treatment group, ranging from 6-8 blood vessels per image field.

Again, the average number of blood vessels was measured to determine the observed changes in LRP on cerebral blood vessels was due to differing levels of blood vessels within the images taken. No statistical difference was found across different genotypes or between treatment groups by either a single factor ANOVA with $\alpha=0.05$ or two-tailed t tests with 95% significance (for WT: F = 1.205, p-value <0.307; for APP: F = 2.713, p-value<0.0745). Average values ranged from 6-8 blood vessels per image. This suggests that changes in the observed LRP levels are not due

to differences in the number of blood vessels per image. The data also suggest that the blood vessel density does not change significantly with simvastatin treatment.

The average intensity of LRP was also measured on neurons. Bar graphs showed that the average intensity of LRP on neurons increased during treatment with simvastatin for both WT and APP groups. This difference was statistically significant in the WT groups (single factor ANOVA, F = 3.997, p-value<0.023, α=0.05), but insignificant in the APP group (F=2.074, p-value<0.134, α=0.05). One-tailed t tests showed that the difference between control WT and 2 week WT was statistically significant (p-value<0.004), as well as the difference between control APP and 8 week APP (p-value<0.033). There was no statistical difference between control WT and 8 week WT or control APP and 2 week APP.
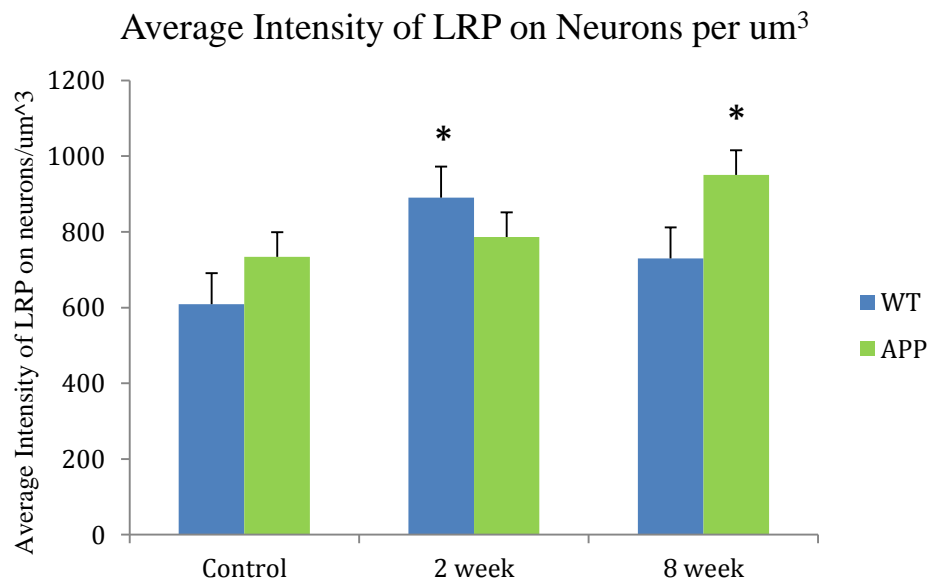

Figure 39: *Average Intensity of LRP on Neurons:* Although LRP was increased on neurons in all groups, this difference was only statistically significant on the control WT/2 week WT and control APP/8 week APP groups (p-values<0.004 and 0.033, respectively).

Overall, the levels of LRP increased on both cerebral blood vessels and on neurons in all treatment groups, however this increase was only statistically significant in 2 week WT (blood vessels and neurons), 8 week WT (blood vessels) and 8 week APP (neurons). This corresponds with the data that shows that brain cholesterol levels were significantly decreased in the 2 and 8 week WT mice, while brain cholesterol was lowest in the 8 week treatment APP mice (of all other APP mice), suggesting that decreased brain cholesterol is associated with an increase in LRP on cerebral blood vessels (an inverse relationship). This was somewhat unexpected since both LRP and brain cholesterol have been shown to be decreased in AD patients, and decreased LRP has been associated with increased levels of APP and ApoE. Also, since LRP expression levels are usually directly related to IL-1 (inflammation) and cholesterol levels, a decrease in LRP would have been the expected result. One explanation for this result is that simvastatin treatment helps to increase LRP expression by a method not previously described.

It is interesting to note that if the ratio of LRP on blood vessels to LRP on neurons is plotted, it follows a symmetric curve similar in shape to the curve that was obtained for blood vessel density in images. These seems to imply that although the neuron density is not statistically different across treatment groups, there may be an artificial increase in the LRP levels on blood vessels due to this minor difference. This may help to explain the observed increase in LRP in the 2 week WT group.

The 8 week APP group is somewhat easier to interpret. Cholesterol levels in this group were on par with those of the control group, suggesting that although simvastatin treatment lowered these cholesterol levels slightly (though not

significantly), astrocytes still appeared in an activated state (associated with an increase in inflammation). Since increased inflammation and levels of IL-1 are associated with increased LRP expression, it is reasonable to conclude that increased inflammation in the 8 week APP group led to this increase in LRP, though further experiments on the levels of IL-1 would be needed to confirm this definitely.
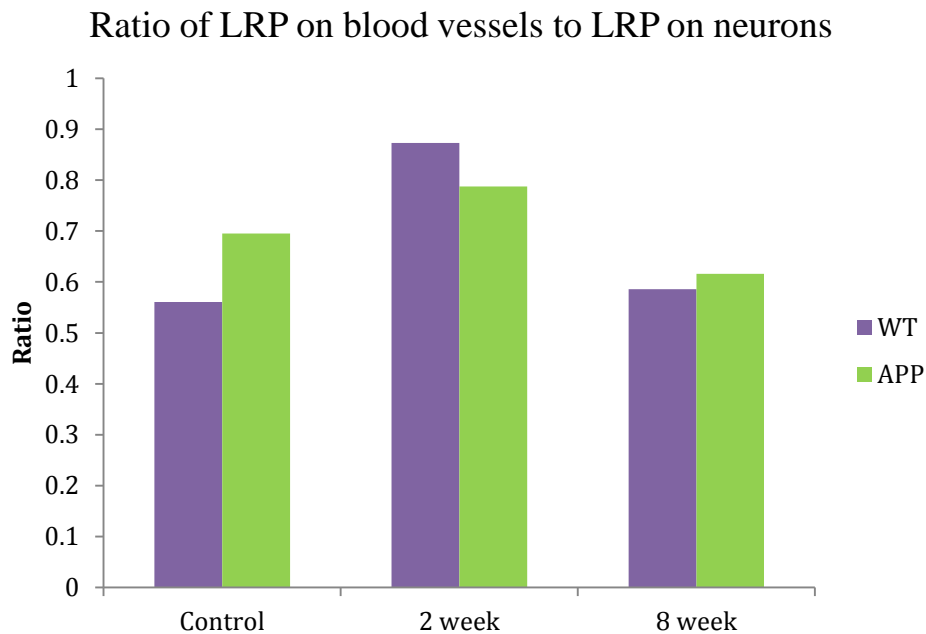
Ratio of LRP on blood vessels to LRP on neurons

Figure 40: *Ratio of LRP on blood vessels to LRP on neurons:* The ratio of LRP on blood vessels and on neurons followed a trend very similar to that observed for the number of blood vessels per image. This suggests that the increase in LRP observed in the 2 week groups is more related to the increased number of blood vessels than an actual increase in LRP. This data represents the ratio of the averages, thus no standard error bars are included.

Conclusions

Data from the experiments to test the effects of short and long-term simvastatin treatment on WT and APP mice has been presented. Simvastatin treatment led to statistically significant decreases in brain cholesterol in WT mice treated with simvastatin for 2 or 8 weeks. APP transgenic mice treated with

simvastatin showed a decreasing trend in brain cholesterol levels, though the trend was not statistically significant. Plasma cholesterol levels increased during both the control treatment and the simvastatin treatment. This was believed to be due to an effect of the high fat content of the peanut butter causing an increase in plasma cholesterol, as opposed to differences in the ages of the mice (verified via correlation analysis). Two week treatment with simvastatin decreased the difference between pre- and post-treatment plasma cholesterol concentrations, and was significant in the 2 week APP group, suggesting that 2 week treatment with simvastatin was able to decrease both brain and plasma cholesterol in these groups. The 8 week treatment group for both WT and APP transgenic mice showed no difference when compared to the respective control groups. This could possibly be due to a rebounding effect that has been observed in animals and humans exposed to statins: after an initial treatment period where the cholesterol levels are significantly reduced, the liver adapts, leading cholesterol levels to initially overshoot before returning to baseline [50]. Also, as stated before, the cholesterol levels in the brain and plasma for the 8 week treatment group may have been slightly inaccurate due to changing the dosage method from peanut butter to baby food temporarily. Definitively, though, plasma cholesterol levels in the 2 week treatment groups for both WT and APP were decreased significantly, while brain cholesterol levels were significantly decreased in 2 week WT (only a trend exists in 2 week APP).

Immunohistochemistry analysis showed several interesting alterations in protein expression. The Aβ plaque density increased significantly in all groups treated with simvastatin (both WT and APP). This increase was not correlated with

the age of the mouse. Since only the 2 week treatment groups showed significant decreases in brain and plasma cholesterol, these results suggest that decreased cholesterol levels correlate with increased Aβ levels. The results of the 8 week group are harder to discuss since there was no statistically significant decrease in brain cholesterol observed in these groups. It is thus suggested that decreased cholesterol levels provided by simvastatin treatment leads to an increase of beta amyloid levels, though further experiments are still needed to definitively make this statement.

ApoE levels increased in the 2 week treated groups in both APP and WT mice (only WT mice were statistically significant though), while mice on 8 week treatment had a decrease in ApoE levels. This would correspond with the expected result that as cholesterol levels decreased, ApoE would increase. The 8 week group can be explained by the fact that cholesterol levels were not statistically decreased and astrocytes appeared to be activated in images when compared to control or 2 week treatment images. Inflammation is correlated directly with an increase in ApoE. The results for LRP were a bit more difficult to interpret, since the increased levels of LRP in the 2 week group do not seem to agree with what is known in the literature (LRP is decreased in AD and in models where APP is increased). The observed trend in the data (increased LRP at 2 weeks on both cerebral blood vessels and on neurons; increased in 8 weeks on neurons) is believed to be explained by the fact that there is a similar trend in the number of blood vessels per image in these groups, which, although is not enough to be statistically different, may be artificially increasing the LRP levels. Alternatively, simvastatin treatment for 2 weeks may increase LRP levels by a previously unknown mechanism, which warrants further study.

Western blotting data for nearly all groups were not statistically significant. Beta amyloid, ApoE and GFAP data showed no clear trends, while APP showed a decreasing trend across the APP group and LRP showed and increasing trend across the WT (but not APP) group. In both WT and APP mice, synaptophysin showed a trend of decreasing expression with simvastatin treatment. PSD95 levels also showed a decreasing trend amongst APP transgenics, though no trend was observed in the WT group. This decreased expression levels of Sy38 and PSD95 in the APP group suggests that as brain cholesterol levels decrease, the levels of proteins associated with synapses also decreases. This follows logically from the fact that cholesterol is needed to form and maintain synapses, and the loss of cholesterol in the brain should hypothetically lead to a decreased number of synapses. Immunohistochemistry could be used to determine synaptic density in order to further understand this relationship. One reason that the western blot data may have had no statistical significance is the loss of information from the homogenization method that was used since all cell types and cellular compartments are lumped together. This implies that there may have been changes that were specific to neurons, astrocytes or other cell types, but the Western method that was used was not able to distinguish this. In future experiments, a differential centrifugation method could be used to separate cell types and cell components.

Chapter 6: When experimental data meets math: final systems biology model incorporating data & inflammatory pathway

Model Assumptions:

The brain can be considered a system consisting of interactions between several key cell types: neurons, astrocytes, microglia, and brain endothelial cells (ECs). The brain parenchymal space, filled with a combination of cerebral spinal fluid and a predominantly proteoglycan mesh extracellular matrix network, surrounds all cell types, except for brain ECs, which contact the blood on one side. At an even higher level, the brain can be effectively modeled as two main compartments: the cerebral blood vessels and the parenchymal space. The ventricles and the areas outside of this described region are neglected from this model.

The brain has a finite volume, thus, there exists a limit, or carrying capacity or concentration threshold, for the number of cells, proteins, signaling molecules, lipids and other biomolecules that can be contained in this volume. Above these concentration thresholds, regulatory systems are triggered in an effort to return the system back to a state of homeostasis. Independent of these regulatory mechanisms, cellular damage can occur due to activation of inflammatory pathways, mechanical loading, activation of apoptosis or necrosis, or changes in local osmolarity. In this model, the blood is considered to be a relatively infinite sink (as in previous models that we have developed) since the rate of blood flow is considered to be sufficient

enough to transport any molecule that is transported across the BBB and out of the brain.

The key cell types in the brain and their interactions with each other can be represented as a directed graph with both weak and strong connection strengths. Not all cell types interact with each other, and only the brain ECs have a direct connection with the blood for waste removal. Within this cellular network, each cell type possesses its own set of metabolic, lipidomic and proteomic pathways that are expressed depending on what genes are currently active. This cellular sub-network can be considered cell-dependent topology.
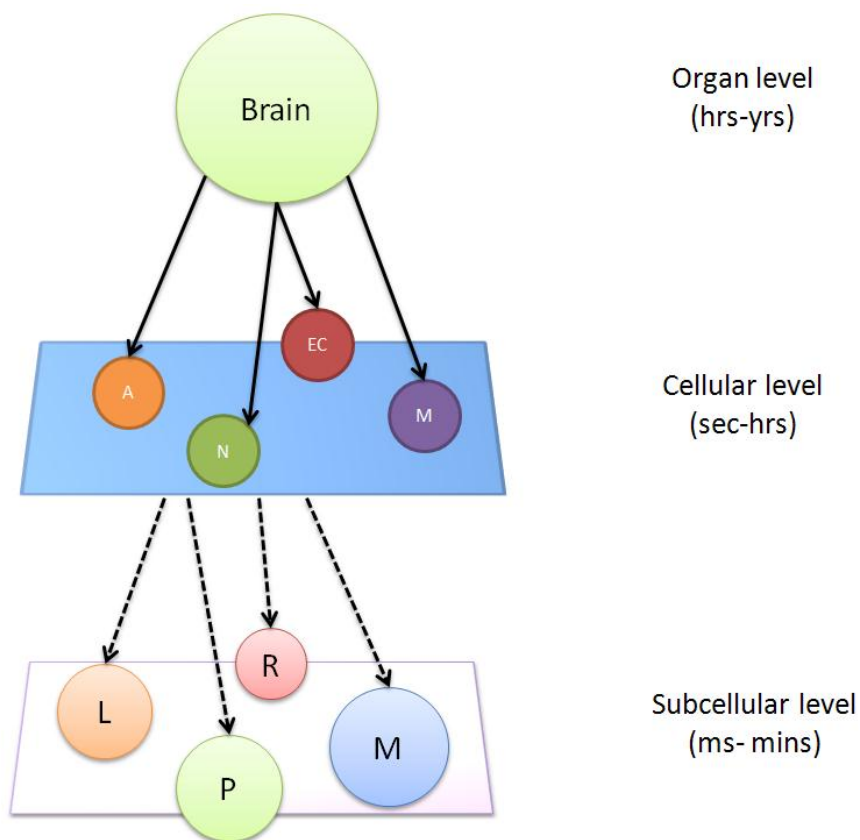

Figure 41: *Two-level hierarchal network used to model our system*. In this model, the brain has been modeled as a two-level hierarchal network. The higher level consists of the cellular network (neurons (N), astrocytes (A), microglia (M) and brain endothelial cells (EC). Each of these cell types also has a sub-cellular network that models lipid metabolism (L), protein metabolism (P), energy metabolism (M) and regulatory pathways (R).

As discussed in chapter 4 briefly, the brain can be thought of as having different "states", similar to the idea of a Markovian process. In the case described here, the current overall *state* of the brain can be modeled as the convoluted sum of the individual pathways that are currently being expressed by that cell type. Initially, this sum would be considered the *healthy* state, where pathways are running efficiently, all biomolecules are within the normal, physiological ranges, energy levels are kept constant and inflammatory processes are balanced. Over time though, the system may become perturbed from environmental or other triggers. If not properly adjusted for, the expression of certain molecules or of pathways may be altered such that the system is no longer in a *healthy* state, but has entered into one of many possible *disease* states. These switches from health to disease states can be modeled as discrete logic transitions since they occur only when a critical threshold for a biomolecule or other constraint condition has been reached. The entire network of metabolic, lipidomic and proteomic pathways can still be modeled using continuous-time ordinary differential equations as described in previous chapters, while these discrete switching conditions are used to model regulatory mechanisms that shift the system state. These switches activate the expression of new pathways or significant changes in the expression of currently expressed pathways, such that the new state is represented by an alternative set of ODEs and/or rate constants. In this manner, a model similar to a hybrid automaton will be described to model the system as it evolves over time.

The following figure visually describes how the brain's state can evolve over time depending on the environmental conditions or, in future models, what genes are

activated. The system state is allowed to switch from healthy → disease, from disease state → disease state, and under some conditions, return from a disease state to a healthy state. Disease states can also combine to form conditions which are even further from the healthy state. The farther that a node is removed from the healthy state, the lower the probability that the system will return to the healthy state.
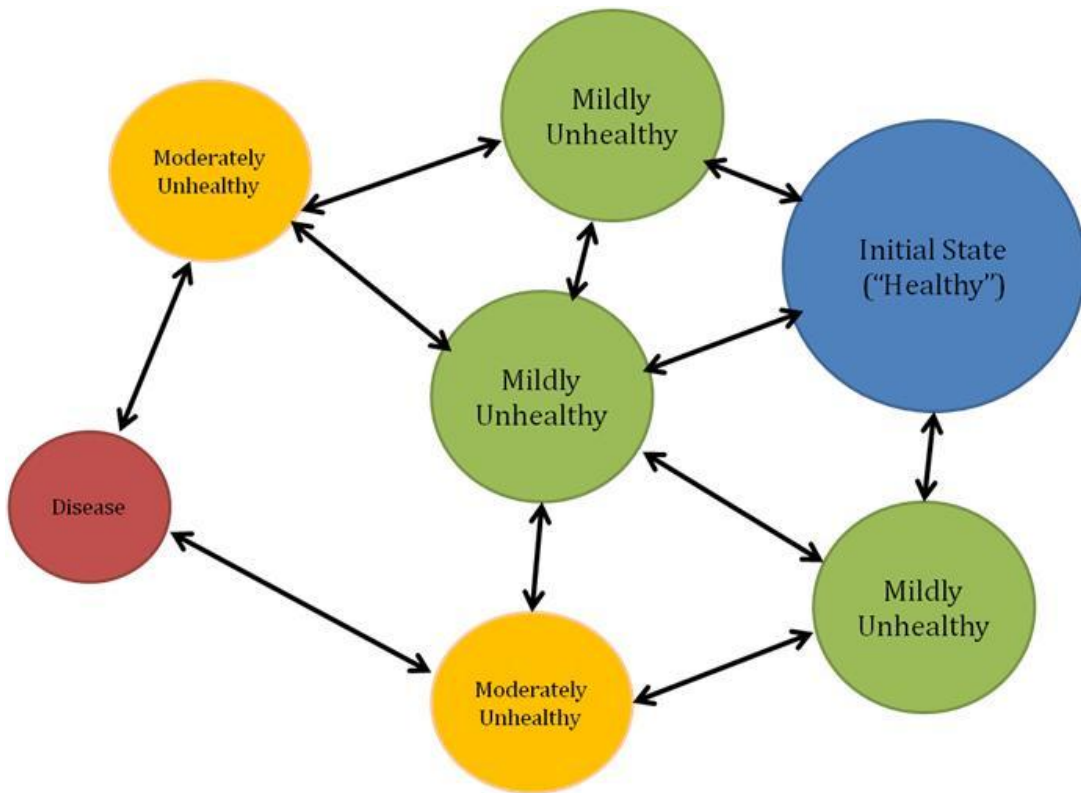

Figure 42: *Disease Processes as a Markovian State Space.* It is being proposed here that diseases, regardless of their underlying pathogenesis mechanisms, can be modeled as Markov state space. The highest probability is to find the system in the *healthy* state, which transitions to other states (*unhealthy states*) upon exposure to an environmental stimulus or other external factor. Over time, these transitions can tend towards a disease state. Depending on the disease, this may be a final, absorbing state, or there may be opportunities to escape this state and return towards a healthier state.

Time delays play a key role in the interaction graph between the cell types, as well as the in the modeling of the biochemical pathways in continuous-time. Delays can be caused by time needed for transcription/translation, diffusion, activation of a specific pathway via a cascade process, or changes in mRNA expression due to such activation. As can be seen in the topology of the two-level hierarchy graph, time scales can vary across levels of the network as well. At the sub-cellular level, most reactions take place in milliseconds-minutes range; while interactions at the cellular level occur in the seconds to hours range. Overall changes at the organ may take hours to years to occur at an observable or measurable rate.

Trends from biological experiments & the literature:

From the biological experiments that were described in the previous chapter, several trends from the data were important in developing the final topology of the network. Decreasing cholesterol levels led to an increase in beta amyloid. This suggests that the proposed role of cholesterol as an inhibitor of BACE activity is correct and has been included as a definitive inhibitory edge in the model. Experimental evidence from other sources also describe a similar trend [1, 33]. Although there is data available that states that cholesterol promotes the generation of beta amyloid by increasing the activity of BACE, the experiments did not take into account the fact that treatment with a statin not only lowers cholesterol, but also decreases inflammation. Additionally, many of these experiments have been done on cell lines which may not give the most accurate or relevant results when compared to the actual body. Decreased cholesterol also led to an increase in ApoE and LRP expression. This trend was included in the model by making ApoE and LRP

generation rates dependent on the astrocytic cholesterol concentration. Increased levels of ApoE are commonly seen in AD brains [42].

From the literature, it is known that increased IL-1 expression levels, as seen during an inflammatory response, decreases cholesterol synthesis by 25-60% [112]. This was modeled by adding an inhibitory rate constant to the equation for modeling cholesterol generation by astrocytes. IL-1 is also known to increase the expression levels of ApoE and LRP, while decreasing the conversion of tryptophan precursors to serotonin, causing a buildup of tryptophan. Finally, IL-1 is also known to stimulate the production of beta amyloid, thus creating a positive feedback loop between beta amyloid (which stimulates production and secretion of IL-1).

Beta amyloid synthesis was set at 5% of the products cleaved from APP, using a rate that has been previously described [28]. It is interesting to note that beta amyloid production is not increased in AD, though a 30% decrease in clearance has been seen [96]. The average half-life for beta amyloid is 2 hours [30]. This half-life includes degradation by proteases, uptake by astrocytes and microglia, and clearance from the brain via the LRP-1 receptor on brain endothelial cells.

The model was derived using Michaelis-Menten rate kinetics since a major assumption was that metabolic reactions were at steady state. These reactions were assumed to proceed much faster than the overall rate at which the system was changing. The steady state value could shift, but the actual rate at which chemical species were flowing through the pathway was trivial.

Network Topology:

Given the hierarchal nature of this model, the biochemical pathways that are being expressed by various cell types have been minimized to those which are either absolutely essential for cell survival, or required for the cell's main function. The pathways have been divided by cell type, though several pathways, such as the need to have functional mitochondria and fatty acid synthesis for maintaining cell membranes, are included in all cell types. Additional pathways are specific to cell type function; proteomic pathways have been limited to include only those proteins that have been implicated in playing a causal role in AD.

Networks for Each Cell Type	
Neurons: - Metabolic (energy, neurotransmitter synthesis) - Fatty acid synthesis - Proteomic (APP, LRP) - 24SOH - Trivial amount of cytokines	*Microglia:* - Metabolic (energy) - Fatty acid/cholesterol synthesis (for self) - Cytokine production (IL-1, TNFα) - Function: phagocytose Aβ
Astrocytes: - Metabolic (energy) - Fatty acid & cholesterol synthesis (for self & neurons) - Proteomic (ApoE, ABCA1)	*Brain ECs:* - Metabolic (energy) - Fatty acid/cholesterol synthesis (for self) - Proteomic (LRP) - Function: transport Aβ across BBB

Table 10: *Networks for Each Cell Type*. Each cell type expresses a distinct set of metabolic pathways, with overlapping networks on key pathways (such as energy metabolism).

The following figures describe in detail the network topology that was used for each cell type. Chemical species are represented as nodes, while chemical reactions or interactions (inhibitory or promoting) are represented by edges. Molecules belonging to metabolic networks have green nodes, lipid molecules are

orange, proteins are blue, cytokines are red, and all other molecules are purple. Inhibitory interactions are represented by red edges; promoting interactions are given by green edges; all chemical reactions are given by black edges.
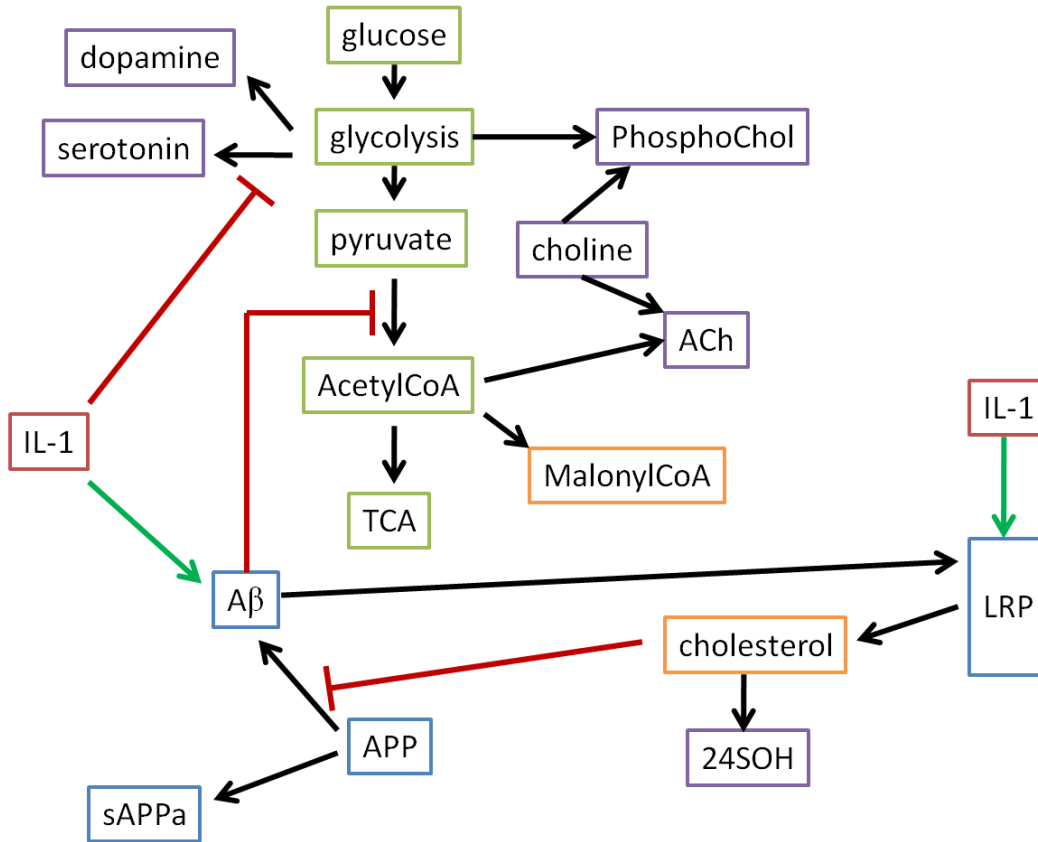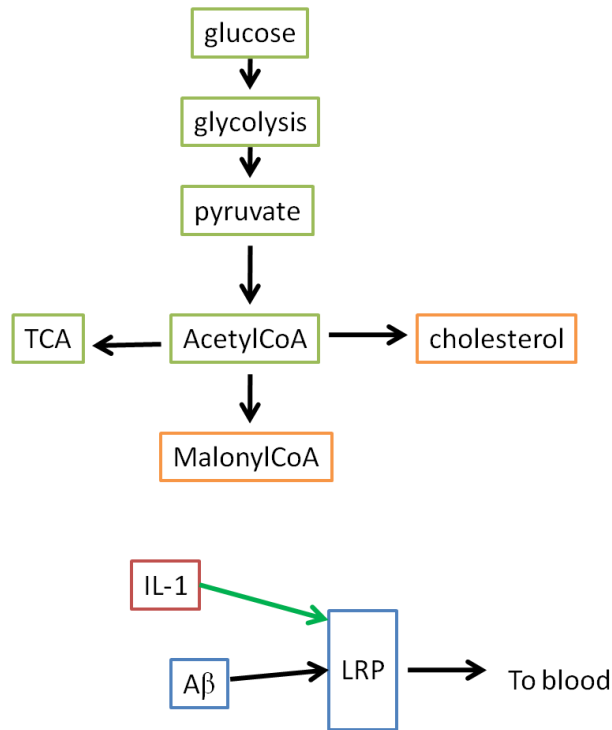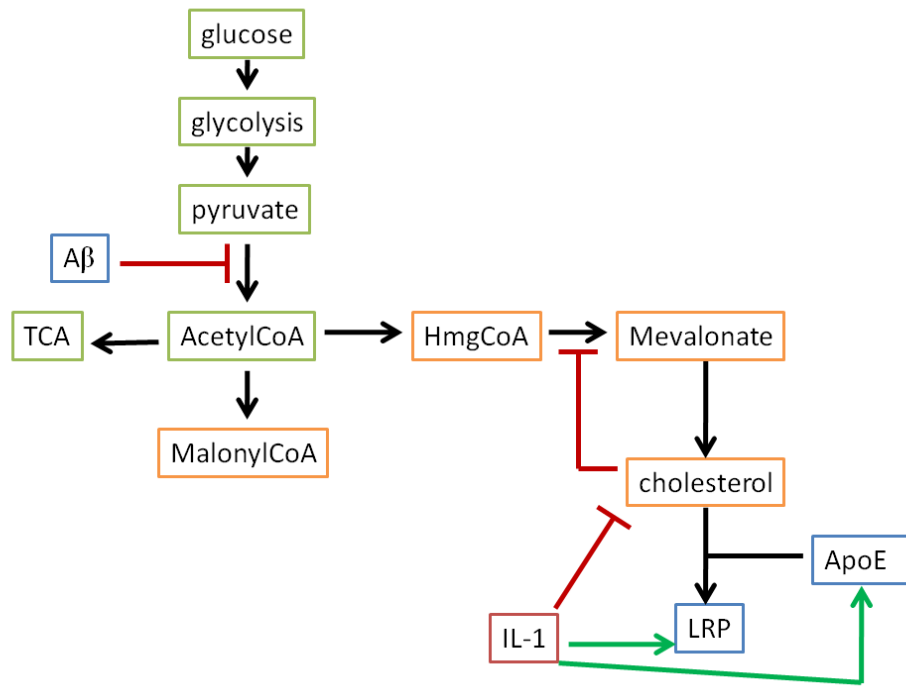

Figure 43: *Network Topology for Neurons*.

Figure 44: *Network Topology for Astrocytes (top) and brain endothelial cells (bottom).*
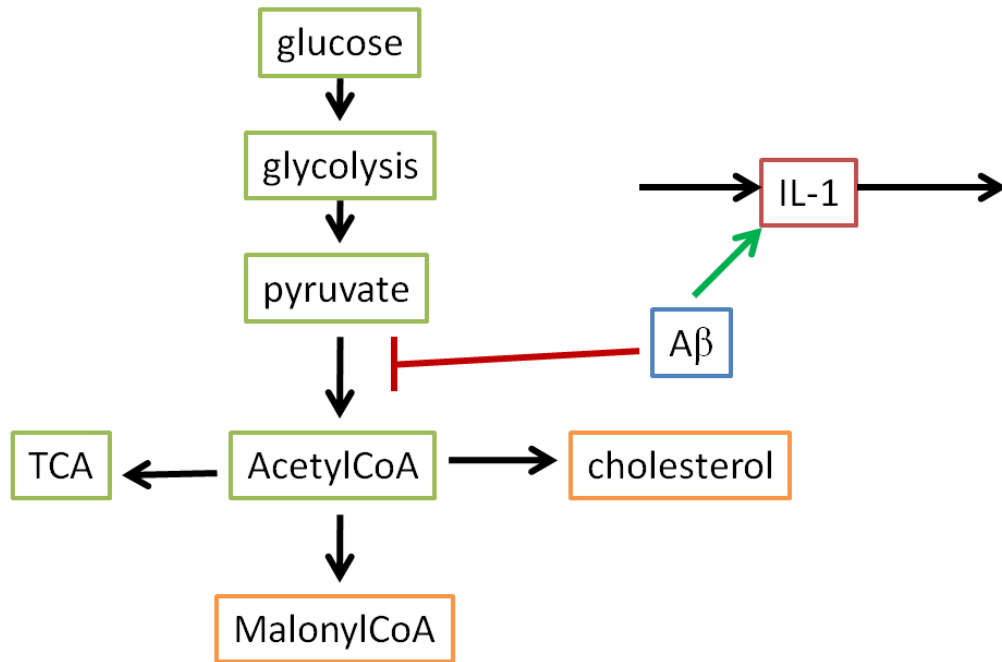
Figure 45: *Network Topology for Microglia*

System of Equations:

A system of equations was derived to describe these interactions. Similar equations were derived for each of the reactions in glycolysis, with only variations in the rate constants used. Glucose metabolism in all cell types was modeled as the conversion of glucose to acetyl coenzyme A, modeling only steps that are key nodes for other important end products or important regulatory steps. In neurons glucose conversion and Acetyl CoA were modeled by the following equations:

$$\frac{dglucose}{dt} = n_1 glucose_T - n_2 glucose$$

$$\frac{dAcoA}{dt} = \frac{n_4}{1 + \alpha A\beta} pyruvate - ACoA(n_5 + n_6 + n_8)$$

Equations for glucose usage and AcetylCoA were similar in other cell types; the only difference was the rate constants. Beta amyloid was modeled as a pseudo-one-step cleavage product of APP. Neuronal cholesterol levels inhibited this generation and were modeled by adding an inhibition term to the Michaelis-Menten rate constant. Beta amyloid could be degraded enzymatically, by astrocyte and microglia uptake or by clearance via LRP-1 on brain endothelial cells:

$$\frac{dAPP}{dt} = g_3 - APP\left(n_9 + d_2 + \left(\frac{n_{10}}{1 + \beta cholN}\right)\right)$$

$$\frac{dA\beta}{dt} = APP\left(\frac{n_{10}}{1 + \beta cholN}\right) + h_7 - A\beta(d_3 + m_7 + b_6 + aLRP_A)$$

LRP was modeled as a simply generation rate minus a degradation rate, with an added generation term (h) that described increased LRP production upon exposure to IL-1:

$$\frac{dLRP_N}{dt} = g_2 + h_1 - d_7 LRP_N$$

In astrocytes, cholesterol metabolism was modeled using simplified equations that studied the conversion of AcetylCoA→HmgCoA→mevalonate→cholesterol, with the key regulatory step being the conversion of HmgCoA to mevalonate:

$$\frac{dmev}{dt} = \frac{a_7}{1 + \beta chol_N} HmgCoA - \frac{a_8}{1 + \delta IL1} mev$$

$$\frac{dchol_A}{dt} = \frac{a_8}{1 + \delta IL1} mev - a_9 apoechol - chol_A(d_8 + d_{13})$$

Derivation of rate constants:

Rate constants for the metabolic network were derived by applying a modified version of Kirchoff's current law to each node in the energy production pathways. This assured that material constraints were being met (conservation of mass). Other rates constants were derived as percentage changes as found in the literature, or estimated from what data was available in the literature or through experiment.

Nodal Analysis:

Nodal analysis is a useful method in identifying possible key nodes in a network. The degree of every node within the sub-cellular level of the hybrid network described here was determined. Nodes were divided between in nodes and out nodes since the graph is directed. No difference in the degree was noted regardless of whether the edge was inhibitory, the step in a chemical reaction, or a promoting factor. Nodes that served roles for transporting other molecules were assigned 1 for node in and 1 for node out. The following table describes both the degree in and degree out for every node.

Network/Chemical Species	Degree In	Degree Out
(Neuron)		
Glucose	1	1
Glycolysis	1	4
Pyruvate	1	1
AcetylCoA	2	3
TCA	1	0
Malonyl CoA	1	0
Serotonin	2	0
Dopamine	1	0
Phosphatidylcholine	2	0
Choline	1	2
Acetylcholine	2	0
APP	1	2
sAPP	1	0
Aβ	3	4
Cholesterol	1	3
LRP	3	1

Astrocyte		
Glucose	1	1
Pyruvate	1	1
AcetylCoA	2	3
TCA	1	0
MalonylCoA	1	0
HmgCoA	1	1
Mevalonate	2	1
cholesterol	2	2
ApoE	2	1
ABCA1	2	1
LRP	3	1
Microglia		
Glucose	1	1
Pyruvate	1	1
AcetylCoA	2	3
TCA	1	0
MalonylCoA	1	0
Cholesterol	1	0
IL-1	2	6
Brain Endothelial Cell		
Glucose	1	1
Pyruvate	1	1
AcetylCoA	1	3
MalonylCoA	1	0
Cholesterol	1	0
TCA	1	0
LRP	3	1

Table 11: *Nodal Analysis.* Descriptions of the degree in and degree out are described.

The degree distribution, which describes the fraction of nodes having degree *k*, was also determined for this network. The most frequent degree in was one, while the most frequent degree out was 0/1. This suggests that many of the molecules that are modeled by this network are terminal reactions in relation to the network topology. There are however several nodes with relatively high degree: AcetylCoA, Aβ, LRP and IL-1 all have degree in or out >=2, suggesting that these are key nodes in this network. Creating the log-log plot of the degree versus the probability of that degree showed a scale-free network given by a power law with an exponent ~2. This

suggests the presence of several hubs (molecules with high degree) and many spokes (terminal reactions).

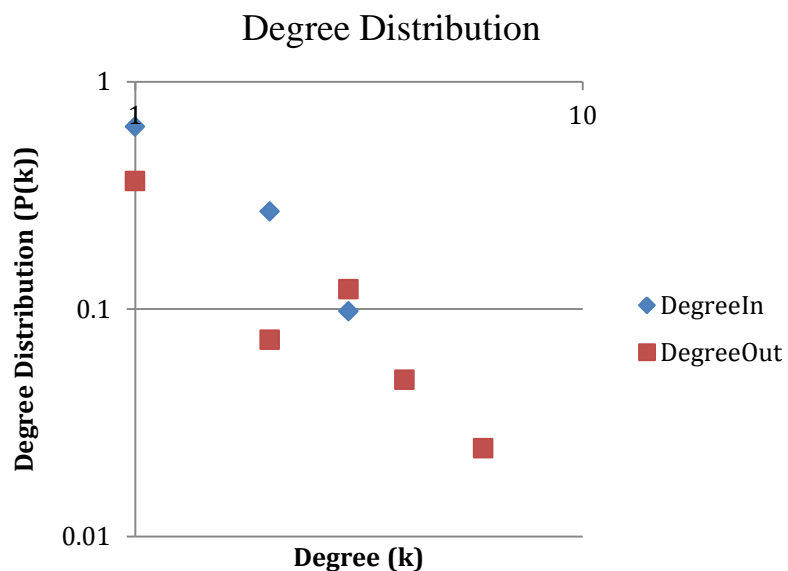| Degree In (k)	0	1	2	3	4	5	6
P(k)	0	26/41	11/41	4/41	0	0	0
Degree Out (l)	0	1	2	3	4	5	6
P(l)	15/41	15/41	3/41	5/41	2/41	0	1/41

Degree Distribution

Figure 46: *Degree Distribution* (top) Degree distribution for the final network topology. (bottom) Log-log of the degree versus the degree distribution, demonstrating a scale-free network.

Simulation Conditions:

Simulations were run for 14600 days (40 years), starting from initial conditions that were supposed to represent the values found in the brain of an average 25 year old. The simulations end time point would be 65 years of age. The system of equations was solved numerically using ODE45 in Matlab. The cases were represented with IF statements that switched the set of differential equations or rate constants being used in the ODEs to those described by the specific case. Figures

describing the temporal concentration distribution of several key molecules were obtained. Results were normalized against their initial values.

Simulation Results:

Reference Simulation:

A reference simulation was run to determine the normal expression levels for all molecules that were being studied. Normal values were as follows: APP- 95; Aβ- 0.132; neuronal cholesterol- 375; astrocytic cholesterol- 37; ApoE- 962; IL-1- 14; LRP on brain ECs- 447. A fast convergence is observed in most simulations.
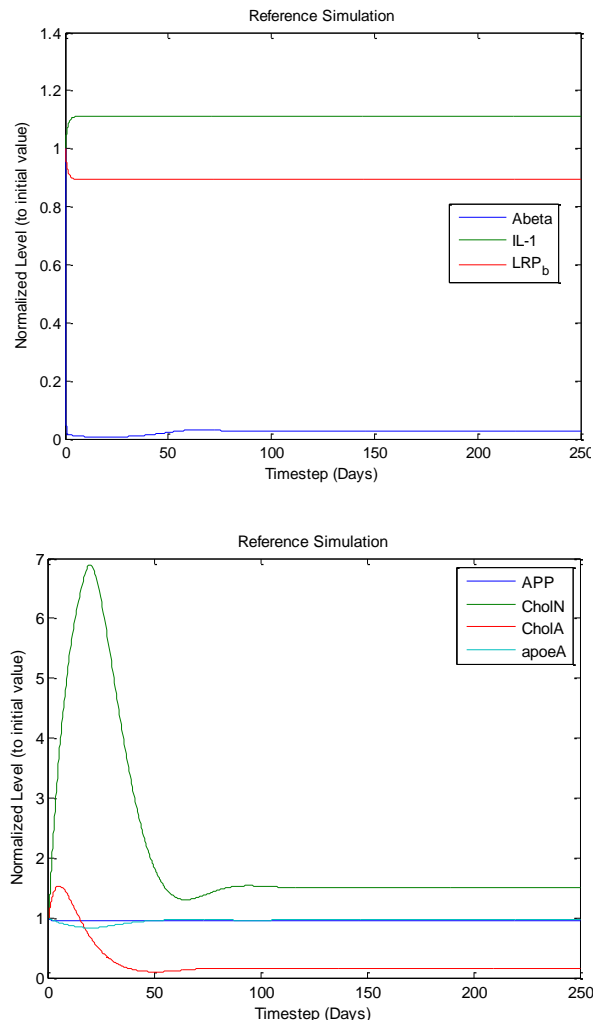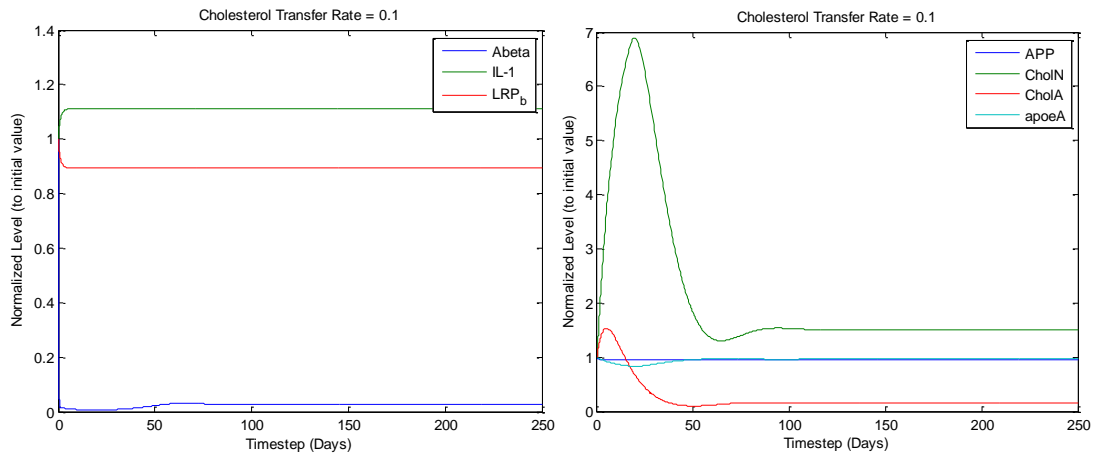

Figure 47: *Reference Simulations.*

Effect of Decreased Cholesterol Transfer Rate:

Decreasing the rate of transfer of cholesterol from astrocytes to neurons led to an increase in beta amyloid levels, a significant increase in neuronal cholesterol, a sustained increase in astrocytic cholesterol and mild increases in APP and ApoE. There are also noticeable changes in the time course at lower transfer rates, leading to a delay.

Effect of Decreasing Cholesterol Production:

Decreasing the cholesterol production rate by astrocytes led to significant increases in Aβ, and mild increases in ApoE, neuronal and astrocytic cholesterol. These results match those that were derived from the experimental section in terms of a similar trend in the data.
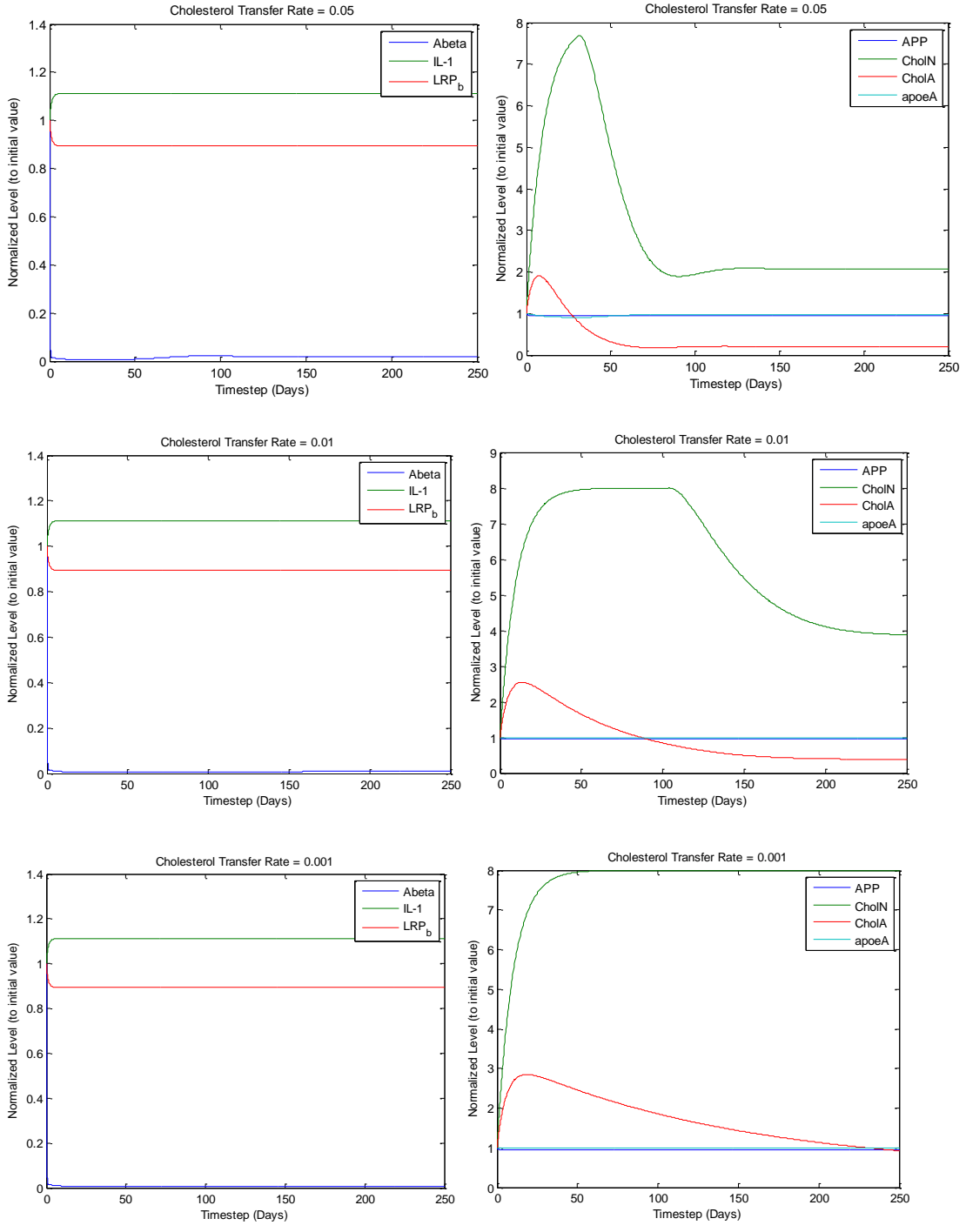
Figure 48: *Effects of Decreased Cholesterol Transfer.* Decreasing the rate at which cholesterol was transferred from astrocytes to neurons led to an increase in steady state beta amyloid, neuronal cholesterol and astrocytic cholesterol.

Figure 49: *Effect of Decreased Acetyl CoA to HmgCoA Conversion:* Decreasing the amount of acetyl CoA to HmgCoA conversion led to a significant increase in steady state levels of beta amyloid. Levels of other molecules only changed slightly or not at all.

Effect of Single Pulse Inflammation:

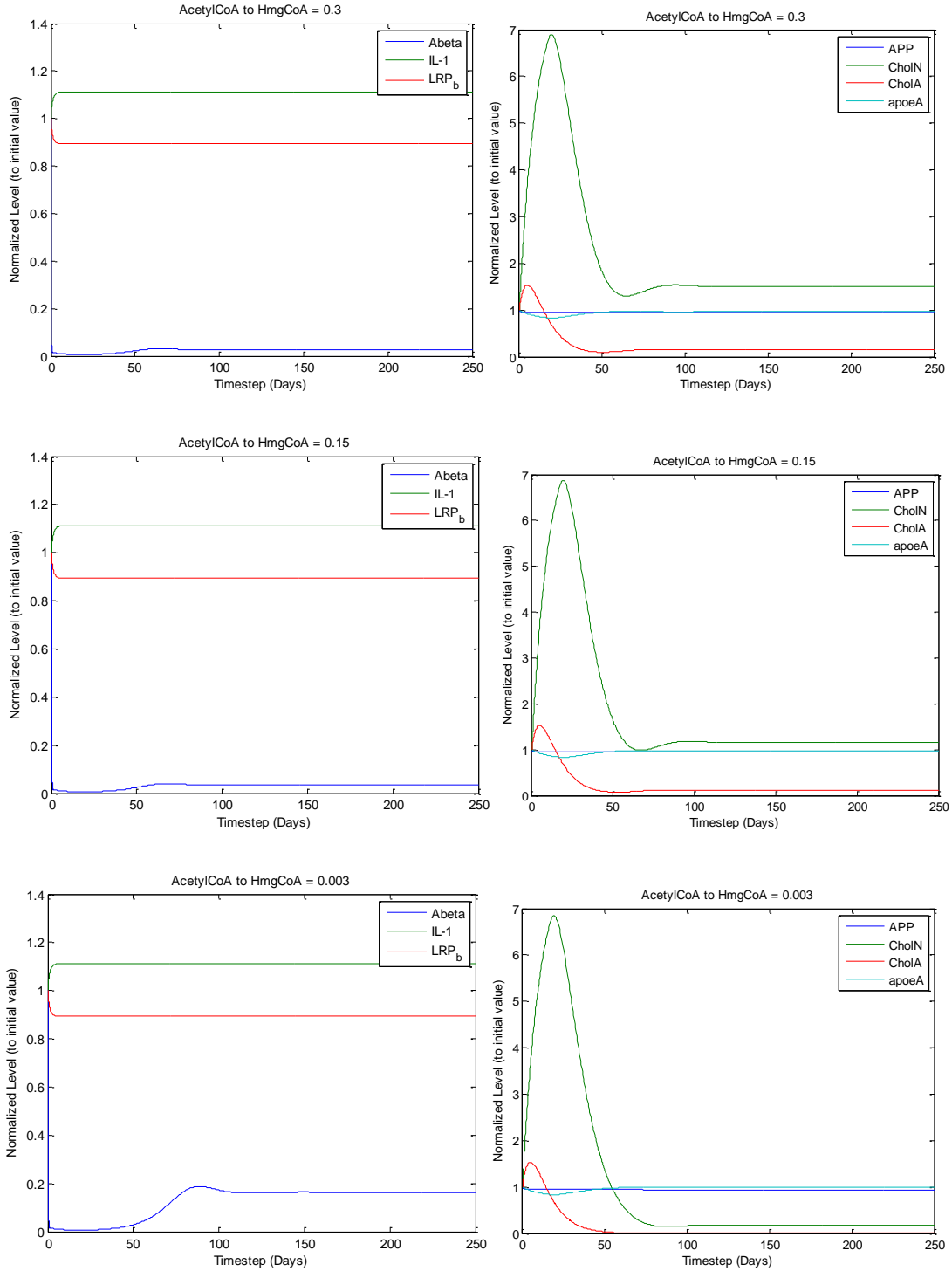Short pulses of increased IL-1 expression (modeled to represent short duration infections) led to sustained increases in ApoE and LRP levels. Neuronal cholesterol levels were perturbed during the duration of the *sickness*, and included an initial decrease, followed by an overshoot, before returning to baseline levels. In all simulations, the final level of Aβ was increased during the duration of the illness, before returning to a level slightly higher than baseline (~5% increase). ApoE levels also increased during the duration of the illness before returning to baseline.

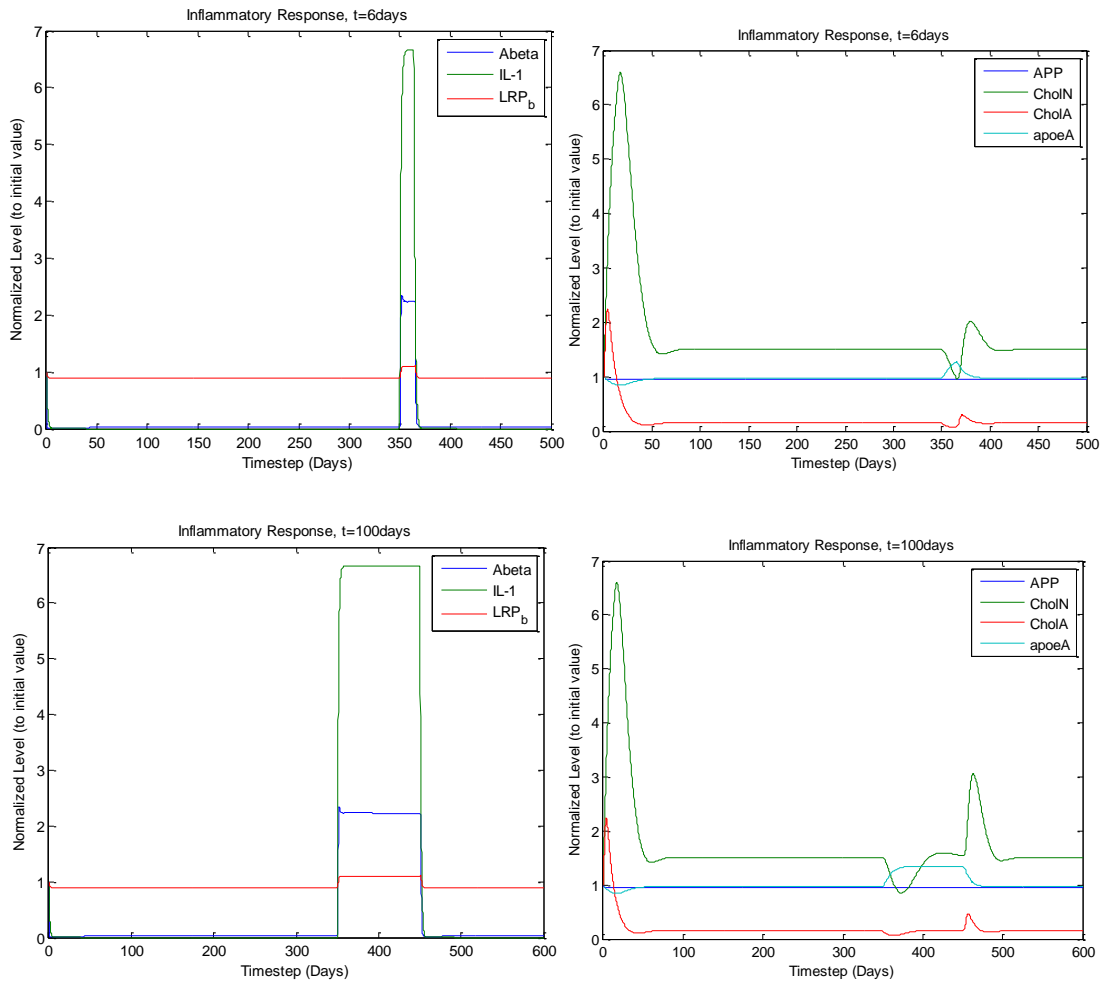**Figure 50**: *Effect of Short-term Inflammatory response*: Short duration inflammatory responses were modeled using step functions to temporarily increase IL-1 levels. This led to a temporally-associated increase in ApoE, neuronal cholesterol and astrocytic cholesterol. Aβ levels were increased significantly during the illness period (~200%), before returning to slightly higher baseline levels (~5% increase).

151

Effects of Periodic Inflammation:

Periodic inflammation that returned to a state of no inflammation (acute inflammation) led to corresponding oscillatory increases in beta amyloid levels, as well as significant increases in ApoE and cholesterol levels during the high inflammatory state. A very weak shift upwards in beta amyloid levels was observed over time (~4%). Under chronic inflammation, beta amyloid levels increased significantly (>10x) that was sustained for the duration of inflammation. Under these conditions, ApoE levels increased significantly (~40%) while LRP levels increased mildly (<10%). Neuronal cholesterol was trivially increased (<1%).
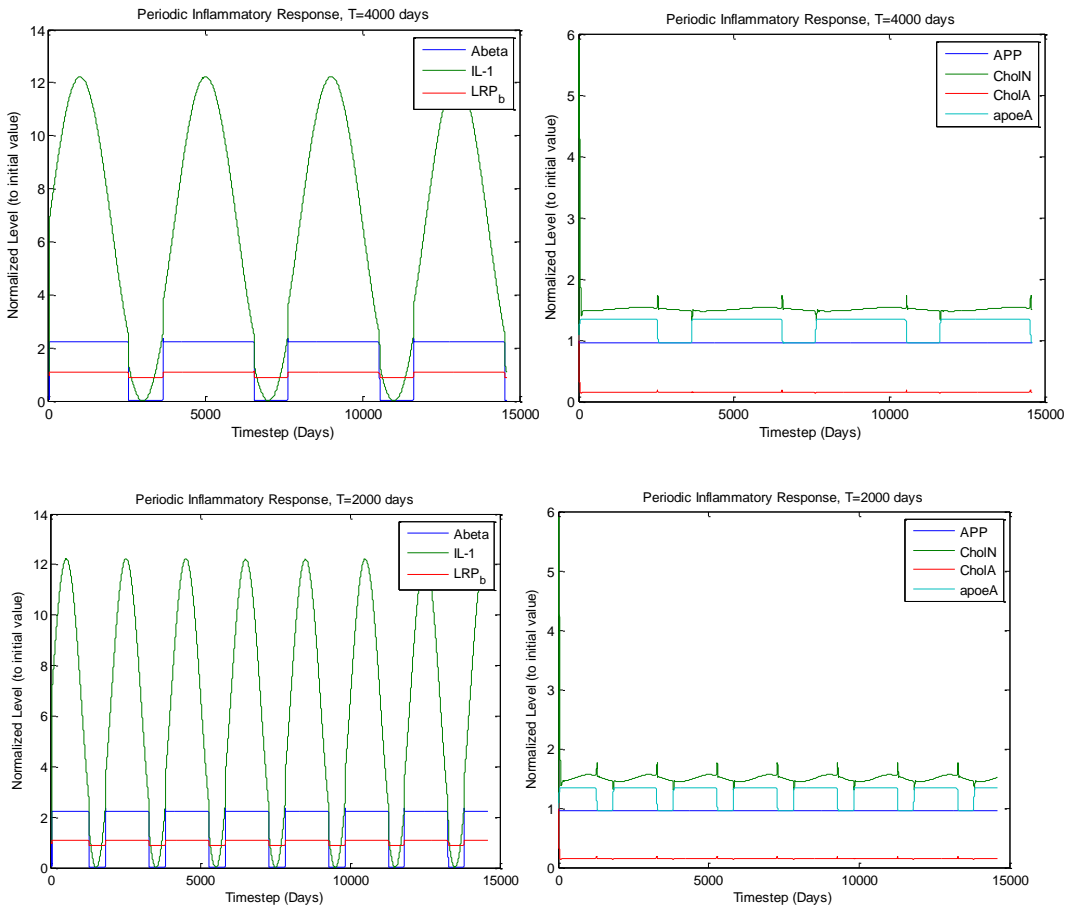
Figure 51: *Effect of Acute Periodic Inflammation.* Levels of different chemical species correspond temporally to increases in IL-1. Beta amyloid levels increased slightly (~5%).

Effect of Decreased Available Glucose:

Decreasing the amount of glucose available to all cells led a significant increase in Aβ levels (~50%) for the most extreme case to be modeled, a significant decrease in both astrocytic and neuronal cholesterol, and a mild increase in ApoE.
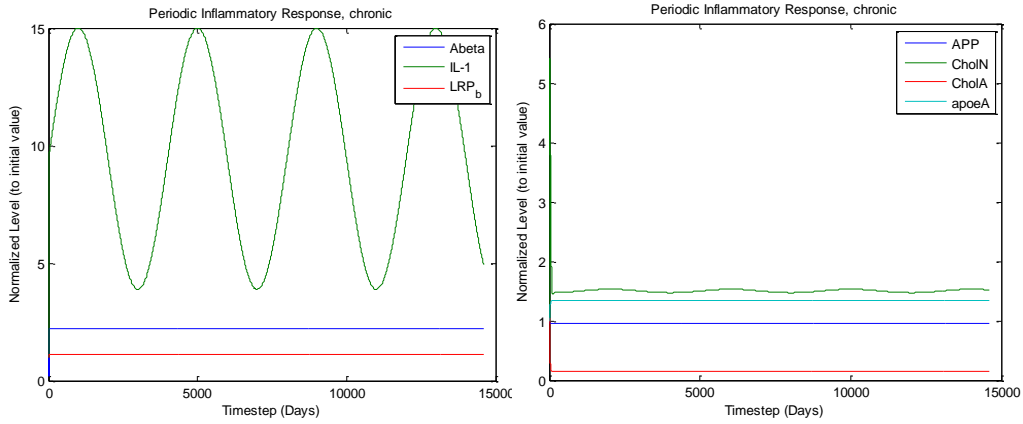
Figure 52: *Effect of Chronic Periodic Inflammation.* Chronic inflammation led to a significant increase in beta amyloid (>10x) and ApoE (~40%). Neuronal cholesterol levels were increased only mildly (<1%)
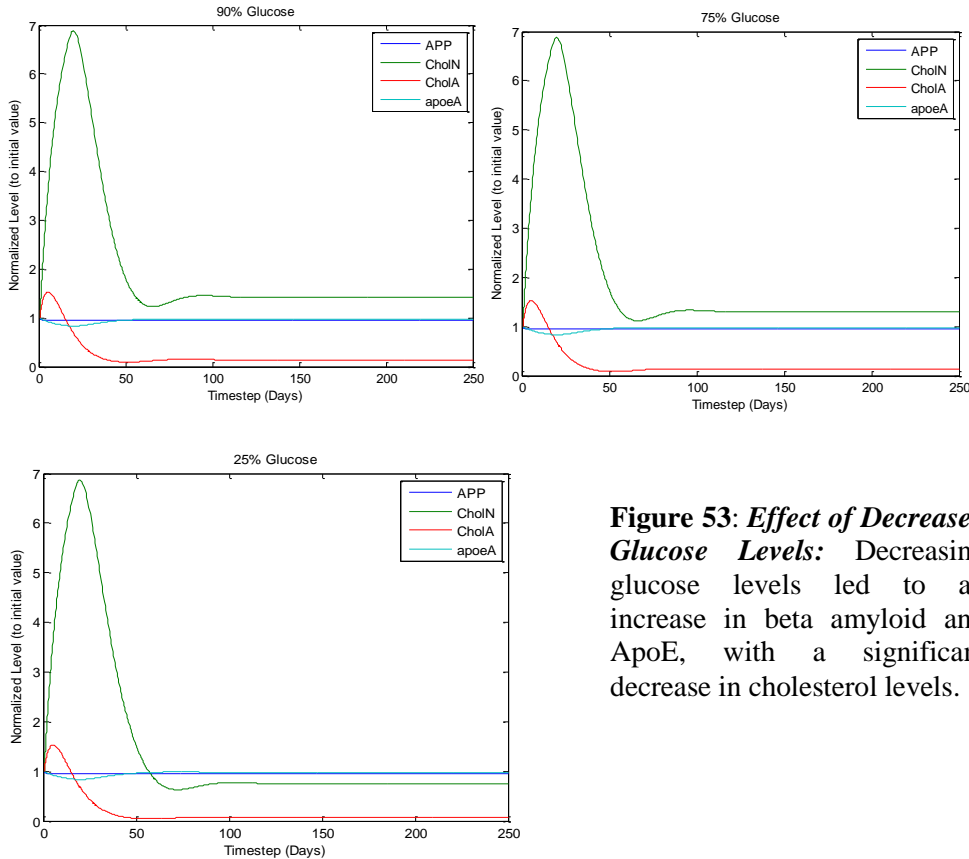
Figure 53: *Effect of Decreased Glucose Levels:* Decreasing glucose levels led to an increase in beta amyloid and ApoE, with a significant decrease in cholesterol levels.

Effect of Increased Aβ Production:

Increasing the production rate of beta amyloid only led to a mild increase in beta amyloid and APP. No other molecules were affected significantly.
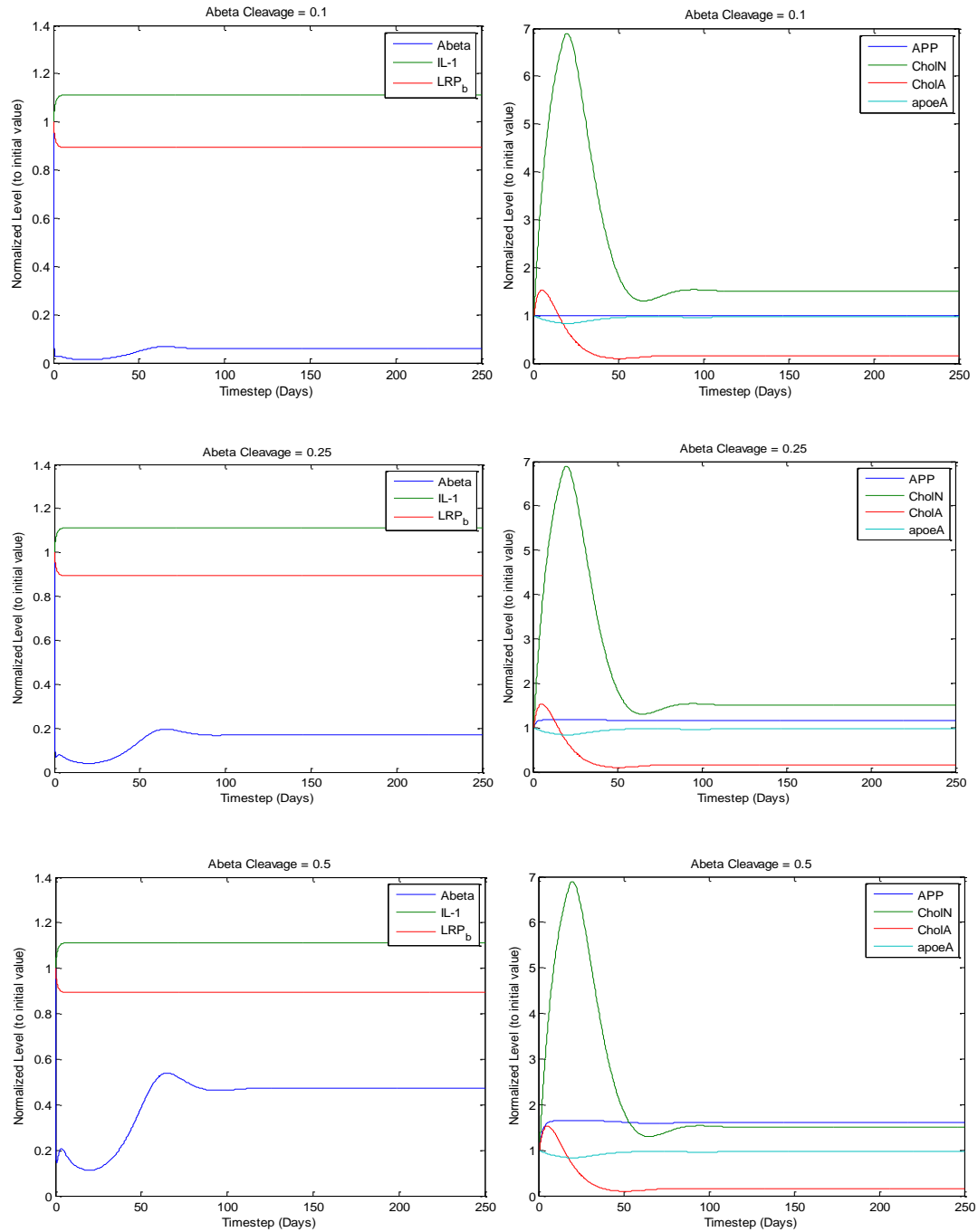
Figure 54: *Effect of increased Aβ cleavage on the network.* Increasing the cleavage rate of beta amyloid from APP led to increased levels of beta amyloid and APP. Other molecules were not significantly affected.

Discussion & Conclusion:

In this chapter, an updated version of the systems biology model that was developed in chapter 4 was developed. This model expanded to include 41 nodes and was compartmentalized into 4 different cell types. The model was expanded to include the role of inflammation, particularly the role of IL-1. Several different simulation runs were made, looking at the roles of decreased cholesterol, increased inflammatory state and increased beta amyloid production.

Decreasing the production rate of cholesterol by astrocytes led to an increase in beta amyloid and ApoE, which was very similar to that which was seen in the biological experiments that studied the effect of simvastatin. Chronic inflammation was found to profoundly affect the system, leading to prolonged increases in the level of ApoE and Aβ. This suggests that inflammation may play a unique causal role in AD pathogenesis that warrants further simulation and experimentation. Increasing the cleavage rate of beta amyloid had little direct effect on other molecules in the system over the range that was studied. This suggests that increased cleavage does not have a significant effect on the network system unless other factors or triggering events are met. This is not to say that increased beta amyloid levels do not play a role in the pathogenesis of AD, such as that seen in familial AD, but that several things may be at play for why increased beta amyloid levels are present and affect the system. For example, significantly increased levels of any protein will negatively affect the state of a biological system, putting strain on resources to clear the protein, possibly competitive interactions between the increased protein and other proteins that share the same receptors or transport proteins, and changing the local osmolarity

and viscosity of the extracellular fluid, all of which could have negative downstream effects. Thus, the increased Aβ generation rates seen in familial AD may initially operate under a different pathogenesis mechanism, before converging onto a similar disease process that is observed in late-onset AD. The model developed here further suggests that unless beta amyloid levels pass a threshold level and initiate an inflammatory response that beta amyloid alone may not be able to initiate the pathologic profile seen in AD.

It should be noted that the simulation results converged quite quickly since the equation used were written to model the steady state approximations and simply study the changes in steady states observed after different perturbations. This model is the first network model for AD for looking not just at cellular interactions, but also at the metabolic, proteomic and lipidomic networks that underlie these cellular interactions, and represents a significant advance forward in using mathematical modeling to better understand disease processes.

Chapter 7: Conclusions & Future Work

Conclusions:

As stated back in Chapter 2, there are an array of risk factors for AD, many of which inflammation plays a significant role in pathology. It is well-accepted in the medical field that metabolic syndrome, another disease caused by general inflammation in the body, that it is not a single or small number of risk factors that lead to initiation of the disease process. The same idea has been proposed for cancer and diabetes. In the same manner of thinking, it is reasonable to propose that having only 1or 2 risk factors for AD (excluding those factors which are purely genetic) does not guarantee that AD will occur in the future. It is only when several or more risk factors are present that disease occurs, that is, that there is a relative 'catastrophe' in the biological system which disrupts multiple interdependent biochemical networks. This concept would help to explain some of the variability seen between studies (aside from the variability due to biased or poorly designed experiments). It also would help to bring together many studies that would otherwise seem unrelated or contradictory, and give the results of epidemiological studies a better understanding.

In addition to this, importance should be placed on how AD pathology relates to disease causation and symptomology. For example, although Aβ levels are increased in the brains of nearly all individuals affected by AD, leading to the traditional belief that these plaques or oligomers are the cause of disease, this perspective fails to take into account the possibility that Aβ buildup may just be a symptom of an underlying disease process, and not the actual cause of the disease.

Just like increased white cell count is not the cause of an infection, but nearly the response to an infection, Aβ may also have a similar role in AD pathogenesis.

Along this same perspective, disease states in general can be viewed as the response of a system to different inputs. Preceding a disease, many different inputs may be received by the body. These inputs must be 'decrypted', processed, interpreted correctly and a decision must be made as to how to keep the organism in a state of homeostasis. A simple survey of regulatory and signal transduction pathways clearly demonstrates that differing inputs often have convergent outputs and moreover these pathways may converge even before a response is taken. For example, intracellular levels of calcium change in response to neurotransmitter binding, ligand binding, and in response to the IP3/DAG pathway. This similarity in network topology, and mutual sharing of common chemical nodes with high traffic, is an evolutionarily advantageous method that living organisms have capitalized on to prevent the need of extra molecules necessary for functioning and putting an upper bound on the amount of genetic material that an organism would need to survive. This does, however, have drawbacks when a mutation occurs in one of these pathways, or if the regulation of a pathway is in disarray. In such a case, the robustness of the system is lost and a disease state is necessitated if balance is not maintained within the system.

Inflammation is perhaps the single most important state that has to be balanced in the human body. Mild to moderate levels of inflammation over short periods of time may actually be beneficial to the body as a system, stimulating the removal of old, dysfunctional or dead cells and promoting regeneration and creation

of new, healthy cells. In AD and many other disease states, this balance is off, leading to cell death and disease. The importance of the inflammatory pathway was demonstrated by the results of the final model, which showed that for even a short duration increase of the pro-inflammatory molecule, IL-1, there are significant and long-term changes the expression patterns of ApoE and LRP-1, in addition to short-term alterations in cholesterol metabolism. It is interesting to note that changes to cholesterol levels were relatively more transient than those to protein expression levels, though it provides nice insight into the possible disease process.

From the experimental results, cholesterol metabolism does seem to play a contributory, if not significant role, in the progression of AD. This role, which may be prominent due to the high interconnectivity of the cholesterol pathway with other key metabolic pathways, has effects on several other pathways that may not directly be connected to cholesterol or its metabolites.

Future Work

Modeling AD and the multitude of pathways and interactions related or possibly related to the disease process is an enormous task. The work presented here just starts to touch the tip of what is possible in terms of using mathematical modeling to better understand disease processes, particularly AD. There are many avenues of open research in this area. Of particular interest to myself would be to look at the role of genetics and epigenetics in AD pathogenesis, as well as the role that chronic stress and adrenal hormones may play in the disease process, in combination with continued biological experiments. Additionally, it would be particularly interesting to study the interaction between the immunological,

psychological, and endocrinological aspects of AD in hopes of creating a unified model for AD pathogenesis that looks at the disease from the various aspects. Future experiments with human subjects would help to gather more relevant data for the model, needed rate constants and further information about the topology of the interacting networks. Expanding this model to include stochastic rate constants, and additional genomic and proteomic interactions would help to make an even more accurate mathematical description for AD pathogenesis that, when combined with biological data and interpreted in the light of such data, could help to create new treatment paradigms in the future.
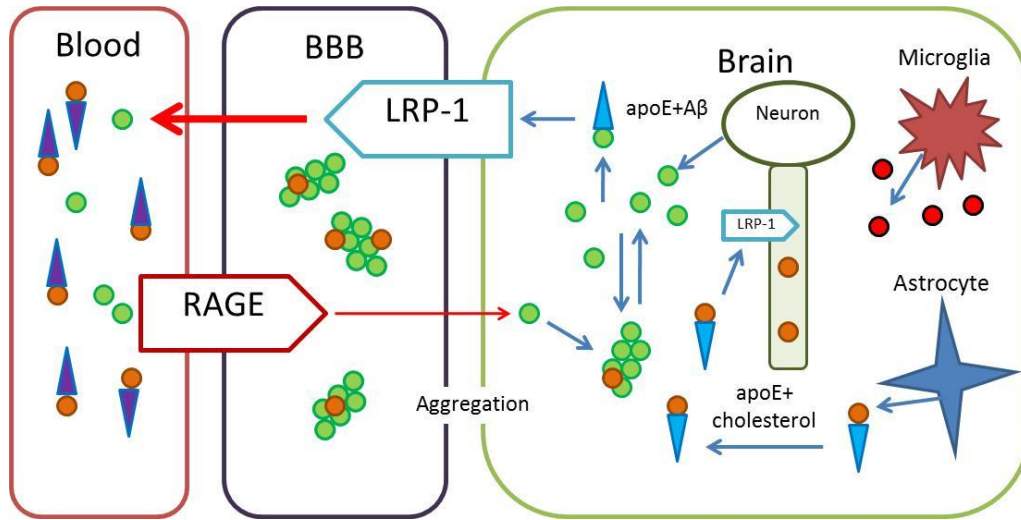
Appendix I

Figure 1: Updated figure for the compartmentalized network used in the final math model.
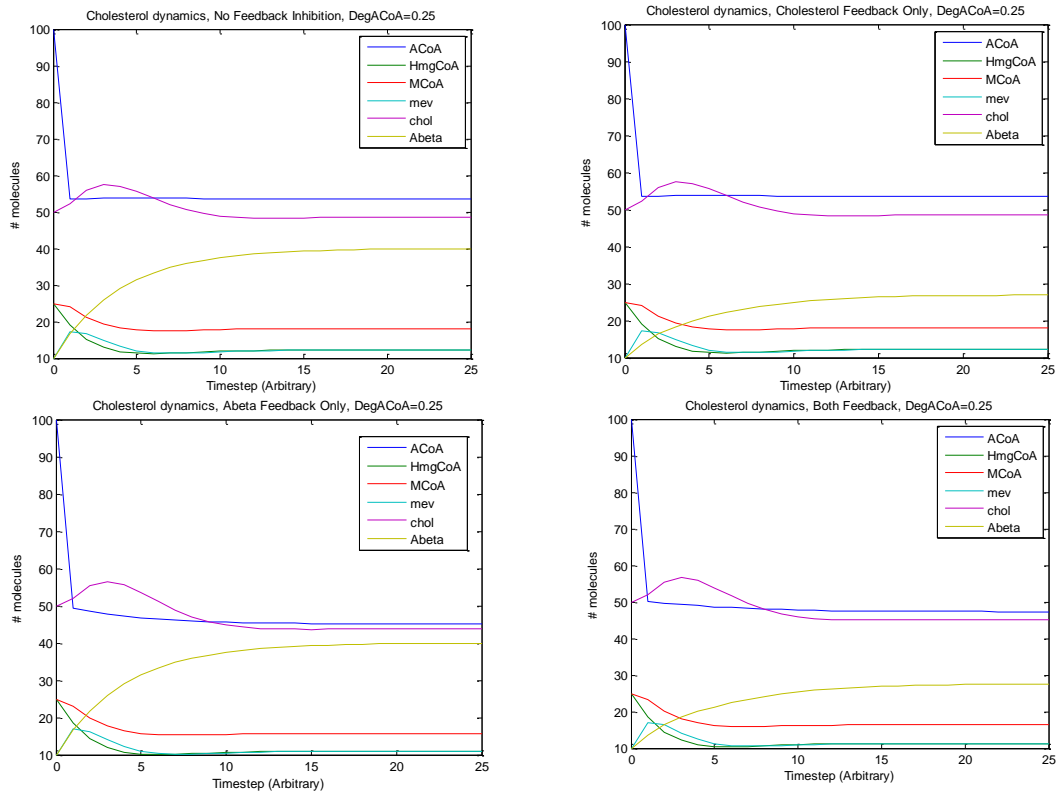
Appendix II

Figure 2: ~50% increased levels of beta amyloid when no feedback control by cholesterol. When feedback by Aβ is removed, normal levels of cholesterol and Aβ observed.

Bibliography

1.   Abad-Rodriguez, J., et al., Neuronal membrane cholesterol loss enhances amyloid peptide generation. J Cell Biol, 2004. 167(5): p. 953-60.
2.   Alarcon, R., et al., Expression of scavenger receptors in glial cells. Comparing the adhesion of astrocytes and microglia from neonatal rats to surface-bound beta-amyloid. J Biol Chem, 2005. 280(34): p. 30406-15.
3.   Alkadhi, K.A., M. Srivareerat, and T.T. Tran, Intensification of long-term memory deficit by chronic stress and prevention by nicotine in a rat model of Alzheimer's disease. Mol Cell Neurosci. 45(3): p. 289-96.
4.   Allan, S.M. and N.J. Rothwell, Inflammation in central nervous system injury. Philos Trans R Soc Lond B Biol Sci, 2003. 358(1438): p. 1669-77.
5.   Arvin, B., et al., The role of inflammation and cytokines in brain injury. Neurosci Biobehav Rev, 1996. 20(3): p. 445-52.
6.   Ball, P., Synthetic biology: starting from scratch. Nature, 2004. 431(7009): p. 624-6.
7.   Ballabh, P., A. Braun, and M. Nedergaard, The blood-brain barrier: an overview: structure, regulation, and clinical implications. Neurobiol Dis, 2004. 16(1): p. 1-13.
8.   Banati, R.B., et al., Cytotoxicity of microglia. Glia, 1993. 7(1): p. 111-8.
9.   Barone, E., et al., Long-term high-dose atorvastatin decreases brain oxidative and nitrosative stress in a preclinical model of Alzheimer disease: a novel mechanism of action. Pharmacol Res. 63(3): p. 172-80.
10.   Benito-Leon, J., et al., Statins and cognitive functioning in the elderly: a population-based study. J Alzheimers Dis. 21(1): p. 95-102.
11.   Besedovsky, H.O., et al., Cytokines as modulators of the hypothalamus-pituitary-adrenal axis. J Steroid Biochem Mol Biol, 1991. 40(4-6): p. 613-8.
12.   Bjorkhem, I. and S. Meaney, Brain cholesterol: long secret life behind a barrier. Arterioscler Thromb Vasc Biol, 2004. 24(5): p. 806-15.
13.   Bliznakov, E.G., Lipid-lowering drugs (statins), cholesterol, and coenzyme Q10. The Baycol case--a modern Pandora's box. Biomed Pharmacother, 2002. 56(1): p. 56-9.
14.   Bloomfield, I.G., I.H. Johnston, and L.E. Bilston, Effects of proteins, blood cells and glucose on the viscosity of cerebrospinal fluid. Pediatr Neurosurg, 1998. 28(5): p. 246-51.
15.   Bonate, P.L., Animal models for studying transport across the blood-brain barrier. J Neurosci Methods, 1995. 56(1): p. 1-15.
16.   Bravo, R., et al., Sulfated polysaccharides promote the assembly of amyloid beta(1-42) peptide into stable fibrils of reduced cytotoxicity. J Biol Chem, 2008. 283(47): p. 32471-83.
17.   Broersen, K., F. Rousseau, and J. Schymkowitz, The culprit behind amyloid beta peptide related neurotoxicity in Alzheimer's disease: oligomer size or conformation? Alzheimers Res Ther. 2(4): p. 12.
18.   Butterfield, D.A., E. Barone, and C. Mancuso, Cholesterol-independent neuroprotective and neurotoxic activities of statins: Perspectives for statin use in Alzheimer disease and other age-related neurodegenerative disorders. Pharmacol Res. 64(3): p. 180-6.
19.   Butz, M., et al., A theoretical network model to analyse neurogenesis and synaptogenesis in the dentate gyrus. Neural Netw, 2006. 19(10): p. 1490-505.
20.   Cagnin, A., et al., In vivo visualization of activated glia by [11C] (R)-PK11195-PET following herpes encephalitis reveals projected neuronal damage beyond the primary focal lesion. Brain, 2001. 124(Pt 10): p. 2014-27.

21. Calhoun, M.E., et al., Neuronal overexpression of mutant amyloid precursor protein results in prominent deposition of cerebrovascular amyloid. Proc Natl Acad Sci U S A, 1999. 96(24): p. 14088-93.

22. Campbell, S., et al., Lower hippocampal volume in patients suffering from depression: a meta-analysis. Am J Psychiatry, 2004. 161(4): p. 598-607.

23. Capuron, L. and R. Dantzer, Cytokines and depression: the need for a new paradigm. Brain Behav Immun, 2003. 17 Suppl 1: p. S119-24.

24. Capuron, L. and A.H. Miller, Immune system to brain signaling: neuropsychopharmacological implications. Pharmacol Ther. 130(2): p. 226-38.

25. Carbonell, W.S., et al., Migration of perilesional microglia after focal brain injury and modulation by CC chemokine receptor 5: an in situ time-lapse confocal imaging study. J Neurosci, 2005. 25(30): p. 7040-7.

26. Carson, J.A. and A.J. Turner, Beta-amyloid catabolism: roles for neprilysin (NEP) and other metallopeptidases? J Neurochem, 2002. 81(1): p. 1-8.

27. Cecchi, G.A., et al., Unsupervised learning and adaptation in a model of adult neurogenesis. J Comput Neurosci, 2001. 11(2): p. 175-82.

28. Chauhan, N.B., Membrane dynamics, cholesterol homeostasis, and Alzheimer's disease. J Lipid Res, 2003. 44(11): p. 2019-29.

29. Choudhury, R.P., et al., Effects of simvastatin on plasma lipoproteins and response to arterial injury in wild-type and apolipoprotein-E-deficient mice. J Vasc Res, 2004. 41(1): p. 75-83.

30. Cirrito, J.R., et al., In vivo assessment of brain interstitial fluid with microdialysis reveals plaque-associated changes in amyloid-beta metabolism and half-life. J Neurosci, 2003. 23(26): p. 8844-53.

31. Cizas, P., et al., Size-dependent neurotoxicity of beta-amyloid oligomers. Arch Biochem Biophys. 496(2): p. 84-92.

32. Craft, D.L., L.M. Wein, and D.J. Selkoe, A mathematical model of the impact of novel treatments on the A beta burden in the Alzheimer's brain, CSF and plasma. Bull Math Biol, 2002. 64(5): p. 1011-31.

33. Crameri, A., et al., The role of seladin-1/DHCR24 in cholesterol biosynthesis, APP processing and Abeta generation in vivo. Embo J, 2006. 25(2): p. 432-43.

34. Cunningham, C., et al., Systemic inflammation induces acute behavioral and cognitive changes and accelerates neurodegenerative disease. Biol Psychiatry, 2009. 65(4): p. 304-12.

35. Danielsson, J., et al., 15N relaxation study of the amyloid beta-peptide: structural propensities and persistence length. Magn Reson Chem, 2006. 44 Spec No: p. S114-21.

36. Deane, R., et al., Clearance of amyloid-beta peptide across the blood-brain barrier: implication for therapies in Alzheimer's disease. CNS Neurol Disord Drug Targets, 2009. 8(1): p. 16-30.

37. Deane, R., A. Sagare, and B.V. Zlokovic, The role of the cell surface LRP and soluble LRP in blood-brain barrier Abeta clearance in Alzheimer's disease. Curr Pharm Des, 2008. 14(16): p. 1601-5.

38. Deane, R., et al., LRP/amyloid beta-peptide interaction mediates differential brain efflux of Abeta isoforms. Neuron, 2004. 43(3): p. 333-44.

39. Deane, R. and B.V. Zlokovic, Role of the blood-brain barrier in the pathogenesis of Alzheimer's disease. Curr Alzheimer Res, 2007. 4(2): p. 191-7.

40. DeBarber, A.E., et al., Liquid chromatography-tandem mass spectrometry determination of plasma 24S-hydroxycholesterol with chromatographic separation of 25-hydroxycholesterol. Anal Biochem, 2008. 381(1): p. 151-3.

41. Dermietzel, R., D.C. Spray, and M. Nedergaard, Blood-brain barriers : from ontogeny to artificial interfaces. 2006, Weinheim, Germany: Wiley-VCH. 2 v. (xxxii, 741 p.).

42. Diedrich, J.F., et al., Neuropathological changes in scrapie and Alzheimer's disease are associated with increased expression of apolipoprotein E and cathepsin D in astrocytes. J Virol, 1991. 65(9): p. 4759-68.

43. Donahue, J.E., et al., RAGE, LRP-1, and amyloid-beta protein in Alzheimer's disease. Acta Neuropathol, 2006. 112(4): p. 405-15.

44. Donnini, S., et al., FGF-2 overexpression opposes the beta amyloid toxic injuries to the vascular endothelium. Cell Death Differ, 2006. 13(7): p. 1088-96.

45. Dzeletovic, S., et al., Determination of cholesterol oxidation products in human plasma by isotope dilution-mass spectrometry. Anal Biochem, 1995. 225(1): p. 73-80.

46. Edelstein-keshet, L. and A. Spiros, Exploring the formation of Alzheimer's disease senile plaques in silico. J Theor Biol, 2002. 216(3): p. 301-26.

47. Edelstein-keshet, L. and A. Spiros, Exploring the formation of Alzheimer's disease senile plaques in silico. J Theor Biol, 2002. 216(3): p. 301-26.

48. Elias, P.K., et al., Serum cholesterol and cognitive performance in the Framingham Heart Study. Psychosom Med, 2005. 67(1): p. 24-30.

49. Eroglu, C. and B.A. Barres, Regulation of synaptic connectivity by glia. Nature. 468(7321): p. 223-31.

50. Evans, B.A., et al., Long-term statin therapy and CSF cholesterol levels: implications for Alzheimer's disease. Dement Geriatr Cogn Disord, 2009. 27(6): p. 519-24.

51. Fassbender, K., et al., Simvastatin strongly reduces levels of Alzheimer's disease beta -amyloid peptides Abeta 42 and Abeta 40 in vitro and in vivo. Proc Natl Acad Sci U S A, 2001. 98(10): p. 5856-61.

52. Feldman, H.H., et al., Randomized controlled trial of atorvastatin in mild to moderate Alzheimer disease: LEADe. Neurology. 74(12): p. 956-64.

53. Francis, P.T. and E.K. Perry, Cholinergic and other neurotransmitter mechanisms in Parkinson's disease, Parkinson's disease dementia, and dementia with Lewy bodies. Mov Disord, 2007. 22 Suppl 17: p. S351-7.

54. French, A.P., et al., Colocalization of fluorescent markers in confocal microscope images of plant cells. Nat Protoc, 2008. 3(4): p. 619-28.

55. Gee, J.R. and J.N. Keller, Astrocytes: regulation of brain homeostasis via apolipoprotein E. Int J Biochem Cell Biol, 2005. 37(6): p. 1145-50.

56. Gonzalez-Velasquez, F.J., J.A. Kotarek, and M.A. Moss, Soluble aggregates of the amyloid-beta protein selectively stimulate permeability in human brain microvascular endothelial monolayers. J Neurochem, 2008. 107(2): p. 466-77.

57. Grace, E.A., C.A. Rabiner, and J. Busciglio, Characterization of neuronal dystrophy induced by fibrillar amyloid beta: implications for Alzheimer's disease. Neuroscience, 2002. 114(1): p. 265-73.

58. Gray, H., et al., Gray's anatomy, descriptive and applied. 32d [centenary] ed ed. 1958, London, New York,: Longmans. xxiii, 1604 p.

59. Green, K.N., et al., Glucocorticoids increase amyloid-beta and tau pathology in a mouse model of Alzheimer's disease. J Neurosci, 2006. 26(35): p. 9047-56.

60. Guntert, A., H. Dobeli, and B. Bohrmann, High sensitivity analysis of amyloid-beta peptide composition in amyloid deposits from human and PS2APP mouse brain. Neuroscience, 2006. 143(2): p. 461-75.

61. Haas, H.S. and K. Schauenstein, Neuroimmunomodulation via limbic structures--the neuroanatomy of psychoimmunology. Prog Neurobiol, 1997. 51(2): p. 195-222.

62.   Haass, C. and D.J. Selkoe, Soluble protein oligomers in neurodegeneration: lessons from the Alzheimer's amyloid beta-peptide. Nat Rev Mol Cell Biol, 2007. 8(2): p. 101-12.

63.   Halford, R.W. and D.W. Russell, Reduction of cholesterol synthesis in the mouse brain does not affect amyloid formation in Alzheimer's disease, but does extend lifespan. Proc Natl Acad Sci U S A, 2009. 106(9): p. 3502-6.

64.   Hamanaka, H., et al., Altered cholesterol metabolism in human apolipoprotein E4 knock-in mice. Hum Mol Genet, 2000. 9(3): p. 353-61.

65.   Hebert, L.E., et al., Alzheimer disease in the US population: prevalence estimates using the 2000 census. Arch Neurol, 2003. 60(8): p. 1119-22.

66.   Hoshi, M., et al., Regulation of mitochondrial pyruvate dehydrogenase activity by tau protein kinase I/glycogen synthase kinase 3beta in brain. Proc Natl Acad Sci U S A, 1996. 93(7): p. 2719-23.

67.   Heneka, M.T. and M.K. O'Banion, Inflammatory processes in Alzheimer's disease. J Neuroimmunol, 2007. 184(1-2): p. 69-91.

68.   Hippisley-Cox, J. and C. Coupland, Unintended effects of statins in men and women in England and Wales: population based cohort study using the QResearch database. Bmj. 340: p. c2197.

69.   Hortschansky, P., et al., The aggregation kinetics of Alzheimer's beta-amyloid peptide is controlled by stochastic nucleation. Protein Sci, 2005. 14(7): p. 1753-9.

70.   Hrabe, J., S. Hrabetova, and K. Segeth, A model of effective diffusion and tortuosity in the extracellular space of the brain. Biophys J, 2004. 87(3): p. 1606-17.

71.   Huang, Y., et al., Apolipoprotein E: diversity of cellular origins, structural and biophysical properties, and effects in Alzheimer's disease. J Mol Neurosci, 2004. 23(3): p. 189-204.

72.   Hudry, E., et al., Adeno-associated Virus Gene Therapy With Cholesterol 24-Hydroxylase Reduces the Amyloid Pathology Before or After the Onset of Amyloid Plaques in Mouse Models of Alzheimer's Disease. Mol Ther, 2009.

73.   Iadecola, C., Neurovascular regulation in the normal brain and in Alzheimer's disease. Nat Rev Neurosci, 2004. 5(5): p. 347-60.

74.   Iadecola, C. and M. Nedergaard, Glial regulation of the cerebral microvasculature. Nat Neurosci, 2007. 10(11): p. 1369-76.

75.   Isaksen, J.G., et al., Determination of wall tension in cerebral artery aneurysms by numerical simulation. Stroke, 2008. 39(12): p. 3172-8.

76.   Jeong, Y.H., et al., Chronic stress accelerates learning and memory impairments and increases amyloid deposition in APPV717I-CT100 transgenic mice, an Alzheimer's disease model. Faseb J, 2006. 20(6): p. 729-31.

77.   Jeynes, B. and J. Provias, Evidence for altered LRP/RAGE expression in Alzheimer lesion pathogenesis. Curr Alzheimer Res, 2008. 5(5): p. 432-7.

78.   Jin, S., Z. Zador, and A.S. Verkman, Random-walk model of diffusion in three dimensions in brain extracellular space: comparison with microfiberoptic photobleaching measurements. Biophys J, 2008. 95(4): p. 1785-94.

79.   Kettenmann, H., et al., Physiology of microglia. Physiol Rev. 91(2): p. 461-553.

80.   Koehler, R.C., R.J. Roman, and D.R. Harder, Astrocytes and the regulation of cerebral blood flow. Trends Neurosci, 2009. 32(3): p. 160-9.

81.   Kolsch, H., et al., Alterations of cholesterol precursor levels in Alzheimer's disease. Biochim Biophys Acta. 1801(8): p. 945-50.

82.   Koistinaho, M. and J. Koistinaho, Interactions between Alzheimer's disease and cerebral ischemia--focus on inflammation. Brain Res Brain Res Rev, 2005. 48(2): p. 240-50.

83. Kronqvist, R., et al., The effect of interleukin 1 beta on the biosynthesis of cholesterol, phosphatidylcholine, and sphingomyelin in fibroblasts, and on their efflux from cells to lipid-free apolipoprotein A-I. Eur J Biochem, 1999. 262(3): p. 939-46.

84. Lacor, P.N., 2003.

85. Lacor, P.N., et al., Abeta oligomer-induced aberrations in synapse composition, shape, and density provide a molecular basis for loss of connectivity in Alzheimer's disease. J Neurosci, 2007. 27(4): p. 796-807.

86. Ledesma, M.D., et al., Raft disorganization leads to reduced plasmin activity in Alzheimer's disease brains. EMBO Rep, 2003. 4(12): p. 1190-6.

87. Ledesma, M.D. and C.G. Dotti, Amyloid excess in Alzheimer's disease: what is cholesterol to be blamed for? FEBS Lett, 2006. 580(23): p. 5525-32.

88. Lee, J.M., et al., Matrix metalloproteinase-9 and spontaneous hemorrhage in an animal model of cerebral amyloid angiopathy. Ann Neurol, 2003. 54(3): p. 379-82.

89. Lim, G.P., et al., Ibuprofen suppresses plaque pathology and inflammation in a mouse model for Alzheimer's disease. J Neurosci, 2000. 20(15): p. 5709-14.

90. Liu, Q., et al., Amyloid precursor protein regulates brain apolipoprotein E and cholesterol metabolism through lipoprotein receptor LRP1. Neuron, 2007. 56(1): p. 66-78.

91. Lomakin, A., et al., On the nucleation and growth of amyloid beta-protein fibrils: detection of nuclei and quantitation of rate constants. Proc Natl Acad Sci U S A, 1996. 93(3): p. 1125-9.

92. Luca, M., et al., Chemotactic signaling, microglia, and Alzheimer's disease senile plaques: is there a connection? Bull Math Biol, 2003. 65(4): p. 693-730.

93. Luca, M., et al., Chemotactic signaling, microglia, and Alzheimer's disease senile plaques: is there a connection? Bull Math Biol, 2003. 65(4): p. 693-730.

94. Maccioni, R.B., J.P. Munoz, and L. Barbeito, The molecular bases of Alzheimer's disease and other neurodegenerative disorders. Arch Med Res, 2001. 32(5): p. 367-81.

95. Marzolo, M.P. and G. Bu, Lipoprotein receptors and cholesterol in APP trafficking and proteolytic processing, implications for Alzheimer's disease. Semin Cell Dev Biol, 2009. 20(2): p. 191-200.

96. Mawuenyega, K.G., et al., Decreased clearance of CNS beta-amyloid in Alzheimer's disease. Science. 330(6012): p. 1774.

97. McEwen, B.S., Stressed or stressed out: what is the difference? J Psychiatry Neurosci, 2005. 30(5): p. 315-8.

98. McGeer, P.L. and E.G. McGeer, Inflammation, autotoxicity and Alzheimer disease. Neurobiol Aging, 2001. 22(6): p. 799-809.

99. Michikawa, M., et al., Apolipoprotein E exhibits isoform-specific promotion of lipid efflux from astrocytes and neurons in culture. J Neurochem, 2000. 74(3): p. 1008-16.

100. Miller, D.B. and J.P. O'Callaghan, Neuroendocrine aspects of the response to stress. Metabolism, 2002. 51(6 Suppl 1): p. 5-10.

101. Miller, M.C., et al., Hippocampal RAGE immunoreactivity in early and advanced Alzheimer's disease. Brain Res, 2008. 1230: p. 273-80.

102. Minghetti, L., Cyclooxygenase-2 (COX-2) in inflammatory and degenerative brain diseases. J Neuropathol Exp Neurol, 2004. 63(9): p. 901-10.

103. Minghetti, L., Role of inflammation in neurodegenerative diseases. Curr Opin Neurol, 2005. 18(3): p. 315-21.

104. Mun-Bryce, S. and G.A. Rosenberg, Gelatinase B modulates selective opening of the blood-brain barrier during inflammation. Am J Physiol, 1998. 274(5 Pt 2): p. R1203-11.

105. Murphy, M.P., et al., Changes in cognition and amyloid-beta processing with long term cholesterol reduction using atorvastatin in aged dogs. J Alzheimers Dis. 22(1): p. 135-50.

106. Nazer, B., S. Hong, and D.J. Selkoe, LRP promotes endocytosis and degradation, but not transcytosis, of the amyloid-beta peptide in a blood-brain barrier in vitro model. Neurobiol Dis, 2008. 30(1): p. 94-102.

107. Pallitto, M.M. and R.M. Murphy, A mathematical model of the kinetics of beta-amyloid fibril growth from the denatured state. Biophys J, 2001. 81(3): p. 1805-22.

108. Pampaloni, F., E.G. Reynaud, and E.H. Stelzer, The third dimension bridges the gap between cell culture and live tissue. Nat Rev Mol Cell Biol, 2007. 8(10): p. 839-45.

109. Parker, R.A., Q. Huang, and B. Tesfamariam, Influence of 3-hydroxy-3-methylglutaryl-CoA (HMG-CoA) reductase inhibitors on endothelial nitric oxide synthase and the formation of oxidants in the vasculature. Atherosclerosis, 2003. 169(1): p. 19-29.

110. Poirier, J., Apolipoprotein E4, cholinergic integrity and the pharmacogenetics of Alzheimer's disease. J Psychiatry Neurosci, 1999. 24(2): p. 147-53.

111. Poirier, J., Apolipoprotein E represents a potent gene-based therapeutic target for the treatment of sporadic Alzheimer's disease. Alzheimers Dement, 2008. 4(1 Suppl 1): p. S91-7.

112. Poirier, J., et al., Cholesterol synthesis and lipoprotein reuptake during synaptic remodelling in hippocampus in adult rats. Neuroscience, 1993. 55(1): p. 81-90.

113. Puglielli, L., R.E. Tanzi, and D.M. Kovacs, Alzheimer's disease: the cholesterol connection. Nat Neurosci, 2003. 6(4): p. 345-51.

114. Puri, I.K. and L. Li, Mathematical modeling for the pathogenesis of Alzheimer's disease. PLoS One. 5(12): p. e15176.

115. Purves, D., Neuroscience. 2001, Sinauer Associates: Sunderland, Mass.

116. Quan, N. and W.A. Banks, Brain-immune communication pathways. Brain Behav Immun, 2007. 21(6): p. 727-35.

117. Raison, C.L., L. Capuron, and A.H. Miller, Cytokines sing the blues: inflammation and the pathogenesis of depression. Trends Immunol, 2006. 27(1): p. 24-31.

118. Refolo, L.M., et al., Hypercholesterolemia accelerates the Alzheimer's amyloid pathology in a transgenic mouse model. Neurobiol Dis, 2000. 7(4): p. 321-31.

119. Refolo, L.M., et al., A cholesterol-lowering drug reduces beta-amyloid pathology in a transgenic mouse model of Alzheimer's disease. Neurobiol Dis, 2001. 8(5): p. 890-9.

120. Rezaie, P. and D. Male, Mesoglia & microglia--a historical review of the concept of mononuclear phagocytes within the central nervous system. J Hist Neurosci, 2002. 11(4): p. 325-74.

121. Rhodin, J.A. and T. Thomas, A vascular connection to Alzheimer's disease. Microcirculation, 2001. 8(4): p. 207-20.

122. Roher, A.E., et al., Circle of willis atherosclerosis is a risk factor for sporadic Alzheimer's disease. Arterioscler Thromb Vasc Biol, 2003. 23(11): p. 2055-62.

123. Rossor, M., et al., Postmortem studies of peptides in Alzheimer's disease and Huntington's disease. Res Publ Assoc Res Nerv Ment Dis, 1986. 64: p. 259-77.

124. Rossor, M.N., Neurotransmitters and CNS disease. Dementia. Lancet, 1982. 2(8309): p. 1200-4.

125. Rothman, S.M. and M.P. Mattson, Adverse stress, hippocampal networks, and Alzheimer's disease. Neuromolecular Med. 12(1): p. 56-70.

126. Ruoslahti, E., Brain extracellular matrix. Glycobiology, 1996. 6(5): p. 489-92.

127.   Salminen, A., et al., Inflammation in Alzheimer's disease: amyloid-beta oligomers trigger innate immunity defence via pattern recognition receptors. Prog Neurobiol, 2009. 87(3): p. 181-94.

128.   Sastre, M., T. Klockgether, and M.T. Heneka, Contribution of inflammatory processes to Alzheimer's disease: molecular mechanisms. Int J Dev Neurosci, 2006. 24(2-3): p. 167-76.

129.   Schmitz, C., et al., Hippocampal neuron loss exceeds amyloid plaque load in a transgenic mouse model of Alzheimer's disease. Am J Pathol, 2004. 164(4): p. 1495-502.

130.   Selkoe, D.J., Soluble oligomers of the amyloid beta-protein impair synaptic plasticity and behavior. Behav Brain Res, 2008. 192(1): p. 106-13.

131.   Shibata, M., et al., Clearance of Alzheimer's amyloid-ss(1-40) peptide from brain by LDL receptor-related protein-1 at the blood-brain barrier. J Clin Invest, 2000. 106(12): p. 1489-99.

132.   Smith, M.M., et al., Whole blood viscosity and microvascular abnormalities in Alzheimer's Disease. Clin Hemorheol Microcirc, 2009. 41(4): p. 229-39.

133.   Snowdon, D.A., Healthy aging and dementia: findings from the Nun Study. Ann Intern Med, 2003. 139(5 Pt 2): p. 450-4.

134.   Sofroniew, M.V., Reactive astrocytes in neural repair and protection. Neuroscientist, 2005. 11(5): p. 400-7.

135.   Sotiropoulos, I., et al., Glucocorticoids trigger Alzheimer disease-like pathobiochemistry in rat neuronal cells expressing human tau. J Neurochem, 2008. 107(2): p. 385-97.

136.   Sparks, D.L., et al., Cholesterol and cognitive performance in normal controls and the influence of elective statin use after conversion to mild cognitive impairment: results in a clinical trial cohort. Neurodegener Dis. 7(1-3): p. 183-6.

137.   Sparks, D.L., et al., Statin therapy in Alzheimer's disease. Acta Neurol Scand Suppl, 2006. 185: p. 78-86.

138.   Srivareerat, M., et al., Chronic psychosocial stress exacerbates impairment of cognition and long-term potentiation in beta-amyloid rat model of Alzheimer's disease. Biol Psychiatry, 2009. 65(11): p. 918-26.

139.   Sterlemann, V., et al., Chronic social stress during adolescence induces cognitive impairment in aged mice. Hippocampus. 20(4): p. 540-9.

140.   Stewart, R., Cardiovascular factors in Alzheimer's disease. J Neurol Neurosurg Psychiatry, 1998. 65(2): p. 143-7.

141.   Stewart, W.F., et al., Risk of Alzheimer's disease and duration of NSAID use. Neurology, 1997. 48(3): p. 626-32.

142.   Streit, W.J., Microglia and Alzheimer's disease pathogenesis. J Neurosci Res, 2004. 77(1): p. 1-8.

143.   Streit, W.J., R.E. Mrak, and W.S. Griffin, Microglia and neuroinflammation: a pathological perspective. J Neuroinflammation, 2004. 1(1): p. 14.

144.   Sun, Z.X., Q.H. Zhou, and S.F. Sui, Cholesterol depletion inhibits the degradation of amyloid beta-peptide in rat pheochromocytoma (PC12) cells. Neurosci Lett, 2005. 391(1-2): p. 71-5.

145.   Suo, Z., et al., Alzheimer's beta-amyloid peptides induce inflammatory cascade in human vascular cells: the roles of cytokines and CD40. Brain Res, 1998. 807(1-2): p. 110-7.

146.   Takano, T., et al., Astrocyte-mediated control of cerebral blood flow. Nat Neurosci, 2006. 9(2): p. 260-7.

147.   Thelen, K.M., et al., Brain cholesterol synthesis in mice is affected by high dose of simvastatin but not of pravastatin. J Pharmacol Exp Ther, 2006. 316(3): p. 1146-52.

148. Timmer, N.M., et al., Amyloid beta induces cellular relocalization and production of agrin and glypican-1. Brain Res, 2009. 1260: p. 38-46.

149. Tolar, M., et al., Truncated apolipoprotein E (ApoE) causes increased intracellular calcium and may mediate ApoE neurotoxicity. J Neurosci, 1999. 19(16): p. 7100-10.

150. Tran, T.T., M. Srivareerat, and K.A. Alkadhi, Chronic psychosocial stress triggers cognitive impairment in a novel at-risk model of Alzheimer's disease. Neurobiol Dis. 37(3): p. 756-63.

151. Tripathy, D. and P. Grammas, Acetaminophen inhibits neuronal inflammation and protects neurons from oxidative stress. J Neuroinflammation, 2009. 6: p. 10.

152. Trompet, S., et al., Pravastatin and cognitive function in the elderly. Results of the PROSPER study. J Neurol. 257(1): p. 85-90.

153. Ullian, E.M., K.S. Christopherson, and B.A. Barres, Role for glia in synaptogenesis. Glia, 2004. 47(3): p. 209-16.

154. Wang, Y., et al., Glucocorticoids Facilitate Astrocytic Amyloid-{beta} Peptide Deposition by Increasing the Expression of APP and BACE1 and Decreasing the Expression of Amyloid-{beta}-Degrading Proteases. Endocrinology. 152(7): p. 2704-15.

155. Waters, D.D., Exploring new indications for statins beyond atherosclerosis: Successes and setbacks. J Cardiol. 55(2): p. 155-62.

156. Weksler, M.E., et al., The immune system, amyloid-beta peptide, and Alzheimer's disease. Immunol Rev, 2005. 205: p. 244-56.

157. Weksler, M.E., et al., The immune system, amyloid-beta peptide, and Alzheimer's disease. Immunol Rev, 2005. 205: p. 244-56.

158. Weller, R.O., et al., Perivascular drainage of amyloid-beta peptides from the brain and its failure in cerebral amyloid angiopathy and Alzheimer's disease. Brain Pathol, 2008. 18(2): p. 253-66.

159. Weller, R.O., et al., Cerebrovascular disease is a major factor in the failure of elimination of Abeta from the aging human brain: implications for therapy of Alzheimer's disease. Ann N Y Acad Sci, 2002. 977: p. 162-8.

160. Wetzel, R., S. Shivaprasad, and A.D. Williams, Plasticity of amyloid fibrils. Biochemistry, 2007. 46(1): p. 1-10.

161. Wyss-Coray, T. and L. Mucke, Inflammation in neurodegenerative disease--a double-edged sword. Neuron, 2002. 35(3): p. 419-32.

162. Yankner, B.A., L.K. Duffy, and D.A. Kirschner, Neurotrophic and neurotoxic effects of amyloid beta protein: reversal by tachykinin neuropeptides. Science, 1990. 250(4978): p. 279-82.

163. Zipfel, G.J., et al., Cerebral amyloid angiopathy: progressive disruption of the neurovascular unit. Stroke, 2009. 40(3 Suppl): p. S16-9.

164. Zlokovic, B.V., Clearing amyloid through the blood-brain barrier. J Neurochem, 2004. 89(4): p. 807-11.

165. Zlokovic, B.V., The blood-brain barrier in health and chronic neurodegenerative disorders. Neuron, 2008. 57(2): p. 178-201.